NASA Technical Memorandum 105888

Application of Jet-Shear-Layer Mixing and Effervescent Atomization to the Development of a Low-NO_x Combustor

Renato Olaf Colantonio
Lewis Research Center
Cleveland, Ohio

June 1993

NASA

Trade names or manufacturers' names are used in this report for identification only. This usage does not constitute an official endorsement, either expressed or implied, by the National Aeronautics and Space Administration.

CONTENTS

APPLICATION OF JET-SHEAR-LAYER MIXING AND EFFERVESCENT ATOMIZATION TO THE DEVELOPMENT OF A LOW-NO_x COMBUSTOR

Renato Olaf Colantonio
National Aeronautics and Space Administration
Lewis Research Center
Cleveland, Ohio 44135

Summary

An investigation was conducted to develop appropriate technologies for a low-NO_x, liquid-fueled combustor. The combustor incorporates an effervescent atomizer used to inject fuel into a premixing duct. Only a fraction of the combustion air is used in the premixing process to avoid autoignition and flashback problems. This fuel-rich mixture is introduced into the remaining combustion air by a rapid jet-shear-layer-mixing process involving radial fuel-air jets impinging on axial air jets in the primary combustion zone. Computational analysis was used to provide a better understanding of the fluid dynamics that occur in jet-shear-layer mixing and to facilitate a parametric analysis appropriate to the design of an optimum low-NO_x combustor. A number of combustor configurations were studied to assess the key combustor technologies and to validate the modeling code.

The results from the experimental testing and computational analysis indicate a low-NO_x potential for the jet-shear-layer combustor. Key parameters found to affect NO_x emissions are the primary combustion zone fuel-air ratio, the number of axial and radial jets, the aspect ratio and radial location of the axial air jets, and the radial jet inlet hole diameter. Each of these key parameters exhibits a low-NO_x point from which an optimized combustor was developed. Using the parametric analysis, NO_x emissions were reduced by a factor of 3 as compared with the emissions from conventional, liquid-fueled combustors operating at cruise conditions. Further development promises even lower NO_x with high combustion efficiency.

Symbols

A_{jet}	jet cross-sectional area, m^2
C_μ	constant for turbulent flows
D	combustor inside diameter, m
D_0	initial drop-size diameter, m
d	hydraulic diameter, m
E	activation energy, J/mole
E_v	fraction of fuel in vapor state

H	mole fraction of CO_2 concentration in dry air
h	humidity of air, moles of water vapor/mole of dry air
K	NO_x rate coefficient
k	turbulent kinetic energy, m^2/s^2
k_i	chemical rate coefficient, cm^3/mole·s
ℓ	turbulent length scale, m
M	atomic weight, kg/kg·mole
P	pressure, MPa
p	turbulence intensity, percent
q	Rosin-Rammler drop-size distribution parameter
R	combustor inside radius, m
$\overline{R}$	universal gas constant, J/mole·K
r	radial direction, m
r_{max}	radius of flametube, m
S	nonuniformity parameter
T	temperature, K
t	time, s
t_a	autoignition time, ms
t_p	slot width, mm
U	axial jet velocity, m/s
u′,v′	rms values of fluctuating velocity components along x and y, respectively, m/s
V	radial jet velocity, m/s
W	traverse jet velocity, m/s
x	axial direction, m
y	vertical direction, m
α	hydrogen-carbon ratio

β	angle of jet interception, deg
γ	angle of deflection of weaker jet, deg
ε	turbulent energy dissipation rate, 1/s
η_c	combustion efficiency, percent
θ	traverse direction, deg
λ_{eff}	effective evaporation constant, mm^2/s
ρ	gas density, kg/m^3
$\overline{\phi}$	average equivalence ratio
ϕ_1	local equivalence ratio
ω	mass flow rate, kg/s

Subscripts:

a	cooling air
air	dry air
C	carbon
EI	emission index, g NO/kg fuel
e	evaporation
g	combustion gas
H	hydrogen
ℓ	liquid droplet burning
M	mean
v	vapor burning
w	wall
0.5	half-width of mean velocity profile
01	exit-plane condition of higher velocity nozzle
02	exit-plane condition of lower velocity nozzle
3	combustor inlet location

Chapter 1

Introduction

As the National Aeronautics and Space Administration (NASA), along with academia and private industry, design and build the next generation of high-speed aircraft, much attention is being given to the discharge of pollutants into the Earth's stratosphere. The stratosphere is an atmospheric region between 12 000 and 31 000 m above the Earth's surface and is the home of the protective ozone layer. Presently most subsonic flight is limited to the troposphere, which is below 12 000 m. The proposed supersonic and hypersonic aircraft will cruise in the ozone layer at altitudes around 20 000 and 31 000 m, respectively. Recent concerns such as the widening of the antarctic ozone holes, the greenhouse effect, and increased skin cancer rates may be linked to the destruction of the ozone layer brought on by pollutants.

One type of ozone-depleting pollutant created during the combustion process is oxides of nitrogen ($NO_x = NO + NO_2$). NO_x is a catalyst for the destruction of ozone O_3 as in the following mechanism:

$$NO + O_3 \rightarrow NO_2 + O_2$$

$$O_3 \rightarrow O + O_2$$

$$O + NO_2 \rightarrow NO + O_2$$

It has been suggested (National Academy of Science, 1975) that a fleet of 300 to 400 supersonic aircraft discharging NO_x (each with an average emissions index of 18 g NO_2/kg fuel) would decrease the ozone density by 10 percent. This could result in a 20-percent increase in skin cancer, damage to vegetation, changes in the nature and growth of some species, and changes in the Earth's average temperature (Miller and Miller, 1989; National Academy of Science, 1977; and Kemp, 1990). Therefore, for high-speed flight to become environmentally acceptable, current combustors must be redesigned to drastically reduce NO_x. NASA is currently developing new technologies and concepts aimed at reducing NO_x to one-tenth of current levels by 1996. Current combustors produce NO_x emissions of 10 to 20 g NO_2/kg fuel at supersonic cruise conditions.

The formation of NO_x has been shown to be an exponential function of the flame temperature. The temperature sensitivity of NO_x production is explained by the fact that the reactions primarily involve atomic oxygen which does not appear in large quantities at low temperatures. The chemical rate reactions are also sensitive to temperature. Therefore, the key to any successful low-NO_x combustor is to provide suffi cient time and temperature for complete combustion but not enough time and temperature for high-NO_x emission levels (Lefebvre, 1983). This requirement has been met by producing a nearly homogeneous fuel-air mixture and burning well away from stoichiometric conditions (lean or rich combustion).

Some of the combustor concepts designed and tested to reduce NO_x emissions are the lean-direct-injection (LDI), lean-premixed-prevaporized (LPP), and rich burn-quick mix-lean burn (RQL) combustors. The idea behind the LDI combustor is to provide a suitable fuel atomizer that will produce exceptionally small droplets. Current atomizers produce droplets that are too large for low-NO_x applications. Small droplet production is essential since large drops burn stoichiometrically via a diffusion-type mechanism and create local hot regions in the flow field. In the LDI concept, fuel droplets are injected into the primary combustion zone in such a way as to provide complete mixing, vaporization, and burning. If these processes are not accomplished fully, some degree of fuel and air nonuniformity will occur and give rise to local hot regions.

The LPP combustor injects the fuel into the air well upstream from the primary combustion zone. This provides sufficient time for the fuel and air to thoroughly mix and vaporize prior to combustion. This combustor concept attempts to eliminate fuel-air nonuniformities and droplet burning. The disadvantages of this concept are the need to provide a relatively long mixing length and the risk of flashback and autoignition in the premixing prevaporizing region.

The RQL combustor concept, as its name implies, consists of three zones. The first zone in the combustor burns fuel at a rich mixture strength. The exhaust gases emerging from this fuel-rich zone then enter a quick-mix zone where additional air is injected and mixed. This process must be accomplished quickly to avoid too long a residence at the stoichiometric crossover condition. Combustion is then completed at well below stoichiometric fuel-air ratios. The main problem with this concept is the need to rapidly dilute the fuel-rich efflux with air.

The present test program examines the effectiveness of an LDI combustor concept incorporating jet-shear-layer mixing to reduce NO_x emissions. A jet-shear-layer-mixing scheme, involving axial air jets impinging directly on radial fuel-air jets near the dome inside the combustor, was shown by Abdul-Hussain et al. (1988) to provide rapid mixing with good combustion stability and low NO_x. However, the work done by Addul-Hussain et al. was limited to gaseous fuels, and the combustor operated at atmospheric pressures only. The use of liquid fuels has been shown to produce higher NO_x as compared with the use of gaseous fuels (Abdul-Aziz et al., 1987).

The goal of this study was to investigate whether the demonstrated low-NO_x potential of the jet-shear-layer (JSL) combustor when burning gaseous fuels was still present for liquid fuels. Based on LPP combustor studies, two key features were added to the JSL combustor concept: a fuel-air premixing region and an effervescent atomizer. Premixing of all the fuel with some of the air prior to combustion permits greater fuel-air uniformity in the combustor and allows some degree of fuel droplet vaporization to take place. This fuel-rich, unignitable premixing region avoids the flashback and autoignition problems encountered in the LPP combustor concept.

To provide a minimal level of large, NO_x-producing fuel droplets, an effervescent fuel atomizer was used in the premixing region of the JSL combustor. In an effervescent atomizer, air bubbles are injected directly into the fuel upstream from the atomizer discharge orifice. Only a small amount of air is needed for this purpose. It has been demonstrated (Roesler, 1988 and Whitlow, 1990) that these bubbles shatter the fuel into fine ligaments which are then ejected from the atomizer orifice at high velocities. The air bubbles explode upon exiting the orifice. These mechanisms all contribute to the production of small droplets (<20-μm Sauter mean diameter SMD).

The simplicity and size of the JSL combustor make it a viable alternative to the LPP, RQL, and other LDI combustors currently being developed. Therefore, for the present study it was hoped that successful low-NO_x results could be achieved by incorporating an effervescent atomizer and partial premixing of the fuel and air in a JSL combustor using liquid fuels. To promote the highest degree of fuel-air mixing in the combustor, a three-dimensional, computational fluid dyanmics (CFD) code was used to facilitate a parametric analysis over a wide range of combustor operating conditions. This analysis led to an optimum configuration for a low-NO_x JSL combustor. A number of combustor configurations were experimentally tested to demonstrate the low-NO_x potential of the liquid-fueled JSL combustor and to verify the CFD model. The best combustor exhibited a threefold reduction in NO_x emissions at altitude cruise conditions when compared with conventional, liquid-fueled aircraft combustors. It is argued that further model development should result in even lower NO_x emissions while high levels of combustion efficiency are still maintained.

Chapter 2

Literature Review

The development of a low-NO_x, jet-shear-layer combustor warrants a literature review of emission production mechanisms and low-NO_x combustor designs. Therefore, a look into the chemical mechanisms of NO_x formation and LPP combustors was undertaken. Previous work on JSL mixing combustors was investigated. The review of two combustor configurations and their performance guided the design work for the combustor configuration used in this research program. The available research on intercepting jets was also investigated. Finally, the merits of using an effervescent fuel atomizer in this program are discussed.

2.1 NO_x Formation

NO can be produced by three different mechanisms (Lefebvre, 1983): thermal, prompt, and fuel-bound. Thermal NO is produced by the oxidation of atmospheric nitrogen. The oxidation process is significant at gas temperatures above 1800 K and is dependent on the residence time at that gas temperature (fig. 2.1). Thermal NO production typically follows the classical Zeldovich mechanism:

$$O_2 \rightarrow 2O$$
$$O + N_2 \rightarrow NO + N$$
$$N + O_2 \rightarrow NO + O$$

Prompt NO is produced by high-speed reactions at the flame front; their kinetics are not well understood. It has been suggested that prompt NO is caused by the attack of carbon or hydrocarbon radicals on nitrogen:

$$CH + N_2 \rightarrow HCN + N$$

Others attribute prompt NO to combustion intermediates (O, OH, and H) not being in chemical equilibrium. Most NO analyses are undertaken by assuming the intermediates to be in equilibrium. Prompt NO has been experimentally determined to be most pronounced in rich burning and is usually negligible in lean burning. Several investigators neglect prompt NO in their combustion analyses.

Fuel-bound NO is produced by the oxidation of the nitrogen contained in the fuel itself. Light distillate fuels such as kerosine, Jet-A, or JP-8 contain small amounts of organic nitrogen (less than 0.06 percent) whereas heavy distillate fuels may contain as much as 1.8 percent organic nitrogen. Fuels used in aircraft turbine combustors are usually the kerosine type; therefore, fuel-bound NO can be ignored.

The other contributor to NO_x, NO_2, is produced when NO is held at temperatures low enough to recombine with O to attain a more chemically stable state. NO_2 may originate from locally cool regions in the combustor, such as the liner walls, or in the gas sampling system.

Nitric oxide formation in combustion was studied by Nelson (1986), who suggests that NO concentration can be predicted for lean to moderately fuel-rich hydrocarbon combustion using an extended Zeldovich mechanism:

$$O + N_2 \rightarrow NO + N$$
$$N + O_2 \rightarrow NO + O$$
$$N + OH \rightarrow NO + H$$

From this extended Zeldovich mechanism, the general rate equation for NO is

$$\frac{\partial(NO)}{\partial t} = k_1(O)(N_2) - k_{-1}(N)(NO) + k_2(N)(O_2) - k_{-2}(O)(NO) + k_3(N)(OH) - k_{-3}(H)(NO)$$

where t is the time and k_1, k_2, and k_3 are the forward chemical rate coefficients for the reactions in the Zeldovich mechanism. The reverse chemical rate coefficients are given as k_{-1}, k_{-2}, and k_{-3}.

A simplified rate production may be determined by assuming that the concentration of N is at equilibrium and the concentration of NO is small. We have (Nelson, 1986)

$$(N) = \frac{(O)[k_1 N_2 + k_2(NO)] + k_3(H)(NO)}{k_1(NO) + k_2(O_2) + k_3(OH)}$$

$$\frac{\partial(NO)}{\partial t} \approx 2k_1(N_2)(O)$$

The steady-state approximation for N concentration is justified since the NO concentration is small compared with the remaining species, and the approximation is true for temperatures of interest in combustion.

Most researchers model low-NO_x combustors by using the simple Zeldovich reaction scheme. The rate equation is similar to that suggested by Nelson:

$$\frac{\partial(NO)}{\partial t} = K(N_2)(O)$$

The rate coefficient K has been determined experimentally to be an exponential function of temperature. Approximating N_2 and O to their local equilibrium values, the following rate equation is commonly used:

$$\frac{\partial(NO)}{\partial t} = A \exp(-E/\overline{R}T)(N_2)(O_2)^{1/2}$$

where A is an experimentally determined constant, E is the activation energy in joules per mole, $\overline{R}$ is the universal gas constant, and T is the gas temperature in degrees Kelvin. Experimental data are used to calibrate and verify this approach.

Other empirical relationships based on experimental observations have also been used successfully. Typical correlations follow the form (Lefebvre, 1983)

$$\ln\left(\frac{NO_{EI}}{t}\right) = B + C\sqrt{T} - \frac{T}{D}$$

where NO_{EI} is the emission index in grams of NO per kilogram fuel, t is the combustion residence time, B, C, and D are experimentally determined constants, and T is the adiabatic flame temperature. Because the reaction $N_2 + O_2 = 2NO$ is a constant volume process, pressure effects on NO production are negligible. However, pressure changes may promote changes in the flame temperature by changing the efficiency of the combustion process.

2.2 Lean-Premixed-Prevaporized (LPP) Combustors

One combustor concept that promises reduced emissions is the LPP. Studies undertaken have indicated NO_x reductions of an order of magnitude as compared with conventional combustors. The LPP concept involves vaporizing all the fuel and thoroughly mixing the resulting vapor with the air upstream from the primary combustion zone. This concept eliminates the presence of fuel droplets in the combustion zone. Droplet combustion occurs by a diffusion flame mechanism. The high temperatures associated with local droplet combustion tend to produce NO_x. Therefore, the key to the success of the LPP combustor is to fully vaporize all the fuel and provide for lean, homogeneous combustion. In this way no portion of the combustor can be at or near stoichiometric conditions where high NO_x formation results. Also, a homogeneous mixture allows more intense burning, resulting in a shorter combustion zone. This shorter combustion zone reduces the time the products of combustion spend at critical NO_x-producing temperatures. However, operating a combustor with a lean, homogeneous mixture creates problems such as autoignition and flashback upstream from the primary zone. Since, for the LPP concept, there are no rich pockets of fuel-air mixture to help maintain combustion at lean equivalence ratios, as occurs in conventional combustors, lean blowout takes place at higher equivalence ratios (typically around 0.5).

2.2.1 LPP Experimental Combustor Performance

Anderson (1973) utilized the rig shown in figure 2.2 to study the effects of premixing on NO_x formation. Inlet conditions included a temperature of 590 K, a pressure of 0.507 MPa and a reference velocity of 23 m/s. Propane (C_3H_8) fuel was used for all tests. An emissions index of less than 1 g NO_2/kg fuel was obtained for an equivalence ratio less than 0.57. Values for conventional combustors with the same inlet conditions range from 3 to 5 g NO_2/kg fuel. Maximum emissions were close to 30 g NO_2/kg fuel for equivalence ratios close to stoichiometric. This investigation employed a flametube with no dilution holes. Anderson noted that, if dilution air holes are introduced at the end of the recirculation region, as is done in conventional combustors, NO_x levels could be reduced even further by quenching chemical reactions. In a later study by Anderson (1975), using the same test rig but higher inlet temperatures (600 and 800 K), he noted that a reduction in residence time leads to a decrease in NO_x levels, especially at high equivalence ratios. Data for different residence times were achieved by axially traversing the sampling probe. The results suggested that, to achieve low NO_x and still maintain high combustion efficiency, burning as lean as possible for the longest residence time is the best approach (fig. 2.3). The combustor inlet temperature also appears to affect NO_x levels (fig. 2.4). At an equivalence ratio of 0.6, the NO_x emissions levels were 1.1 and 6.8 g NO_2/kg fuel for inlet temperatures of 600 and 800 K, respectively.

Roffe (1976) and Roffe and Ferri (1975 and 1976) demonstrated the effectiveness of the premixing, prevaporizing technique at conditions corresponding to gas turbines operating at high altitudes and high

Mach numbers using JP-5 fuel. Figure 2.5 shows the experimental rig used. The inlet temperature and pressure were 833 K and 0.405 MPa. A number of flameholders and fuel injection configurations were tested. Roffe and Ferri noted that the most sensitive problem associated with the design of an LPP burner is the avoidance of mixing tube combustion either as flashback or autoignition. Such events may damage the flameholder and mixing tube. One must select a mixing length that is low enough to avoid autoignition yet high enough to ensure adequate premixing and prevaporization. Also needed is a flameholder with an air-fuel-mixture injection velocity high enough to avoid flashback. The flameholder must also be geometrically designed and assembled such that boundary layer effects are kept to a minimum. This design is critical since flames may propagate upstream from the flameholder through low-velocity boundary layers.

Roffe and Ferri noted that, as the degree of fuel premixing improved, the NO_x level decreased and the combustion efficiency increased. Fuel injection upstream from the mixing duct was achieved by using 12 equally spaced nozzles located flush to the duct wall or via coaxially mounted nozzles positioned streamwise to the flow. The initial fuel droplet diameters ranged from 50 to 150 μm. A single axially mounted pressure atomizer spraying at a 75° angle produced 9 g NO_2/kg fuel with 99 percent combustion efficiency at an equivalence ratio of 0.60. A set of four of these pressure atomizers reduced emissions to 2 g NO_2/kg fuel with 99 percent combustion efficiency. Using a 12-orifice normal injector further reduced emissions to 1.60 g NO_2/kg fuel with 99.7 percent combustion efficiency. Figure 2.6 compares the performances of different low-NO_x combustors.

Roffe and Ferri also investigated the effect of decreasing the mixing duct length from 0.53 to 0.33 m for a constant duct diameter of 89 mm. NO_x levels increased by a factor of 2 over the entire range of equivalence ratios. This behavior is attributed to local increases in equivalence ratios brought on by decreases in the fuel-air uniformity.

Marek and Papathekos (1976) studied exhaust emissions from a premixing, prevaporizing combustor using Jet-A liquid fuel injected into the inlet airstream upstream from a perforated plate flameholder (fig. 2.7). Inlet air temperatures ranged from 640 to 833 K for a constant inlet pressure of 0.567 MPa. The reference velocity was 25 m/s and the equivalence ratio varied from 0.7 to the lean blowout limit value. Autoignition occurred above 650 K when the residence time upstream from the flameholder was 104 ms (2.60-m-long mixture tube). When this time was shortened to 24 ms (0.61-m-long mixing tube), autoignition was eliminated at inlet temperatures below 833 K. In a later work by Marek, Papathekos, and Verbulecz (1977), autoignition times decreased with increasing temperature and pressure according to the equation

$$t_a = \frac{A_0 e^{(-E/\bar{R}T)}}{p^n}$$

where t_a is the autoignition time; A_0 and n are experimental constants; E is the activation energy (for Jet-A fuel, E was determined experimentally to be 41 840 J/mole); $\bar{R}$ is the universal gas constant; and T is the inlet temperature in degrees Kelvin. For an inlet temperature of 640 K, NO_x values were as low as 0.6 and 1.1 g NO_2/kg fuel for equivalence ratios of 0.55 and 0.60, respectively. For an inlet temperature of 833 K, NO_x values were as low as 0.3 and 4.5 g NO_2/kg fuel for equivalence ratios of 0.40 and 0.60, respectively. High combustion efficiencies of 99 percent were achieved for conditions close to the lean blowout limits.

2.2.2 Influence of Degree of Vaporization on NO_x

Cooper (1980) investigated the effect of the degree of fuel vaporization on NO_x emissions for a premixed combustor. He suggests that the total NO_x created for a partially vaporized mixture can be separated as

$$(NO_x)_{total} = E_v(NO_x)_{vapor\ burning} + (1 - E_v)(NO_x)_{droplet\ burning}$$

where E_v is the fraction of fuel in the vapor state, and $(1 - E_v)$ is the fraction in the liquid droplet state; $(NO_x)_{vapor\ burning}$ and $(NO_x)_{droplet\ burning}$ can be determined from a knowledge of the equivalence ratio and experimental data and/or analytical models. $(NO_x)_{droplet\ burning}$ is known from the adiabatic flame temperature T_ℓ at an equivalence ratio of unity, and $(NO_x)_{vapor\ burning}$ is known from the vapor phase adiabatic flame temperature T_v at a vapor equivalence ratio equal to E_v (total equivalence ratio). Cooper determined that if, for a given combustor inlet temperature and total equivalence ratio, T_v falls below 2050 K, decreases in E_v increase NO_x emissions. For values of T_v between 2050 and 2200 K, E_v has little effect on NO_x emissions whereas, for a T_v above 2200 K, decreases in E_v decrease NO_x emissions. In the first case, the liquid droplet NO_x contribution dominates whereas in the latter case the vapor phase NO_x contribution dominates. Cooper's investigation suggests that, for any given NO_x emissions standard, a degree of vaporization and equivalence ratio can be selected to meet those standards without complete vaporization of the fuel being necessary. A completely vaporized system poses problems of autoignition and flashback, as discussed earlier in section 2.2.1.

2.2.3 Influence of Degree of Fuel-Air Nonuniformity on NO_x

Lyons (1981) investigated the effect of fuel-air nonuniformity on NO_x emissions in order to define the degree of premixing required in the LPP combustor. Nonuniformity was accomplished by varying the amount of fuel supplied to different zones of a multipoint fuel injector upstream from the flameholder. Lyons defined a nonuniformity parameter S as

$$S = \left(\int_0^{r_{max}} (\phi_1 - \overline{\phi})^2 r\,dr \Big/ \int_0^{r_{max}} r\,dr \right)^{1/2}$$

where r_{max} is the radius of the flametube, and ϕ_1 and $\overline{\phi}$ are the local and average equivalence ratios, respectively. It was determined that, for equivalence ratios less than 0.7, increases in S increase NO_x levels whereas, for equivalence ratios near unity, increases in S decrease NO_x levels (fig. 2.8). The decrease in NO_x levels in the latter case occurs because some regions in the combustion zone must be fuel rich or fuel lean, leading to lower than stoichiometric temperatures in those regions.

2.3 Direct-Injection Low-NO_x Combustors

As an alternative to LPP combustors, where complete evaporation and mixing of fuel and air are accomplished before they enter the primary combustion zone, many researchers developed combustors with direct fuel injection into the primary zone and still achieved adequate mixing of the fuel and air. The key to the success of the lean-direct-injection (LDI) combustors is to provide rapid mixing of fuel and air in a limited combustion volume.

Abdul-Aziz et al. (1987), Abdul-Hussain et al. (1988), Al-Dabbagh and Andrews (1981), and Andrews, Abdul-Aziz, and Al-Dabbagh (1983) studied jet-shear-layer-mixing combustion using the jet mix flame stabilizer shown in figure 2.9. A central pipe provides eight radial fuel jets which pass through eight radial air passages. These radial air passages provide time for all the fuel to partially mix with a portion of the combustion air prior to its entry into the primary zone. Two 140-mm-diameter combustor configurations were used. The first configuration had radial air-fuel jets directly impinging on axial air jets. The second configuration had radial air-fuel jets ejecting between axial air jets. The radial distance of the axial air jets from the combustor axis was varied to investigate its effect. Tests were carried out using gas oil, natural gas, propane, and kerosine as fuels. All tests were conducted at normal atmospheric pressure with inlet air temperatures ranging from 400 to 600 K.

The results obtained by Abdul-Aziz et al. (1987), Abdul-Hussain et al. (1988), Al-Dabbagh and Andrews (1981), and Andrews, Abdul-Aziz, and Al-Dabbagh (1983) showed that their concepts can achieve ultralow emissions of NO_x with good stability margins as compared with totally premixed combustors. The in-line jet configuration provides direct impingement and rapid mixing with no chance of any combustion taking place in the rich radial jets. This configuration yielded the lowest NO_x levels but had the poorest stability limits. However, the offset configuration provides a means for local burning in the rich radial jets and shows greater stability with slightly higher NO_x levels (fig. 2.10). Al-Dabbagh and Andrews (1981) determined that mixing for both configurations is complete within 20 percent of the mean at a downstream distance of four axial jet diameters. Because NO_x production is dependent on residence time, this combustor feature is a dominant force in reducing such emissions.

The amount of radial air used affected combustion stability and NO_x production. Using 15 to 30 percent of the total combustion air through the radial air passages yielded the lowest NO_x; greater than 30 percent created stability problems and less then 15 percent yielded high NO_x levels. Abdul-Hussain et al. (1988) used a nominal radial airflow of 32 percent. The radial position of the axial air jets also affected emissions and stability levels. For the in-line configuration, the inner axial jets generated the most intense mixing, which resulted in low NO_x but poor flame stability. For the offset configuration, inner axial jets maximized the opportunity for combustion in the rich radial jets, which resulted in high NO_x but good flame stability.

2.4 Intercepting Jets

Al-Dabbagh and Andrews (1981) demonstrated the effectiveness of jet-shear-layer mixing in combustor design. They carried out water visualization tests on radial and axial jet mixing using a conductivity technique with salt added to the radial jets. They found that mixing was very rapid and was 90 percent complete within five axial hole diameters. Abdul-Aziz et al. (1987), using a nonpremixed jet mix technique with kerosine fuel, found that the weak extinction limit approached that of a propane-air premixed system. This finding established the attributes of the jet mix design. Not much work has been done on two unequal jets intercepting one another at 90°. However, Al-Dabbagh and Andrews suggest that the good performance of the jet mix design is attributed to the influence of the radial jet increasing the rate of spreading of the axial jet. Water flow visualization studies indicated a jet spreading angle of 90° as compared with a spreading angle of 10° without radial jet interaction. They concluded that the combined jet entrainment rate was much greater than that for a single axial jet and that a more uniform radial velocity profile does exist. The increased entrainment rate and the rapid reduction in jet velocity was suggested to aid flame stability.

Elbanna and Sabbagh (1985) studied the interaction of two, equal-flow, slotted jets at various impingement angles. The slot width t_p was 12 mm and the two jets were spaced 0.15 m apart. They

found that the mutual entrainment of the surrounding air creates a subatmospheric region between the jets. This local pressure is observed to increase downstream from the subatmospheric region because of the confluence of the jets. Downstream from this confluence region the pressure energy converts to kinetic energy and the fluids attain a maximum velocity (minimum static pressure). The pressure then gradually attains the level of the surrounding pressure. The mean velocity profile of the combined jet is similar to that of a single jet and exhibits a saddleback shape which disappears as the interception angle increases. Similarity is also observed for axial, lateral, and transverse velocity fluctuations as compared with a single jet. Figures 2.11 and 2.12 illustrate the velocity profiles resulting from two jets intercepting at 100° where x/t_p is the nondimensionalized downstream distance from the jet orifices, and $y/y_{0.5}$ is the nondimensionalized vertical distance from the combined jet centerline.

Elbanna and Sabbagh (1986) also investigated two, nonequal-flow, slotted jets intercepting at 100°. The slots were 12 mm and spaced 0.15 m apart. The deflection angle γ of the weaker jet for the zero-pressure effect was determined to be

$$\gamma = \cot^{-1}\left[\cot\beta + \left(\frac{U_{02}}{U_{01}}\right)^2 \frac{1}{\sin\beta}\right]$$

where β is the angle of interception and U_{01} and U_{02} are the mean velocities of the high- and low-velocity jets, respectively. However, since there is a subatmospheric region between the jets, they merge upstream of the geometric intercept. As can be seen in figures 2.11 and 2.12, the velocity and turbulence levels are similar to those of a single jet at all the mean jet velocity ratios tested.

2.5 Effervescent Atomizers

Effervescent atomization has been the subject of much research over the past few years. The results of these investigations suggest their possible application to gas turbine combustors (Lefebvre, 1988).

Roesler (1988) investigated the internal and external flow characteristics of effervescent atomizers spraying into ambient air (fig. 2.13). Water and air were used as the working fluids. Water injection pressures ranged from 173 to 690 kPa, with gas-liquid ratios ranging from 0.001 to 0.05 by mass. Three separate orifice diameters of 1.5, 2.0, and 2.5 mm were used. A laser diffraction technique was used to measure the SMD and the Rosin-Rammler drop-size distribution parameter q. Figure 2.14 shows the mean drop size plotted against the gas-liquid ratio for four different injection pressures. The gas-liquid ratios were limited because of the spray becoming unstable above a certain value. This instability occurs because the bubble density, generated via aeration, may reach a critical point when bubbles start to coalesce and create air gaps, or voids. This effect induces instabilities and intermittent fluctuations in the spray. A higher injection pressure allows a higher gas-liquid mass ratio before the onset of this instability. Further increases in gas-liquid ratio result in the formation of a gas core surrounded by a thin liquid film flowing along the inside wall of the atomizer tube. Roesler found this annular flow regime to be stable with no fluctuations in the spray. He concluded that increases in pressure and gas-liquid ratio decrease the mean drop size. Figure 2.14 illustrates the SMD's independence of the discharge orifice diameter. The distribution parameter q was in the range of 1.7 as compared with typical atomizers which vary between 1.5 and 2.5. This finding suggests a broader drop-size distribution for this particular effervescent atomizer.

Because plain-orifice atomizers produce spray angles that are too narrow for most combustor applications (<20°), Whitlow (1990) investigated the spray performance of single-hole and four-hole orifice effervescent atomizers spraying into air at atmospheric pressure (fig. 2.15). Water injection pressures ranged from 69 to 689 kPa and air-liquid ratios from 0 to 0.06 for the single-hole atomizer. This study included investigations in the transitional and annular flow regions. Results similar to Roesler's were obtained for the stable, bubbly flow region. Drop sizes as low as 10 μm SMD were obtained in the annular flow regime at a 689-kPa injection pressure. This was attributed to the high-velocity aerated air imparting kinetic energy to the fluid. This annular flow regime is analogous to what is seen in an air-assist atomizer rather than in an effervescent atomizer. Similar results were obtained for the four-hole atomizer. Effective spray angles achieved for the single orifice in the bubbly and annular flow regimes were 23° and 16°, respectively, at a 689-kPa injection pressure.

Whitlow (1990) also investigated conical-sheet atomizers at operating pressures between 69 and 552 kPa and at gas-liquid ratios between 0 and 0.12 using pintle gap widths between 0.1 and 0.37 mm (fig. 2.16). Unlike the plain-orifice effervescent atomizer, the conical-sheet effervescent atomizer exhibited no instability regions across a wide spectrum of injection pressures, gas-liquid ratios, and gap widths. Whitlow attributed this stable behavior to the annular passage and the exit throat "dampening out" adverse effects by providing an area around the annulus for the large air voids to spread out and break up. As with plain-orifice effervescent atomizers, increases in pressure and gas-liquid ratio decreased the SMD (fig. 2.17). In this figure, position B is located 90° around the spray axis from position A. The SMD was relatively independent of the discharge gap width, especially at high injection pressures.

Lefebvre, Chin, and Rollbuhler (1991, Purdue University, Indiana, NASA Lewis Research Center, Cleveland, unpublished report) utilized a conical-sheet effervescent atomizer (fig. 2.18) in an actual combustor to evaluate combustion efficiencies over wide ranges of pressure and inlet temperature. The atomizer was fitted to an T–56 combustor. Combustion pressures ranged from 0.101 to 0.760 MPa; air inlet temperatures ranged from 270 to 530 K; and the nominal atomizing air-fuel ratio was 0.2 by mass. The combustion efficiency was measured using 21 Chromel-Alumel thermocouples arranged in a cruciform pattern at the combustor exit. This efficiency was compared with that of the T-56 combustor fitted with a standard dual-orifice atomizer. Figure 2.19 shows the improvement in efficiency from using the effervescent atomizer. Over the entire range of pressures and inlet temperatures, the combustion efficiency was higher, presumably because of better fuel atomization.

A review of the literature on NO_x formation is crucial to the development of a low-NO_x, liquid-fueled combustor. Therefore, with respect to their effect on NO_x emissions, the relevance of the fuel-air ratio, fuel-air uniformity, and fuel vaporization was apparent. Further, understanding these key parameters revealed the potential application of jet-shear-layer mixing, fuel-air premixing, and effervescent atomization to low-NO_x combustor development.

Chapter 3

Test Facility Flow Systems

An effective evaluation of a low-NO_x combustor requires extensive flow systems. The test facility used, the Thermal Sciences and Propulsion Center (TSPC), is located at Purdue University. In this chapter, an overview of the air, fuel, ignition, water, and gas analysis systems used in this research is presented. Rink (1987) gives a more detailed description of these systems.

3.1 High-Pressure Air System

The high-pressure air system, shown schematically in figures 3.1 and 3.2, is divided into the main air system, which supplies air for combustion, and the effervescent air system, which supplies air for fuel atomization. High-pressure air is stored in four 56.7-m^3 aboveground storage tanks that are periodically pressurized up to 15.2 MPa using a piston-type compressor. The pressurized tanks are blown down during testing. All air is dried and filtered at 440 μm.

3.1.1 Main Air System

The main air system is shown in figure 3.1. The test rig is designed for pressures up to 2.41 MPa with maximum flow rates up to 1.5 kg/s. The desired rig pressure is achieved via a dome-loading pressure regulator. The rig is protected from overpressure by a burst disk (rated at 4.94 MPa) and a relief valve (set at 4.14 MPa) downstream from the pneumatic pressure regulator. The flow is measured with a 34.9-mm-diameter ASME standard orifice plate housed in a 102-mm-diameter pipe. Measurements from a differential pressure transducer and an upstream Chromel-Alumel thermocouple are used to calculate flow rates. An electropneumatic plug valve regulates the desired flow rate.

For heated air, a nonvitiating natural-gas-fueled heater is used (fig. 3.1). The heater is rated for pressures up to 2.03 MPa and is protected by an upstream burst disk (set at 2.41 MPa). Three natural gas burners are used to heat a 76.2-mm-diameter coiled pipe inside the heater. Test section inlet temperatures as high as 623 K can be safely attained. The heater system is protected from overtemperature via shutdowns commanded by thermocouples mounted on the coiled pipe (set at 1000 K) and near the chimney of the heater (set at 1400 K) to monitor preheater exhaust temperatures.

3.1.2 Effervescent Air System

High-pressure air is also required for the effervescent fuel atomizer (fig. 3.2). The atomizer air line is capable of supplying air at a rate of 100 g/s at 10.3 MPa, and it is protected by a relief valve set at 2.75 MPa. The pressure and flow rate are regulated by a dome-loaded pressure regulator and needle valve, respectively. Flow rates are measured using an 8.9-mm-diameter ASME standard orifice housed in a 44.4-mm-diameter pipe along with a Validyne differential pressure transducer and an orifice inlet Chromel-Alumel thermocouple. The effervescent air is not preheated but is supplied at ambient temperatures.

3.2 Fuel and Ignition Systems

The fuel system, shown schematically in figure 3.3, is designed to deliver a maximum flow rate and pressure of 11.5 liters/min and 3.5 MPa, respectively. The fuel is housed in a 206-liter drum. The fuel system has a recirculation line to preset the fuel flow prior to ignition and a nitrogen purge system to safely eject the fuel from the fuel lines after a test run. A 1.5-kW electric motor runs a gear pump to supply fuel to the effervescent atomizer. A turbine flowmeter monitors the fuel flow rate; two parallel needle valves regulate coarse and fine fuel flow; and a rheostat regulates the motor speed to give the desired fuel pressure. The fuel system is protected by a 3.8-MPa relief valve downstream from the pump.

The ignition system is shown in figure 3.4. Ignition is accomplished by using a 10 000-V electrically sparked, propane-oxygen jet. The spark is initiated by a contact switch in the control room. The switch energizes the ignitor transformer and opens the shutoff valves in the propane and oxygen lines that feed the ignitor. Upon release of this contact switch, the ignitor is deactivated and the shutoff valves close. Propane and oxygen are supplied from two pressurized cylinders. The propane and oxygen are regulated down to 186 and 310 kPa, respectively, for optimum ignitor performance.

3.3 Water System

A schematic diagram of the water cooling system is shown in figure 3.5. High-pressure water is used to cool the gas sampling probe and low-pressure water is used to cool the ignitor housing. Water for the system is supplied from a 516-kPa city water supply. Higher pressures are achieved using a 22.4-kW electric motor to drive a centrifugal pump, which is capable of supplying water at a flow rate of 132 liters/min at pressures up to 2.86 MPa. The water pressure is regulated via a hand valve in the water recirculation loop. The pump and 80 PVC piping are protected from overpressure by a 2.75-MPa relief valve in the recirculation loop. Water pressure at the gas sampling probe is set to 1.72 MPa. City water is fed directly to the ignitor housing and regulated by a hand valve. All effluent water is discharged, untreated, into the cell drainage system.

3.4 Gas Analysis System

The gas analysis system is schematically shown in figure 3.6. The design is based on SAE Aerospace Recommended Practice (Society of Automotive Engineering, 1980) to correctly represent the combustor emissions.

A single-port, water-cooled traversing probe (fig. 3.7) was used to sample emissions on one radial axis of the combustor exit. The probe has a 12.7-mm-diameter stainless steel housing which contains a concentric 4.76-mm-diameter Inconel gas sampling collection tube that protrudes from the probe housing tip. The collection tube has a 3.18-mm-diameter hole, 12.7 mm from its tip, through which combustion gases flow. The probe tip is thermally coated with zirconium oxide to better withstand high-temperature environments. Pressurized city water flows through the annular gap inside the housing for cooling purposes. The probe feeds through a 152.4-mm stainless steel flange via a 12.7-mm Conax fitting. An actuator and controller are used to traverse the probe 102 mm downstream from the combustor exit.

Nonisokinetic gas sampling was employed in this test program. Isokinetic sampling occurs when the velocity inside the probe is equal to the velocity of the free stream. If the free-stream velocity decelerates inside the sampling port, a greater portion of higher density gas will reach the gas analyzers; the opposite trend occurs if the flow accelerates. Generally, isokinetic sampling is considered important when the gas

contains large particles (>10 μm in diam) such as soot and unburnt fuel droplets in a high-velocity gas flow. Isokinetic sampling becomes less important when gases such as NO_x and CO are sampled. Because NO_x and CO concentrations are of prime interest in this program and the combustor exit velocity is generally low, nonisokinetic sampling was considered acceptable.

As soon as they enter the sampling probe, the hot gases are quenched by heat transfer to the water that cools the probe housing, thus preventing further chemical reactions. Upon exiting the probe, the gas travels through a thermistor-controlled heated line that is maintained at 505 K. The gas is then fed to its respective analyzers. According to the SAE Aerospace Recommended Practice, the sampling flow rate and line length must be such that the measured or calculated sample transport time from the probe to the analyzers is less than 10 sec. Some of the sample gases are dumped to the atmosphere through two bypass lines in order to reduce the travel time to under 2 sec from the combustor exit to the analyzers. This reduced travel time allows the analyzers to respond and stabilize quickly to operational changes in the combustor and minimizes chemical recombinations in the sampling line.

A Thermo Electron Model 10A chemiluminescent analyzer is used to measure NO and NO_2. Nitric oxides (0 to 10 000 ppm) are detected by light emitted when the NO molecules in the sampling gas react with the ozone molecules generated in the instrument. The reaction creates NO_2 and also emits light, the intensity of which is proportional to the NO concentration. To measure NO_2, the gas sample is first heated to high temperatures (923 K) to convert all the NO_2 to NO. The emission measured is NO_x. Determining NO_2 concentration is simply a matter of subtracting NO from NO_x. The NO_x analyzer is calibrated before each test run using 25- and 250-ppm NO calibration gases stored in pressurized cylinders. Nitrogen gas at 99.995 percent purity is used to zero the NO_x analyzer, which has an accuracy of 1 percent of full scale.

Carbon dioxide (0 to 20 percent) is measured with a MEXA-311GE portable nondispersive infrared analyzer. The analyzer measures CO_2 by making a differential measurement of the absorption of infrared energy. The percentage of radiation absorbed is proportional to the concentration of CO_2. The analyzer has an accuracy of 0.3 percent CO_2. For calibration purposes, 5 percent CO_2 is used with 99.995 percent N_2 gas to zero the analyzer.

A portable MEXA-224GE nondispersive infrared analyzer is used to measure unburnt hydrocarbons (0 to 10 000 ppm). For calibration and zeroing, 0.5 percent propane and 99.995 percent N_2 gases are used, respectively. The analyzer has an accuracy of 10 ppm.

Carbon monoxide (0 to 5 percent) is measured on a Beckman 864 infrared analyzer. For calibration and zeroing, 0.3 percent CO and 99.995 percent N_2 gases are used, respectively. The analyzer has an accuracy of 0.02 percent.

Chapter 4

Test Section Hardware

Various approaches to reducing NO_x were studied in some detail. Based on these reviews, a T-56 combustor was modified to incorporate some key features of different experimental low-NO_x combustors. These key features include jet-shear-layer mixing in the primary zone, studied by Abdul-Aziz et al. (1987), Abdul-Hussain et al. (1988), Al-Dabbagh and Andrews (1981), and Andrews, Abdul-Aziz, and Al-Dabbagh (1983); a premixed region upstream from the primary zone, studied by Anderson (1973 and 1975) and Roffe and Ferri (1975 and 1976); and an effervescent atomizer, studied by Lefebvre (1983), Lefebvre, Chin, and Rollbuhler (1991, Purdue University, Indiana, NASA Lewis Ressearch Center, Cleveland, unpublished report), Roesler (1988), and Whitlow (1990).

4.1 Test Section Configuration

The experimental combustor is configured in the test facility as shown in figures 4.1 and 4.2. The 0.635-m-long test section that houses the combustor tapers in diameter from 0.191 to 0.140 m. Flow straighteners are located upstream from the test section to smooth the airflow. Because, for turbulent flow, fully developed profiles are achieved at pipe length-to-diameter ratios of around 40, a bundle of pipe segments 0.459 m long and 10 mm in diameter are inserted in a 76-mm-diameter line that feeds air to the test section. Downstream from the flow straighteners are two concentric diffusers used to expand the air to the 191-mm-diameter test section inlet.

The inlet temperature and pressure are monitored by a Chromel-Alumel thermocouple and a pressure tap located in the test section housing. A traversing gas sampling probe, located directly downstream from the test section housing, is used to collect gaseous emissions. The combustor exit temperatures are monitored by replacing the gas sampling probe with 21 Chromel-Alumel thermocouples arranged in a cruciform pattern. The combustion exhaust gases exit the test section into a fixed-geometry converging nozzle which governs back pressure at a given flow condition. The exhaust gases are then expelled to the atmosphere.

4.2 T-56 Combustor Modifications

The modified T-56 combustors are shown in figures 4.3 to 4.6. Each combustor has a diameter of 0.138 m and an overall length of 0.432 m. The combustor liner length is 0.369 m. The front dome sections of the T-56 combustors were removed and replaced by dome plates incorporating axial slots and a premixing duct from which radial jets eject a fuel and air mixture. All the fuel and some of the air are premixed upstream from the primary combustion zone. Fuel is injected into the 38.1-mm-diameter premixing duct by an effervescent atomizer which can be moved axially to adjust the premixing length. The premixing duct is 0.102 m long.

During the initial testing period, the central hub of the premixing duct that protrudes into the primary combustion zone partially ablated away. This was attributed to the central hub acting as a flameholder. To eliminate this problem, 36 2.54-mm-diameter holes were drilled 10° apart around the

outer perimeter of the hub (fig. 4.3). These holes provide direct convective cooling to the hub. The combustor configurations tested are described in the following sections.

4.2.1 Four-Slotted Combustor Configurations

A baseline combustor (JSL4A) was fabricated and tested (figs. 4.3 and 4.4). It was used primarily to calibrate the NO_x model and to confirm its low-NO_x potential. The dome plate consists of 1.59-mm-thick Hastalloy-X. The premixing duct is a 38.1-mm-diameter Hastalloy-X tube. The combustor includes four axial slots in line with four radial slots. The axial slots have an aspect ratio AR of 2.49. The aspect ratio is calculated as follows:

$$AR = \text{Slot arc length/Slot width}$$

The arc length is calculated from the slot circumferential centerline at an r/R of 0.72 where r is the radial direction and R is the inside radius of the combustor. The radial jet inlets are 14.7 mm in diameter. The airflow splits for the JSL4A combustor configurations are given in table 4.1. Airflow splits were determined by measuring pressure drops across the combustor at various cold flow rates. Specific slots were blocked and pressure drops and flow rates were measured to determine the fraction of air going to each slot in the combustor. The JSL4A combustor used 50 percent of the total air in combustion. Additional cooling air slots on the JSL4A liner were later blocked to allow more air to participate in combustion while at the same time reduce liner cooling air. The JSL4B and C combustor configurations, having the same JSL4A dome section and liner, used 60 and 75 percent of the total air in combustion, respectively. The airflow splits for the JSL4B and C combustors are shown in table 4.1.

TABLE 4.1.–AIRFLOW SPLITS FOR JSL COMBUSTORS

Air slots	Combustor					
	JSL4A	JSL4B	JSL4C	JSL4D	JSL4E	JSL6
	Airflow splits, percentage of total airflow[a]					
Liner cooling	50	40	25	25	25	25
Axial combustion	32	39	48	48	47	48
Radial combustion	14	16	20	20	22	20
Hub cooling	4	5	7	7	6	7

[a]Nominal combustor airflow rate, 0.70 kg/s.

4.2.2 Optimized Four-Slotted Combustor Configurations

Based on CFD results, two jet-shear-layer combustor configurations, JSL4D (figs. 4.3 and 4.5) and E, were fabricated and tested. The dome plate consists of a 4.75-mm-thick Haynes 231 material. The premixing duct is a 38.1-mm-diameter Haynes 231 tube. The inside of the combustor is coated with zirconium oxide for additional thermal protection. The combustor includes four axial slots in line with four radial slots. The axial slots have an aspect ratio of 1.00. The radial position of the axial slots is located at an r/R of 0.72. Cooling slots are blocked to permit 75 percent of the total air to participate in combustion. JSL4D has a radial jet inlet diameter of 14.7 mm. JSL4E has a radial jet inlet diameter of 17.5 mm. Apart from the radial jet inlet diameters, all other combustor dimensions remain the same for both JSL4D and E. The airflow splits for the JSL4D and E combustors are shown in table 4.1.

4.2.3 Six-Slotted Combustor Configuration

A six-slotted combustor, JSL6 (figs. 4.3 and 4.6), was fabricated and tested. The dome plate is made from 4.75-mm-thick Haynes 231 material. The premixing duct is a 38.1-mm-diameter Haynes 231 tube. The inside of the combustor is coated with zirconium oxide for additional thermal protection. The JSL6 combustor has six axial slots in line with six radial slots. The axial slots have an aspect ratio of 1.00. The radial position of the axial slots is located at an r/R of 0.72. Cooling slots are blocked to permit 75 percent of the total air to participate in combustion. The radial jet inlets have a diameter of 12.3 mm. The airflow splits for the JSL6 are shown in table 4.1.

4.3 Effervescent Atomizer

The effervescent atomizer used in this research program is shown in figures 4.3 and 2.18. Its geometry and flow characteristics are based on work done by Whitlow (1990); it was tested in an actual combustor by Lefebvre, Chin, and Rollbuhler (1991, Purdue University, Indiana, NASA Lewis Research Center, Cleveland, unpublished report). The atomizer consists of two concentric tubes, 25.4 and 12.7 mm in diameter. The inner tube supplies effervescent air to the annular gap region where fuel is flowing. Thirteen sets of 0.79-mm-diameter holes, spaced 3.18 mm apart in the inner tube, are used to inject air bubbles into the fuel. The pintle gap width is 0.51 mm and produces a spray having an included angle of 90°.

Chapter 5

Computational Analysis

The goal of the combustor modeling is to utilize a three-dimensional numerical program to investigate reacting flows generated by a fuel-rich radial jet intercepting an axial air jet. Parametric variations of key combustor parameters were carried out to evaluate NO_x concentrations exiting the combustor. The program modeled the primary combustion zone and incorporated the effects of liner cooling air. The model was calibrated and verified using gas emissions and temperature data obtained from the preliminary testing of a JSL combustor.

5.1 Modeling Code

REFLEQS (REactive FLow EQuation Solver) is an advanced CFD package specifically designed for turbulent flow and heat transfer problems with and without chemical reactions (CFD Research Corporation, 1990). REFLEQS solves the full two- and three-dimensional Navier-Stokes equations for fluid flow in a generalized coordinate system. For reactive flows, additional energy and species concentration equations are solved.

REFLEQS is a well-documented program and has been validated by many users. Over 30 validation cases have been performed and good-to-excellent agreement between benchmark data and prediction has been shown (Ratcliff and Smith, 1989 and Smith et al., 1989). Talpallikar et al. (1991) have used REFLEQS with excellent results to predict NO_x in the RQL combustor. The general capabilities of REFLEQS are as follows:

(1) Cartesian, polar, and boundary-fitted coordinates
(2) Automated geometry specification and grid distribution
(3) Porosity-resistivity technique for flows with internal objects
(4) Arbitrary placement of boundary conditions
(5) Compressible and incompressible flow
(6) Steady-state and transient calculations
(7) Standard JANNAF thermodynamic properties and stoichiometric relations
(8) Standard and extended k-ϵ turbulence models and the two-scale turbulence model of Chen
(9) Single-, two-, and four-step hydrocarbon combustion models
(10) Eulerian-Lagrangian technique for dispersed two-phase flow analysis
(11) Fully implicit and conservative formulation
(12) Symmetric whole field solver
(13) Pressure-based solution algorithms
(14) Upwind, hybrid, and central differencing schemes

5.2 Computational Grid

The combustors tested in this research program have a number of axial and radial in-line jets. To preserve combustor symmetry, the geometry of the computational grid volume consists of only one axial and one radial jet in a pie section of the combustor (fig. 5.1). The pie section has a 120°, 90°, or 60°

angle for a three-, four-, or six-jet configuration, respectively. Polar coordinates, the x-, r- and θ-directions, are used. The radial direction extends from the combustor centerline to its wall; the axial direction extends from the axial air slot to the exit of the combustor. A baseline grid of 11 550 cells ($35\times22\times15$ in the x-, r-, and θ-directions) was selected for modeling the combustor. The axial grid spacing is dense near the jet interception region and becomes coarser farther downstream to ensure adequate representation of all key flow features.

5.3 Boundary Conditions

Boundary conditions (table 5.1) selected for REFLEQS are based on reviews of previous combustor modeling and testing and on data obtained from preliminary JSL combustor testing.

TABLE 5.1.-BOUNDARY CONDITIONS

Property	Location							
	Inlets				Walls		Center-line	Exit boundary
	Axial jet	Liner cooling air	Hub cooling air	Radial jet	Liner	Traverse		
Jet velocity, m/s Axial, U Radial, V Traverse, W	 (a) 0 0	 (a) 0 0	 (a) 0 0	 0 (a) 0	 0 0 0	Planes of symmetry		Zero-gradient boundary conditions
Turbulent kinetic energy, k, m^2/s^2	$k = 1.5\ (p\times \text{jet velocity})^2$				(b)			
	p = 15%	p = 15%	p = 15%	p = 30%				
Turbulent intensity dissipation rate, ϵ,1/s	$\epsilon = 0.09\ k^{1.5/\ell}$							
	$\ell/d = 0.13$	$\ell/d = 0.13$	$\ell/d = 0.13$	$\ell/d = 0.13$				
Temperature, T, K	551	551	551	551	(c)			
Pressure, P, MPa	0.48	0.48	0.48	0.48	(d)			
Oxygen, O_2, percent	23.2	23.2	23.2	(e)	0			
Nitrogen, N_2, percent	76.8	76.8	76.8	(e)	0			
Propane, C_3H_8, percent	0	0	0	(e)	0			

[a]Specified (see table 4.1) and uniform.
[b]Specified by wall function.
[c]Specified (see table 5.2).
[d]Calculated from flow field.
[e]Composition specified by fuel-air ratio.

5.3.1 Inflow Boundary Conditions

Velocities for the radial, axial, hub cooling, and liner cooling jets are based on the flow distribution measured in the combustor (table 4.1). Velocities were calculated using the mass flow rate equation

$$U = \frac{\omega}{\rho A_{jet}}$$

where U is the axial jet velocity and ω, ρ, and A_{jet} are the mass flow rate, gas density, and jet cross-sectional area, respectively. The jets are assumed to have a uniform velocity distribution both radially and circumferentially. This assumption was used successfully by other researchers (Talpallikar et al., 1991) who showed that velocity distributions within the jets do not affect the flow field sufficiently to warrant a more complicated boundary condition.

5.3.2 Jet Turbulence

No measurement of turbulence intensity or dissipation in the combustor was possible in the present test facility. Instead, turbulence levels are based on the results obtained by other researchers for turbulent jets. Both inlet turbulent kinetic energies and turbulent dissipation rates are needed for the standard k-ε turbulence model in REFLEQS. The turbulent kinetic energy is defined as

$$k = \frac{3}{2}(pU)^2$$

where p is the turbulence intensity. The turbulent energy dissipation rate is defined as

$$\varepsilon = C_\mu \frac{k^{1.5}}{\ell}$$

where C_μ is a constant commonly taken as 0.09 for turbulent flows, and ℓ is the turbulent length scale.

The inlet turbulence intensities of the axial, hub, and cooling air are all estimated to be 15 percent based on turbulence measurements of other researchers (Marek and Tacina, 1975) who used similar airflow test facilities. Because the fuel sprayed into the premixing duct creates additional disturbances in the incoming premixing air, the turbulence intensity of the radial jets is assumed to be greater than that of the other jets. A turbulence intensity of 30 percent is assumed for the radial jets.

The length scales are based on values obtained by other researchers (Talpallikar et al., 1991 and Krishnamurthy et al., 1984). For orifice-type jets, an ℓ/d of 0.13 is typically used. The variable d is the hydraulic diameter of either the axial, radial, hub, or cooling jets. These choices of turbulence intensity and dissipation rates proved satisfactory because combustor exit temperature profiles generated by REFLEQS agreed well with those obtained from preliminary combustor testing. Also, in the CFD code the variation of the inlet turbulence intensity of between 10 to 50 percent for the radial jet and 10 to 30 percent for the remaining jets showed too small an effect on the flow field to warrant more accurate values for turbulence intensity.

5.3.3 Jet Composition

The axial, hub, and liner cooling jets are dry air (23.2 percent O_2 and 76.8 percent N_2). The radial jets are a fuel-rich mixture of air and fuel. It is assumed that the fuel ejecting from the radial holes is fully vaporized. Although liquid Jet-A fuel was used in the experimental program, the chemical complexity of

Jet-A combined with the unavailability of a fuel droplet vaporization and burning model in REFLEQS confine the present CFD work to a gaseous fuel, namely propane, C_3H_8. Because the JSL combustor configuration incorporates a premixing duct, significant vaporization of the liquid fuel droplets discharging from the fuel atomizer does occur. Experiments show that, for an effervescent atomizer operating at an air-fuel ratio of 0.20 (by mass), the SMD and the drop-size distribution parameter q are 20 μm and 1.8, respectively. This result suggests that 25, 50, and 90 percent of the liquid fuel volume are contained in drop diameters less than 20, 32, and 63 μm, respectively, according to the Roslin-Rammler distribution relations outlined by Lefebvre (1989). Chin and Lefebvre (1983) defined an effective evaporation constant as

$$\lambda_{eff} = \frac{D_0^2}{t_e}$$

where D_0 is the initial drop-size diameter in meters and t_e is the drop evaporation time in seconds. The constant λ_{eff} increases with ambient temperature, pressure, velocity, and drop size and decreases with increases in normal fuel boiling temperature. Chin and Lefebvre (1983) calculated λ_{eff} for a number of pressures, velocities, boiling temperatures, and droplet diameters. It is estimated that the evaporation constant is 0.10 mm^2/s for sprays subjected to an inlet temperature and pressure of 551 K and 0.480 MPa. Therefore, the time for the complete vaporization of fuel droplets is estimated to be

$$t_{20\ \mu m} = 4 \text{ ms}$$

$$t_{32\ \mu m} = 10 \text{ ms}$$

$$t_{63\ \mu m} = 40 \text{ ms}$$

The evaporation time shows a vaporization of about 70 percent (by volume) in a 76.2-mm premixing length.

It should be noted that, after the fuel and air mixture leave the premixing duct, any unvaporized fuel droplets must travel an additional 25.4 mm before impacting the axial air jets. Also, the surrounding air temperature outside the premixing duct will be higher than the inside premixing duct temperature, thereby accelerating the vaporization process. It is also anticipated that the larger droplets, having more momentum, will impinge on the hot backplate of the premixing duct (fig. 4.3) and vaporize to smaller droplets before exiting through the radial holes. It has been shown by Cooper (1980) that fuel droplets having diameters less than 10 to 15 μm will act in air as a "pseudovapor" and burn as a vapor. Drops as large as 85 μm could vaporize to 15 μm at the jet interception region (assuming a 101.6-mm travel: 76.2 mm axially and 25.4 mm radially towards the axial jets). For these reasons, the assumption of complete fuel vaporization is considered valid for a parametric study of the JSL combustor.

5.3.4 Combustor Liner Wall

The liner wall is defined as the region where the velocities in the x-, r-, and θ-directions are zero. No direct thermocouple temperature measurement was possible with the current test hardware configuration. However, the wall temperature was estimated from thermal indicating paint applied to the outside of the combustor liner and also from empirical relations (Nealy and Reider, 1979). Because the thermal paint indicates the highest temperature it senses, wall temperatures can only be determined at the combustor maximum operating condition during a test run. During combustor testing, the maximum fuel-air ratio was held at 0.025. Wall temperatures at other fuel-air ratios were determined using the empirical relation (Nealy and Reider, 1979) for film-cooling combustor liners

$$\frac{T_g - T_w}{T_w - T_a} = \text{Constant}$$

where T_g is the combustion gas temperature, T_w is the liner wall temperature, and T_a is the cooling air temperature. The constant varies with the amount of cooling air used. The liner temperature profiles generated from the thermal paint do not exhibit very high gradients (<100 K) in the axial and traverse directions. Therefore, an average wall temperature was selected to represent the whole combustor. Table 5.2 presents the wall temperatures used at all flow conditions.

TABLE 5.2.–COMBUSTOR LINER TEMPERATURES

Fuel-air ratio	Combustion air, percent		
	50	60	75
	Combustor liner temperature, K		
0.015	604	633	710
.020	627	670	779
.025	638	686	810

5.3.5 Exit, Traverse, and Centerline Boundary Conditions

The exit boundary condition is assumed to be a zero-gradient boundary condition. This assumption is valid for the region downstream from any significant recirculations (nonzero-velocity gradients) in the combustion zone. The traverse plane and centerline are treated as symmetry planes. Although the actual centerline is located at r = 0, because of CFD convergence problems, the centerline is located at a very small radial distance (r = 0.1 mm).

5.4 NO_x Model

The model assumes the NO_x reaction does not contribute to the overall heat release in the combustor. This assumption allows the NO_x reactions to be decoupled from the heat release reactions. NO_x is calculated as a passive scalar after the computation of the reacting flow field. The combustion process is considered mixing controlled, and heat release rates are based on a one-step instantaneous burning of propane, C_3H_8:

$$C_3H_8 + 5O_2 \rightarrow 3CO_2 + 4H_2O$$

The general NO_x rate equation used has the form (Cooper, 1980 and Talpallikar et al., 1991)

$$\frac{\partial NO_x}{\partial t} = A \exp\left(\frac{-E}{\overline{R}T}\right)(N_2)(O_2)^{1/2}$$

The rate constants are determined experimentally based on preliminary combustor testing. Table 5.3 gives the rate constants used to predict NO_x concentration for a wide range of fuel-air ratios. Because the model does not take into account combustion inefficiency and chemical dissociation, the calculated gas

temperatures will be overestimated by varying degrees at all fuel-air ratios. Therefore, it is necessary to change the rate constants at different fuel-air ratio conditions.

The boundary conditions and models used in the computational analysis will provide a qualitative assessment and optimization of a number of JSL combustor configurations. The REFLEQS code will be used as a valuable tool to guide in the development of a low-NO_x combustor.

TABLE 5.3.-NO_x REACTION RATE CONSTANTS

Fuel-air ratio	NO_x reaction rate constants	
	$A, \frac{1}{s}\sqrt{\frac{moles}{m^3}}$	$E/\overline{R}$, K
0.015	2.0×10^{4}	1.09×10^{14}
.020	6.6×10^{3}	1.09×10^{14}
.025	5.0×10^{3}	1.09×10^{14}

Chapter 6

Results

The experimental testing of the JSL combustor used a traversing gas sampling probe (located directly downstream from the test section housing) to collect emissions data. Hydrocarbons, NO, NO_x, CO, and CO_2 were measured. Also, combustor exit temperature profiles were studied by replacing the gas sampling probe with 21 Chromel-Alumel thermocouples arranged in a cruciform pattern.

The combustor pressure and temperature inlet conditions for both the experimental testing and computational analysis were 0.480 MPa and 551 K, respectively. The fuel-air ratios ranged from 0.012 to 0.025 for the rig testing and from 0.015 to 0.025 for the CFD analysis. The nominal airflow rate was 0.70 kg/s. The nominal air-fuel ratio (by mass) of the effervescent atomizer was 0.20. The premixing length was kept constant at 76.2 mm.

6.1 Gas Emissions Data

The gas sample fuel-air ratios were calculated using an equation from the SAE Aerospace Recommended Practice (Society of Automotive Engineering, 1980):

$$\mathrm{Far} = \left(\frac{M_C + \alpha M_H}{M_{air}}\right)\left\{\frac{(1+h)\left[(CO)+(CO_2)+(HC)\right] - 100H}{100 - \left(\frac{\alpha}{4}\right)\left[(CO)+(CO_2)\right] + (HC)}\right\}$$

where M_C, M_H, and M_{air} are the atomic weights of carbon (12.011), hydrogen (1.008), and dry air (28.965), respectively; the hydrogen-carbon ratio α for Jet-A fuel is 1.97; the humidity h of the inlet air is set to zero; and (CO), (CO_2), and (HC) are the percentages of CO, CO_2, and hydrocarbon mole concentrations, respectively. The mole fraction concentration of CO_2, H, in the dry air is set to 0.0032.

A correction factor was introduced for the NO_x concentration to compensate for any deviation of the combustor inlet temperature during the test run. From preliminary experimental testing, a relationship was developed to predict the emission trend with inlet temperature. The following relationship was used to correct all NO_x readings:

$$(NO_x) = A_1 \exp\left(0.0077754 \times T_3\right)$$

where A_1 is an experimentally determined constant, and T_3 is the combustor inlet air temperature in degrees Kelvin.

The combustion efficiencies were calculated using the equation (Roffe and Ferri, 1976)

$$\eta_c = 1 - \frac{0.464(CO) + 1.11(HC) + 0.148(NO_x)10^{-4}}{(CO_2) + (CO) + (HC)}$$

where (NO_x) is the parts per million of NO_x.

6.2 NO_x Model Performance

The NO_x model was calibrated against the experimental data shown in figure 6.1 over a wide range of fuel-air ratios. The model does not take into account combustion inefficiency and chemical dissociation, both of which will lower the actual adiabatic flame temperature in the combustor. Figure 6.2 presents the combustor exit temperature data obtained during the preliminary combustor testing. The CFD results overestimated the combustor outlet temperature because of the one-step instantaneous chemical kinetics model used. Therefore, for making a qualitative analysis to optimize a JSL combustor, the NO_x rate-producing constants were varied at each fuel-air ratio (table 5.2).

Figure 6.1 shows the NO_x trends matching those obtained from experiment. However, the deviation between experimental and CFD results becomes significant at low combustion airflows when the primary combustion zone temperatures are high. High temperatures correspond to high chemical dissociation. Because NO_x is an exponential function of temperature, the CFD model overpredicts NO_x concentration at high temperatures. Low combustion airflows are not of real interest in this test program. Therefore, the current model provides a suitable means of analyzing the NO_x-producing regions in the combustor.

6.3 Effect of Combustion Air Quantity on NO_x

Each of the airflows within the JSL combustor is governed by a pressure differential across the air slots. Therefore, a decrease in liner cooling air necessarily results in increases in the axial, radial, and hub cooling airflows. It is assumed that all the axial, radial, and hub cooling airflows participate in combustion, with negligible liner cooling air interaction. As combustion air is increased for a fixed fuel-air ratio, the primary combustion zone burns leaner, resulting in lower NO_x emissions.

Figures 6.3 and 6.4 show the calculated temperature profiles within the combustor in the xr- and rθ-planes at a fuel-air ratio of 0.020. Fewer hot spots exist in the combustor when more combustion air is used. These hot spots are the principal NO_x-producing regions (>1800 K) in the combustor. Figures 6.1 and 6.5 present the experimental and CFD results obtained by increasing the combustion air. The maximum amount of combustion air is limited to protect the structural integrity of the combustor liner.

Combustion efficiency suffers slightly from increasing the combustion air (fig. 6.6), which is attributed to higher amounts of unburnt hydrocarbons emanating from a cooler combustion zone.

6.4 Effect of Radial Location of Axial Slots on NO_x

It has been determined through CFD analysis that the radial location of the axial air slots has a direct effect on NO_x emissions. The axial slot position was varied from radially inward, toward the central

premixing duct, to radially outward, toward the combustor liner wall. The maximum and minimum radial positions in the CFD analysis were limited because of the axial slot thickness and the position of the hub cooling holes. Therefore, the radial position of an axial slot, having an aspect ratio of 2.49, was varied from an r/R of 0.58 to 0.88.

Figure 6.7 shows the effect of axial slot radial position on NO_x emissions for a four-slotted JSL combustor (JSL4) using 75 percent combustion air. Lower NO_x is produced with axial slots closer to the liner wall as compared with those closer to the central hub. Figures 6.3, 6.8, and 6.9 show the calculated temperature profiles within the JSL4 combustor having axial slots at various radial positions. Hot regions are evident for slots near the premixing duct. These high-temperature zones are the principal NO_x-producing regions.

A fuel-rich radial jet intercepting an axial air jet produces a nominally fuel-lean jet downstream from the interception region. However, jet expansion into the combustor volume is critical for a thorough mixing of all the fuel with the axial air. The gaps between the adjacent axial jets increase with a more outward axial slot. As this gap decreases with a more inward axial slot, the jets are confined to expand and mix in the circumferential direction. Figures 6.3, 6.8, and 6.9 clearly illustrate the confined jet expansion or mixing with an inward axial slot location. As the axial slot is moved radially outward, the axial jet is less confined and can expand freely into the combustor volume in both the circumferential and radial directions. From this analysis it was determined that an outboard axial jet promotes more improvement in the mixing process, thereby reducing NO_x emissions.

6.5 Effect of Axial Slot Aspect Ratio on NO_x

Experimental and CFD results revealed that the aspect ratio AR of the axial air slots has a direct effect on NO_x emissions. The AR was varied from 0.61 to 5.22 while the axial slot area was maintained constant. The outer radius of the axial slots was held at an r/R of 0.82.

Figure 6.10 shows the effect of the axial slot AR on NO_x emissions for a JSL4 combustor with 75 percent combustion air. The lowest NO_x is produced with an AR close to unity. Any change in AR away from unity increases NO_x. Figures 6.3, 6.11, and 6.12 show the calculated temperature profiles within the JSL combustor for AR's of 2.49, 0.62, and 5.22, respectively. Hot regions are evident when the AR is 0.62. These high-temperature zones are the principal NO_x-producing regions.

For an AR of 0.62, the hot regions are concentrated near the center of the combustor. The thin axial jet acts like a wedge for the incoming fuel-rich radial jet. This appears to prevent the radial jet from breaking up the axial jet adequately. Instead, the radial jet only partially breaks up the bottom portion of the axial jet, with high-temperature combustion occurring at the sides of the axial jet (fig. 6.11).

For an AR of 5.22, the increase in NO_x is not quite as severe as for the low-AR case. A higher AR restricts the axial jet from expanding and mixing circumferentially into the combustor volume. It appears that an AR close to unity provides optimum mixing for low-NO_x emissions.

Figures 6.13 and 6.14 show the experimental results obtained for the JSL4D and C combustors having AR's of 1.0 and 2.49, respectively. The higher AR yielded a slightly lower NO_x. However, the combustion efficiency for an AR of 1.0 is greater than that for an AR of 2.49. This suggests that an axial slot AR close to unity yields the lowest NO_x and provides better combustion efficiency as compared with that of a higher AR axial slot.

6.6 Effect of Number of Axial and Radial In-Line Jets on NO_x

Experimental and CFD analysis revealed that the number of axial and radial in-line jets has a direct effect on NO_x emissions. The axial and radial jet pairs varied from 3 to 6. In each case the axial and radial slot areas remained constant. Also, the AR of the axial slot was kept constant at 1.00.

Figure 6.15 shows the effect of the number of in-line jets on NO_x emissions. Lower NO_x was produced with fewer in-line jets. Figures 6.16 and 6.17 show the calculated temperature profiles within a three- and six-slotted JSL combustor using 75 percent combustion air. Hot zones are more prevalent in the six-slotted combustor. These high-temperature zones are the main NO_x-producing regions.

The gap between adjacent axial jets decreases with an increase in the number of in-line jets. As this gap becomes narrower, the axial jets cannot expand and mix adequately in the combustor volume. Figure 6.17 illustrates that a higher number of in-line jets creates a hotter primary combustion zone. This suggests that inadequate mixing of the fuel and axial air is taking place.

Figures 6.18 and 6.19 show the experimental results obtained from JSL combustors having four and six pairs of in-line jets, respectively. The four-slotted combustor produced lower NO_x emissions with higher combustion efficiency as compared with that produced by the six-slotted combustor. These results verify the CFD trends in varying the number of in-line jets.

6.7 Effect of Radial Inlet Hole Diameter on NO_x

Experimental and CFD results revealed that the radial jet hole diameter has a direct effect on NO_x emissions. The radial hole diameter was varied from 9.93 to 17.46 mm.

Increases in premixing air lower NO_x emissions. However, an increase in radial hole diameter does not, in all cases, decrease NO_x emissions. The flow through all the air ports in the combustor is governed by the pressure differential, hole area, and discharge coefficients. The annular gap cross-sectional area between the effervescent atomizer and the inner wall of the premixing duct is fixed (fig. 4.3). If the total radial jet hole area is greater than the total annular gap area, then the airflow through the premixing tube will be controlled by the annular gap region. As the hole diameter is continually increased, a critical radial hole diameter is reached at which further increases in hole diameter cannot increase the premixing flow rate. At this point, the flow rate is metered by the annular gap region and the radial jet velocity is reduced.

Figures 6.20 and 6.21 show the effect of radial hole diameter on NO_x. The lowest NO_x was produced with a radial hole diameter of about 15 mm and increases for smaller and larger diameter holes. Figures 6.22 and 6.23 show the calculated temperature profiles in the JSL4 combustor for radial hole diameters of 9.93 and 17.46 mm, respectively. Hot regions are evident for the small- and large-diameter cases. For small-diameter holes, hot regions are caused by low premixing air; for large-diameter holes, hot regions are caused by the low-velocity radial jets not mixing adequately with the axial jet air. Also, the large- diameter radial jet appears to spread a fuel-rich mixture in between the axial jets. This mixture does not mix with the axial air in the most effective manner.

Figures 6.20 and 6.24 show the experimental results obtained for the JSL4 combustor having an axial slot AR of unity. Experimental results verify the NO_x trends of the CFD results. The large holes produce high NO_x emissions and low combustion efficiency. From this parametric study it appears that the radial hole diameter is critical for a given premixing duct size. A radial hole area that does not exceed the annular cross-sectional area within the premixing duct should be selected.

6.8 Comparison of Low-NO_x Results

The degree of NO_x emissions improvement due to the CFD parametric analysis and optimization is shown in figure 6.25. NO_x emissions between the baseline combustor, JSL4A, and the optimized combustor, JSL4D, were decreased by a factor of 3. Also, the combustion efficiency improved slightly (fig. 6.26).

Most fundamental low-NO_x combustor tests utilize flametubes with no cooling air requirements; all the air is used for combustion purposes. The adiabatic walls of these flametubes are generally constructed of a high-temperature ceramic able to withstand temperatures over 2500 K. Because NO_x is an exponential function of the combustion air quantity (fig. 6.5), comparing the JSL combustor NO_x emissions to those of flametube combustors is not of real interest. Therefore, to gauge the NO_x emission performance of the JSL combustor, a more meaningful comparison is made (fig. 6.27) with a conventional T-56 combustor having a direct-injection, dual-orifice atomizer. Because different combustors use different fuels, an emission index (grams of NO_2/kilograms of fuel) is commonly used instead of parts per million of NO_x. Also, different combustor operating conditions make the combustor exit temperature a more useful point of comparison than the fuel-air ratio. NO_x emissions were over three times lower for the JSL4D combustor as compared with those of a conventional T-56 combustor. Small differences in combustion efficiencies were noted: for the JSL and conventional T-56 combustors, efficiencies were 98 and 99 percent, respectively.

Chapter 7

Conclusions and Recommendations

7.1 Conclusions

A liquid-fueled JSL combustor successfully demonstrated a low-NO_x potential. The incorporation of an effervescent atomizer in a premixing duct of a JSL combustor configuration produced lower NO_x emissions as compared with those produced by conventional combustors. NO_x emissions were reduced by a factor of 3 with no adverse effect on the combustion efficiency in comparison with a T-56 combustor at similar operating conditions.

The viability of using a three-dimensional CFD code to model the JSL combustor was also successfully demonstrated. The CFD code was used as a tool to facilitate a parametric analysis that led to optimum fuel-air mixing and low-NO_x production within the combustor. Key parameters found to affect NO_x emissions are the primary combustion zone fuel-air ratio, the number of in-line jets, the aspect ratio and radial location of the axial air slots, and the radial jet inlet hole diameter. The CFD analysis provided optimization of the above combustor parameters for minimum NO_x.

The experimental and CFD analysis revealed that the percentage of total air employed in combustion had the strongest effect on NO_x emissions. A high combustion air quantity leads to a cooler primary zone temperature. Optimum fuel-air mixing was demonstrated by varying a number of geometrical features of the basic JSL configuration: a low number of in-line jets and an outboard axial air slot having an aspect ratio of near unity produced the highest degree of fuel-air mixing within the combustor; an optimum radial hole diameter provided the largest amount of fuel-air premixing with the highest radial jet velocity for a given JSL geometry.

A low-NO_x, liquid-fueled JSL combustor was successfully developed by incorporating an effervescent atomizer in a fuel-air premixing duct and using a three-dimensional CFD code to optimize the fuel-air mixing in the primary combustion zone. Further combustor development promises even lower NO_x while high combustion efficiency is maintained, thus making the JSL concept highly competitive with that of other low-NO_x combustors. The simplicity and size of the JSL combustor also make it a viable alternative to the lean-premixed-prevaporized (LPP), rich burn-quick mix-lean burn (RQL), and other lean-direct-injection (LDI) combustors currently being developed.

7.2 Recommendations

Based on the investigation reported herein, the following research should continue.

The present study has demonstrated that increases in combustion air quantity have a powerful effect on reducing NO_x emissions. Although only 25 percent of the total air was used to cool and protect the liner, visual inspection showed little liner degradation. With even less liner cooling, more air could be added to the axial and radial jets, thereby providing a leaner combustion zone. Also, a greater fraction of the total air could be used in premixing. An existing T-56 combustor liner was used for this study. Alternative liner construction should be investigated for better liner integrity for the minimal amount of cooling air. In addition, flametube studies that permit operation at more severe conditions but require no liner cooling air

should be performed for direct comparions with other studies of low-NO_x flametube combustors, such as the LPP, RQL, and LDI.

An existing conical-sheet effervescent atomizer was used in this study. No attempt was made to optimize this effervescent atomizer although it restricted the amount of air flowing into the premixing duct. A smaller diameter atomizer should be designed to allow more premixing air and a resulting higher radial jet velocity. Also, continued development of effervescent atomizers should be undertaken to enhance fuel premixing and prevaporization for a particular JSL combustor configuration.

Only rectangular axial air slots were investigated in this study. Based on the experimental and CFD results, an axial slot aspect ratio of near unity produced the lowest NO_x. This suggests that round axial holes might be superior to rectangular axial slots.

CFD modeling was proven to be a valuable tool in designing and optimizing a JSL combustor. A more accurate assessment of gas temperatures in this combustor could be attained if chemical dissociation were taken into consideration. Thus, one could avoid having to vary the coefficients in the NO_x rate equations at different fuel-air ratios as is required in the present CFD analysis. Combustion with chemical dissociation can be modeled using a multistep chemical kinetics code.

Further combustor and fuel atomizer development can make possible a continued reduction in NO_x emissions. The JSL combustor has proven its potential for low-NO_x emissions and should be regarded as an environmentally safe candidate, along with the LPP, RQL, and other LDI combusotrs, for use in future aircraft engines.

References

1. Abdul-Aziz, M.M, et al.: Lean Primary Zones: Pressure Loss and Residence Time Influences on Combustion Performance and NO_x Emissions. Presented at the Tokyo International Gas Turbine Congress, Tokyo, Japan, Oct. 26-31, 1987.

2. Abdul-Hussain, U.S., et al.: Low NO_x Primary Zones Using Jet Shear Layer Combustion. ASME Paper 88-GT-308, 1988.

3. Al-Dabbagh, N.A.; and Andrews, G.E.: The Influence of Premixed Combustion Flame Stabilizer Geometry on Flame Stability and Emissions. J. Eng. Power, vol. 103, Oct. 1981, pp. 749-758.

4. Anderson, D.: Effects of Premixing on Nitric Oxide Formation. NASA TMX-68220, 1973.

5. Anderson D.: Effects of Equivalence Ratio and Dwell Time on Exhaust Emissions from an Experimental Premixing Prevaporizing Burner. NASA TMX-71592, 1975.

6. Andrews, G.E.; Abdul-Aziz, M.M.; and Al-Dabbagh, N.A.: Mixing and Fuel Atomization Effects on Premixed Combustion Performance. ASME Paper 83-GT-55, 1983.

7. Chin, J.S.; and Lefebvre, A.H.: Effective Values of Evaporation Constant for Hydrocarbon Drops. Proceedings of the Twentieth Automotive Technology Development Contrators' Coordination Meeting, SAE, Warrendale, PA, 1983, pp. 325-331.

8. Cooper, L.P.: Effects of Degree of Fuel Vaporization Upon Emissions for a Premixed Partially Vaporized Combustion System. NASA TP-1582, 1980.

9. Elbanna, H.; and Sabbagh, J.A.: Interception of Two Equal Turbulent Jets. AIAA J., vol. 23, July 1985, pp. 985-986.

10. Elbanna, H.; and Sabbagh, J.A.: Interaction of Two Nonequal Jets. AIAA J., vol. 24, Apr. 1986, pp. 686-687.

11. Environmental Impact of Stratospheric Flight. National Academy of Sciences, Washington, D.C., 1975.

12. Kemp D.D.: Global Environmental Issues–A Climatological Approach. Routledge, New York, 1990.

13. Krishnamurthy, L., et al.: Time-Averaged and Time-Dependent Computations of Isothermal Flow Fields in a Centerbody Combustor. Report AFWAL-TR-84-2081, Wright-Patterson AFB, OH, 1984.

14. Lefebvre, A.H.: Gas Turbine Combustion. Hemisphere Publishing Corp., New York, 1983.

15. Lefebvre, A.H.: A Novel Method of Atomization with Potential Gas Turbine Application. Def. Sci. J., vol. 38, no. 4, Oct. 1988, pp. 353-362.

16. Lefebvre, A.H.: Atomization and Sprays. Hemisphere Publishing Corp., New York, 1989.

17. Lyons, V.J.: Fuel/Air Nonuniformity-Effect on Nitric Oxide Emissions. AIAA J., vol. 20, no. 5, 1981, pp. 660-665.

18. Marek C.J.; and Papathekos, L.C.: Exhaust Emissions from a Premixing, Prevaporizing Flame Tube Using Liquid Jet-A Fuel. NASA TMX-3383, 1976.

19. Marek, C.J.; Papathekos, L.C.; and Verbulecz, P.W.: Preliminary Studies of Autoignition and Flashback in Premixing Flame Tube Using Jet-A Fuel at Lean Equivalence Ratios. NASA TMX-3526, 1977.

20. Marek, C.J.; and Tacina, R.R.: Effect of Free-Stream Turbulence on Film Cooling. NASA TN D-7958, 1975.

21. Miller, E.W.; and Miller, R.: Environmental Hazards: Air Pollution. Contemporary World Issues, Santa Barbara, CA, 1989.

22. Nealy, D.A.; and Reider, S.B.: Evaluation of Laminated Porous Wall Materials for Combustor Liner Cooling. ASME Paper 79-GT-100, 1979.

23. Nelson, H.F.: Nitric Oxide Formation in Combustion. AIAA J., vol. 14, Sept. 1986, pp. 1177-1182.

24. Nitrogen Oxides, National Academy of Sciences, Washington, D.C., 1977.

25. Procedure for the Continuous Sampling and Measurement of Gaseous Emissions from Aircraft Turbine Engines. SAE Aerospace Recommended Practice, ARP 1256A, Society of Automotive Engineering, 1980.

26. Ratcliff, M.L.; and Smith, C.E.: REFLEQS-2D: A Computer Program for Turbulent Flows with and without Chemical Reaction, vol. 2: Validation Manual. CFD Research Corporation, Huntsville, AL, 1989.

27. REFLEQS-3D: A Computer Program for Turbulent Flows with and without Chemical Reactions, vol. 1: User's Manual, Ver. 1.2, CFD Research Corporation, Huntsville, AL, 1990.

28. Rink, K.K.: Pollutant Formation in Heterogeneous Mixtures of Fuel Drops and Air. MS Thesis, Purdue University, West Lafayette, IN, 1987.

29. Roesler, T.C.: An Experimental Study of Aerated-Liquid Atomization. Ph.D. Thesis, Purdue University, West Lafayette, IN, 1988.

30. Roffe, G.: Effect of Inlet Temperature and Pressure on Emissions from a Premixing Gas Turbine Primary Zone Combustor (GASL-TR-227, General Applied Science Labs., Inc., NASA Contract NAS3-18563), NASA CR-2740, 1976.

31. Roffe, G.; and Ferri, A.: Prevaporization and Premixing to Obtain Low Oxides of Nitrogen in Gas Turbine Combustors. (ATL-TR-203, Advanced Technology Labs., Inc., NASA Contract NAS3-17865), NASA CR-2495, 1975.

32. Roffe, G.; and Ferri, A.: Effect of Premixing Quality on Oxides of Nitrogen in Gas Turbine Combustors. (TR-793 General Applied Science Labs., Inc., NASA Contract NAS3-18563), NASA CR-2657, 1976.

33. Smith, C.E., et al.: Validation of an Advanced Turbulent Combustion Code: REFLEQS. Presented at the 7th Space Shuttle Main Engine CFD Workshop, NASA MSFC, Huntsville, AL, 1989.

34. Talpallikar, M.V., et al.: CFD Analysis of Jet Mixing in Low NO_x Flametube Combustors. ASME Paper 91-GT-217, 1991.

35. Whitlow, J.D.: An Experimental Investigation of Internal-Mixing Twin-Fluid Atomizers. MS Thesis, Purdue University, West Lafayette, IN, 1990.

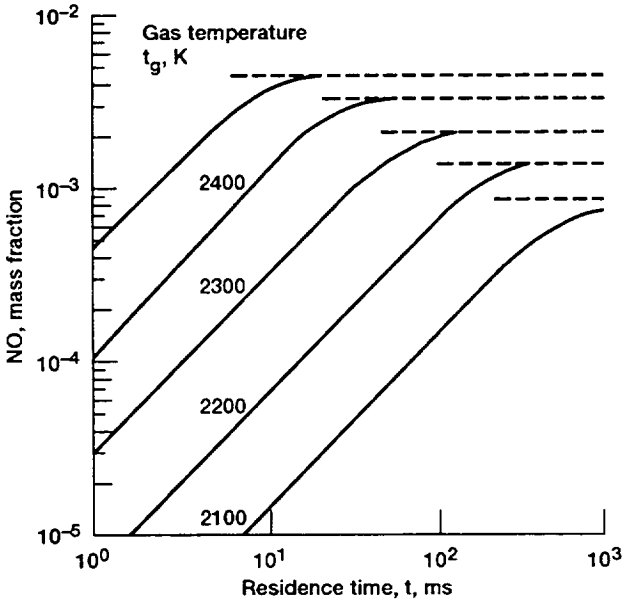

Figure 2.1.—Calculated NO mass fraction as a function of time and temperature; CH_2-air mixture; pressure, 1MPa; equivalence ratio, 1.0 (Lefebvre, 1983).

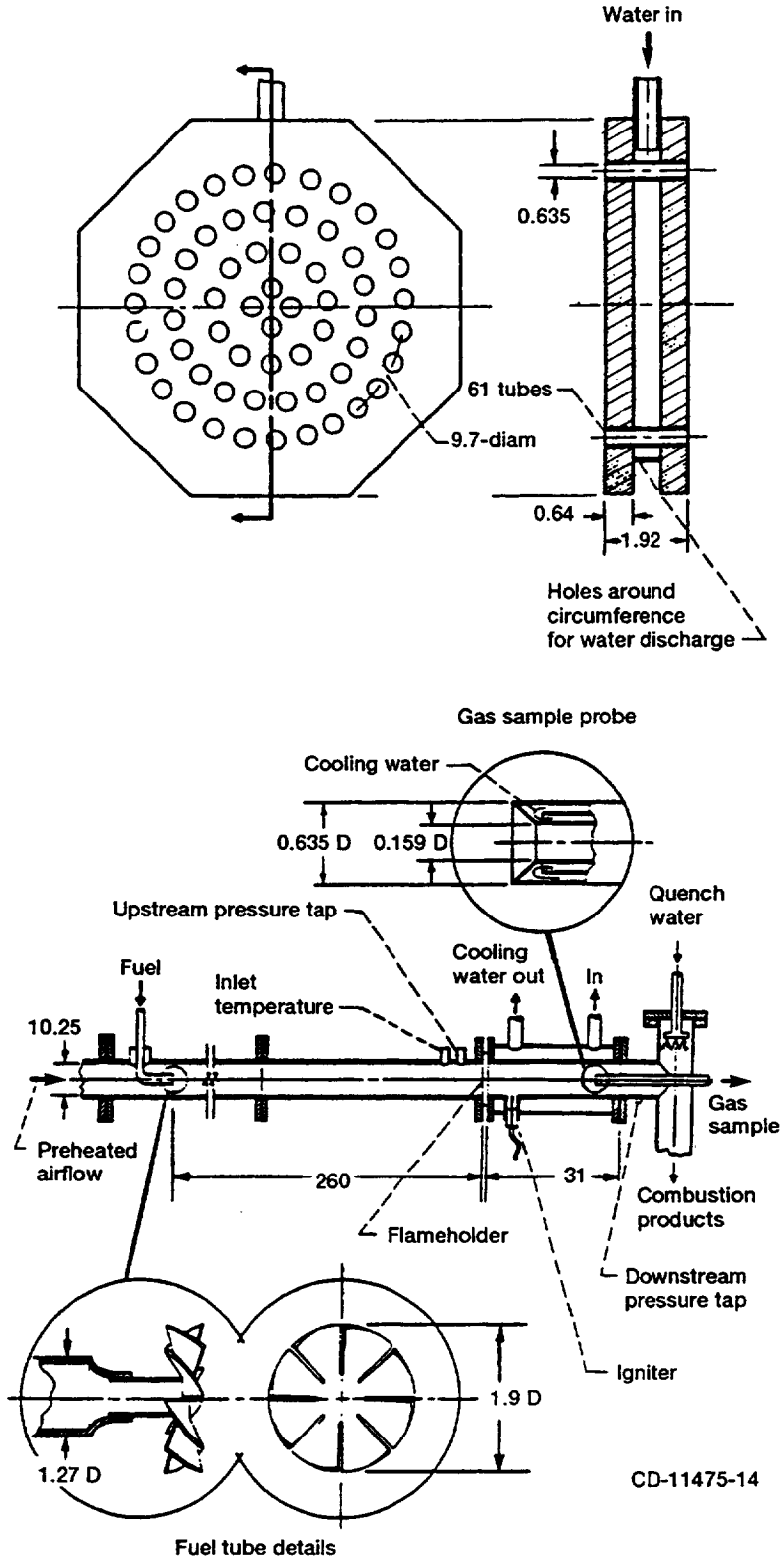

Figure 2.2.—Flameholder assembly (top) and rig (bottom). Dimensions are in cm (Anderson, 1973).

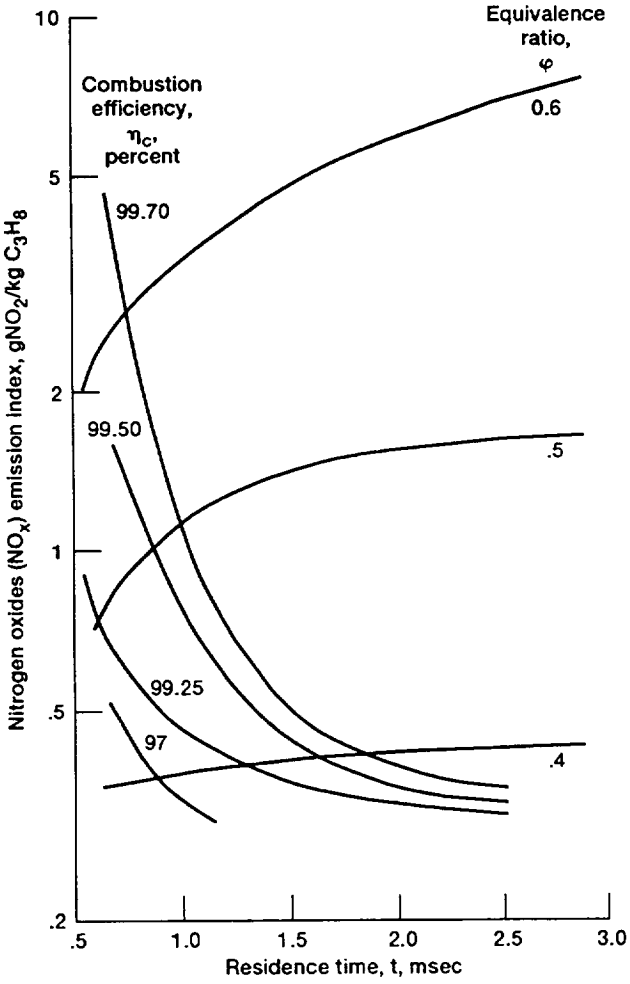

Figure 2.3.—Effect of residence time on emissions of nitrogen oxides; inlet temperature, 800 K; inlet pressure, 0.507 MPa (Anderson, 1975).

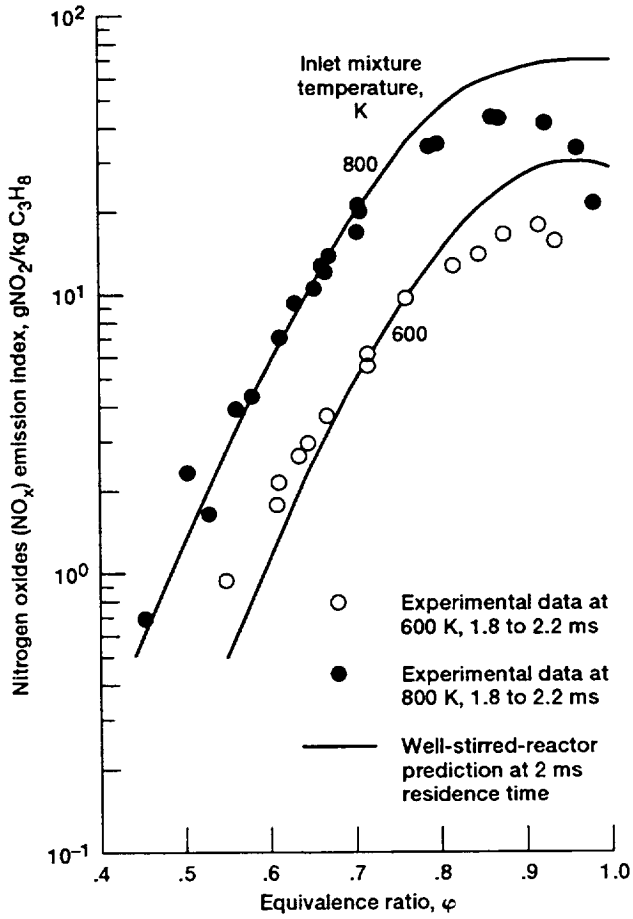

Figure 2.4.—Emissions of nitrogen oxides after 2 ms; inlet pressure, 0.507 MPa; reference velocity, 25 and 30 m/s (Anderson, 1975).

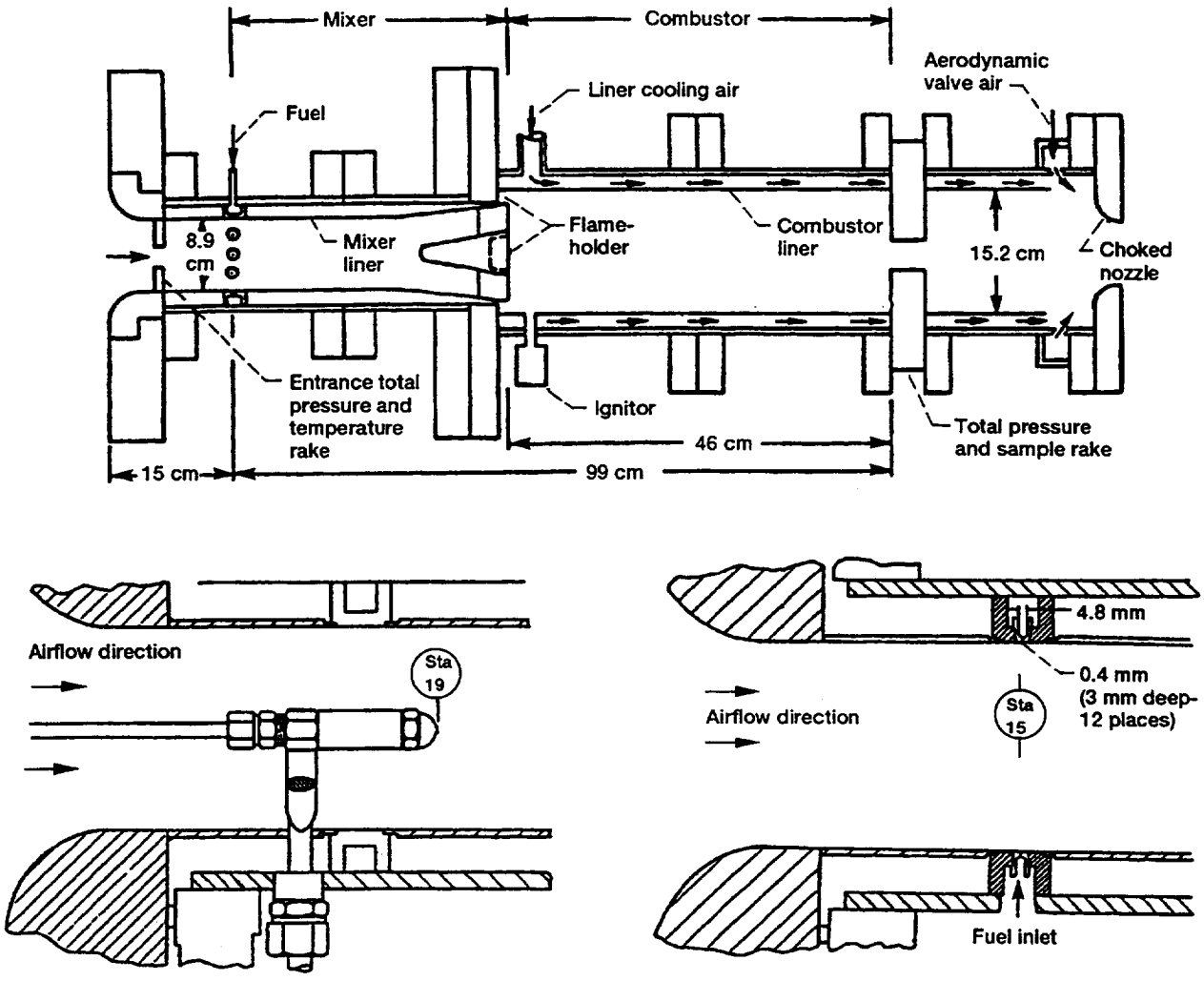

Figure 2.5.—Combustor test apparatus (top). Coaxially mounted streamwise fuel injector (bottom left). Normal fuel-injection ring nozzle (bottom right) (Roffe, 1976).

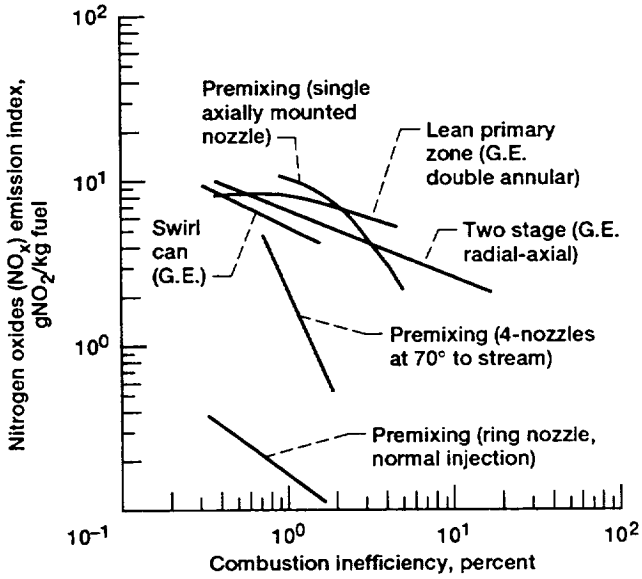

Figure 2.6.—Comparison of results for low-NO_x combustors (Roffe, 1976). Note: All data corrected to supersonic cruise condition.

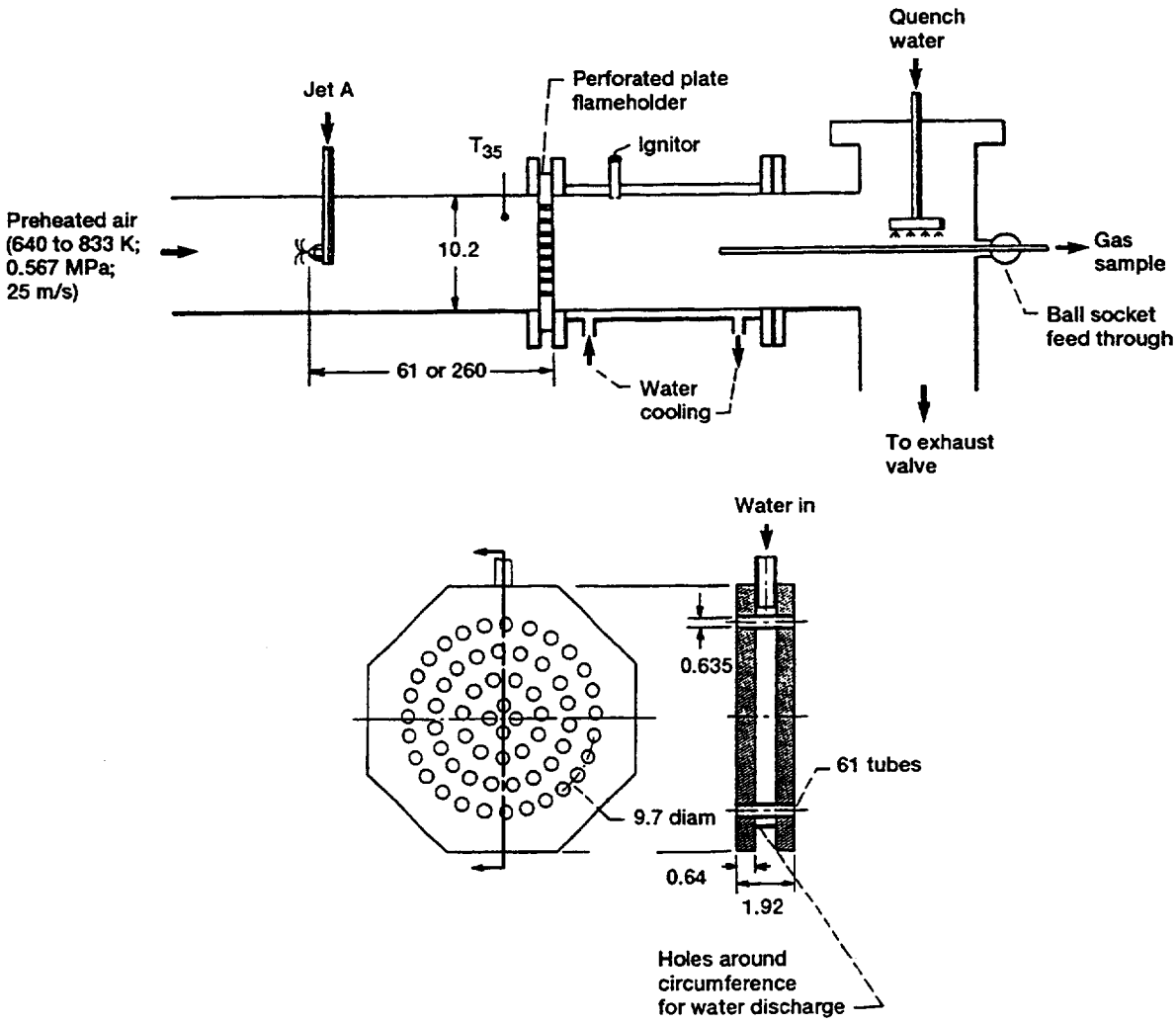

Figure 2.7.—Premixing-prevaporizing combustor (top). Flameholder with 25 percent open area (bottom). Dimensions are in cm (Marek and Papathekos, 1976).

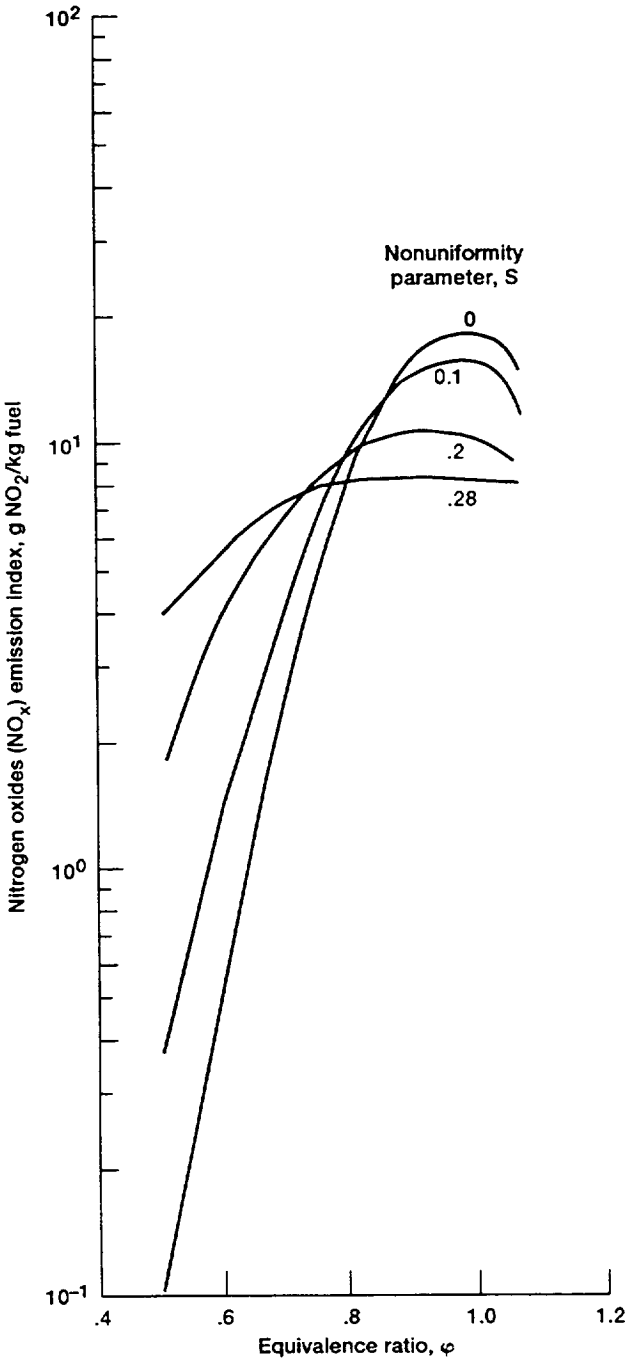

Figure 2.8.—Predictions of the effect of equivalence ratio and fuel-air nonuniformity on NO_x emissions (Lyons, 1981).

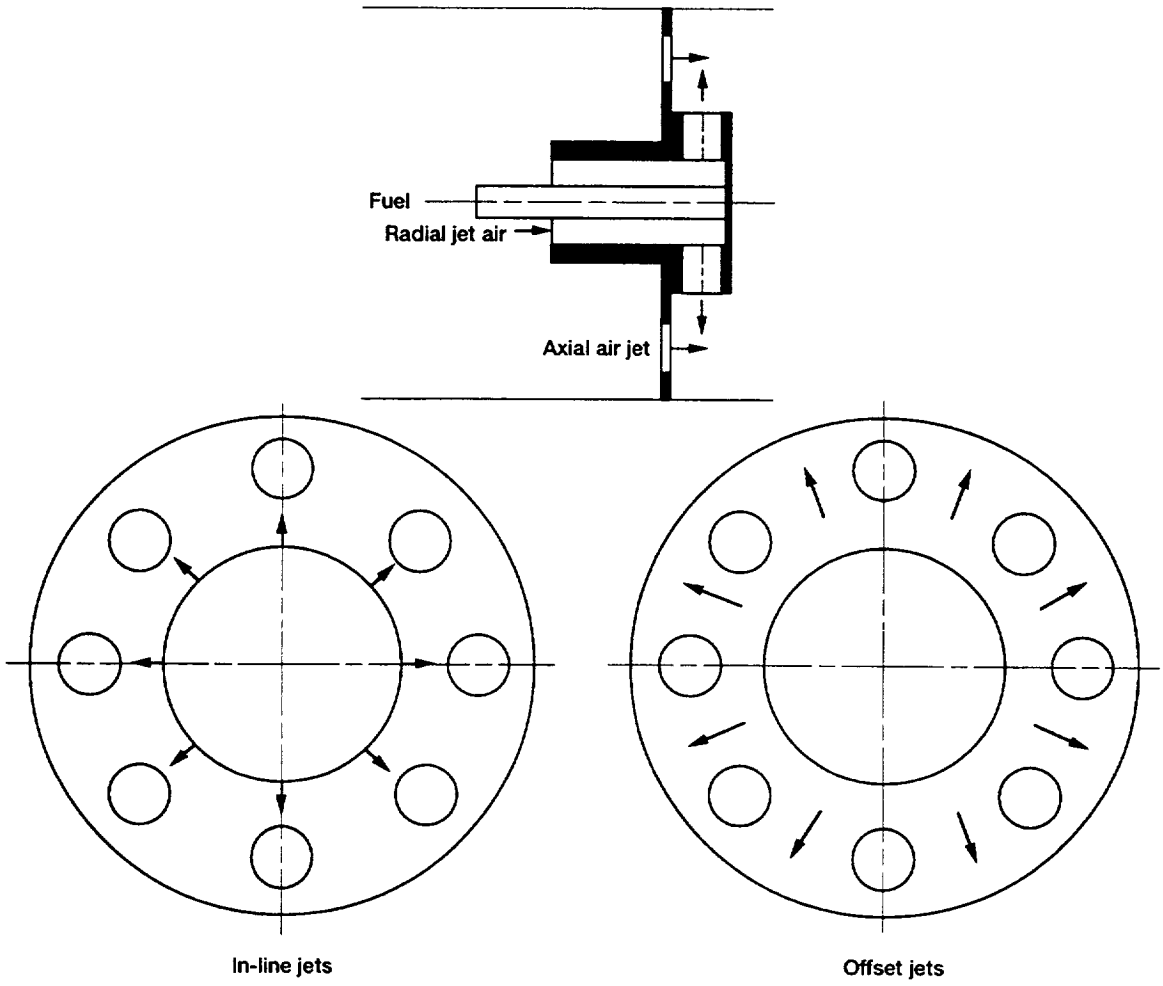

Figure 2.9.—Jet mix combustor (Abdul-Hussain et al., 1988).

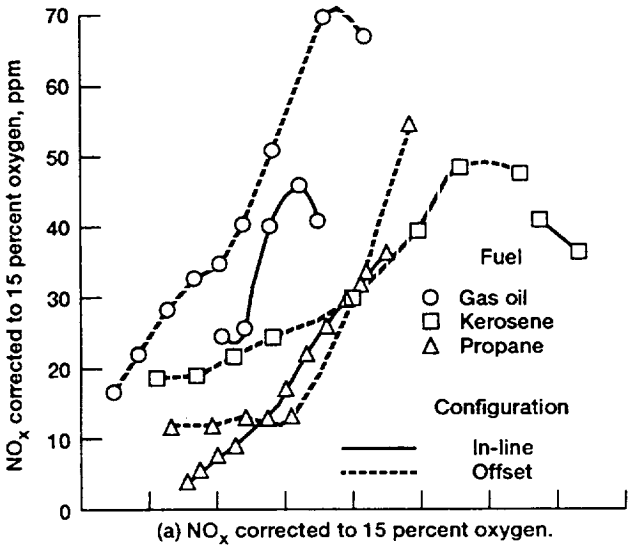

(a) NO_x corrected to 15 percent oxygen.

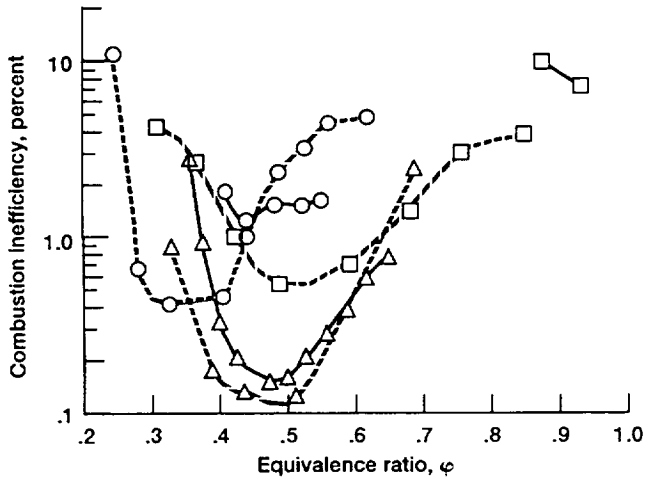

(b) Combustion inefficiency.

Figure 2.10.—Comparison of in-line and offset jet configurations; Mach number, 0.047; inlet air temperature, 600 K (Abdul-Aziz et al., 1987).

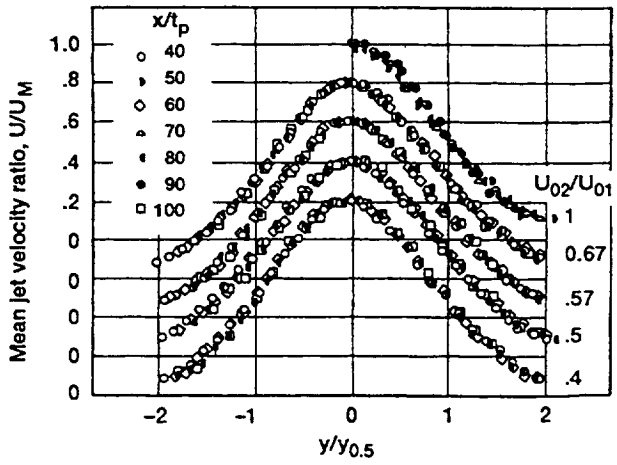

Figure 2.11.—Velocity profile for combined intercepting jets (Elbanna and Sabbagh, 1986).

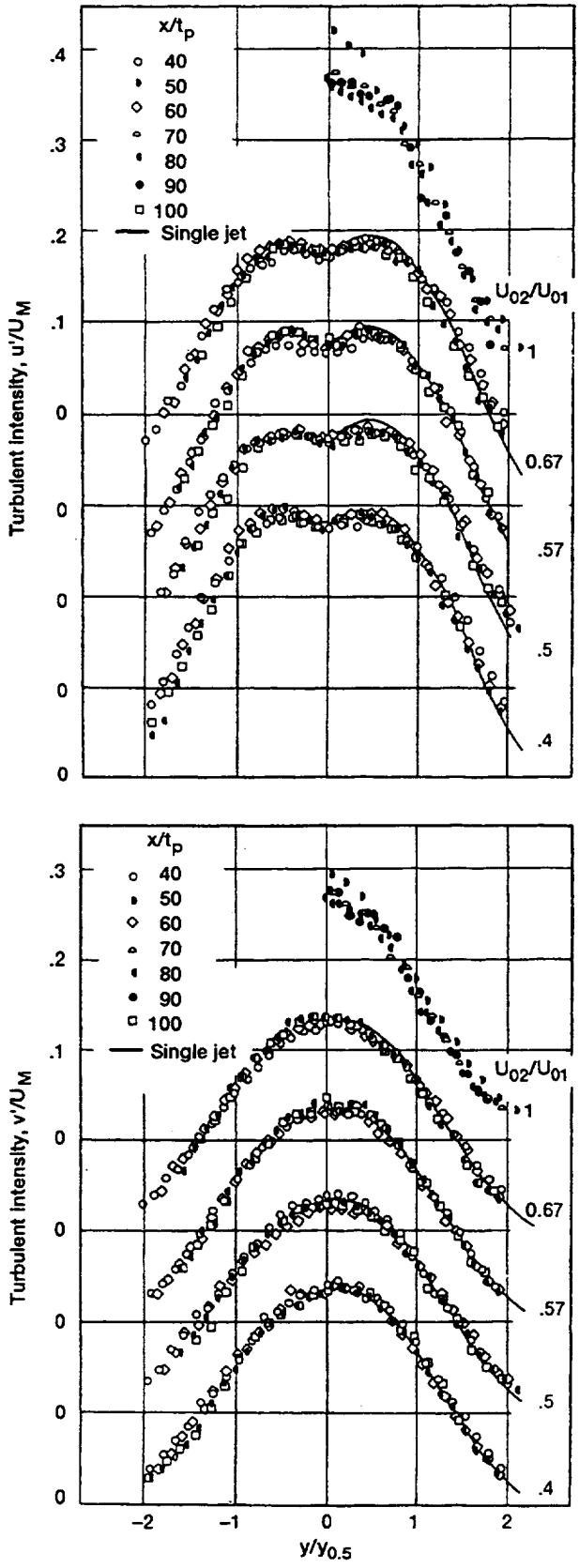

Figure 2.12.—Axial velocity (top) and lateral velocity (bottom) fluctuations for combined intercepting jets (Elbanna and Sabbagh, 1986).

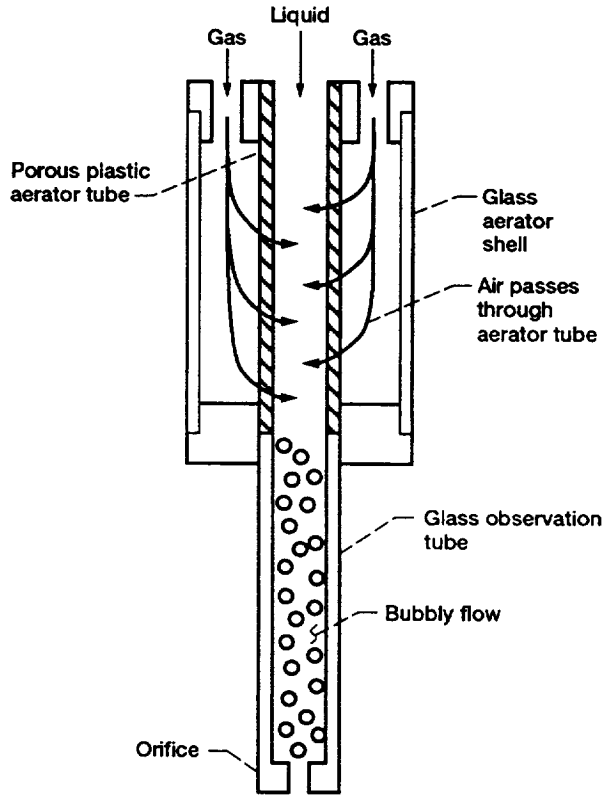

Figure 2.13.—Aerated liquid atomizer (Roesler, 1988).

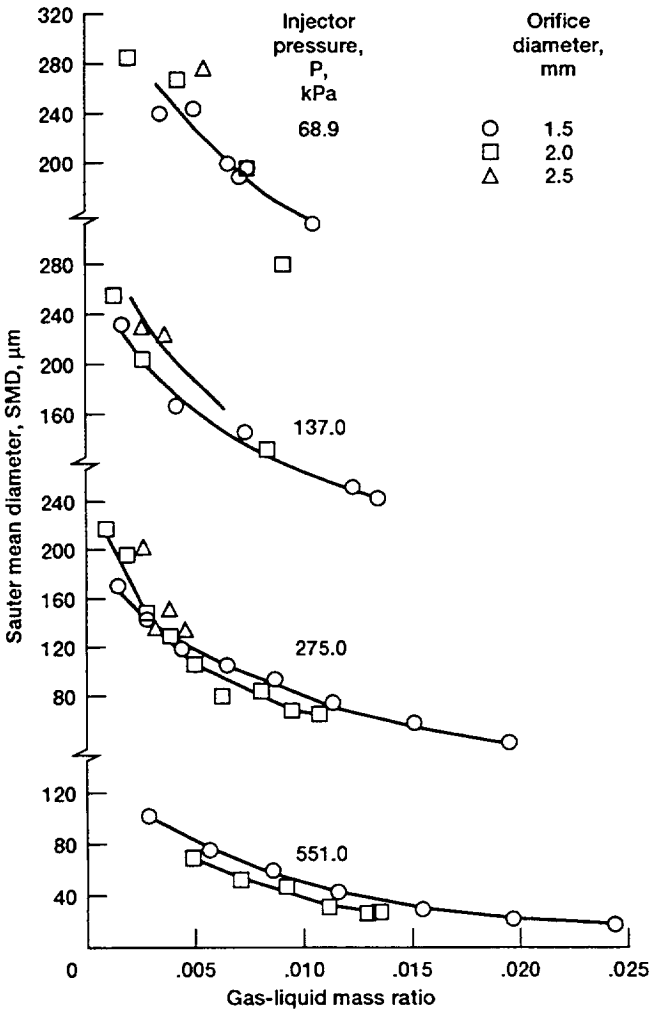

Figure 2.14.—Effect of orifice diameter on SMD; viscosity, 0.001 kg/m·s; aerator porosity, 20 μm (Roesler, 1988).

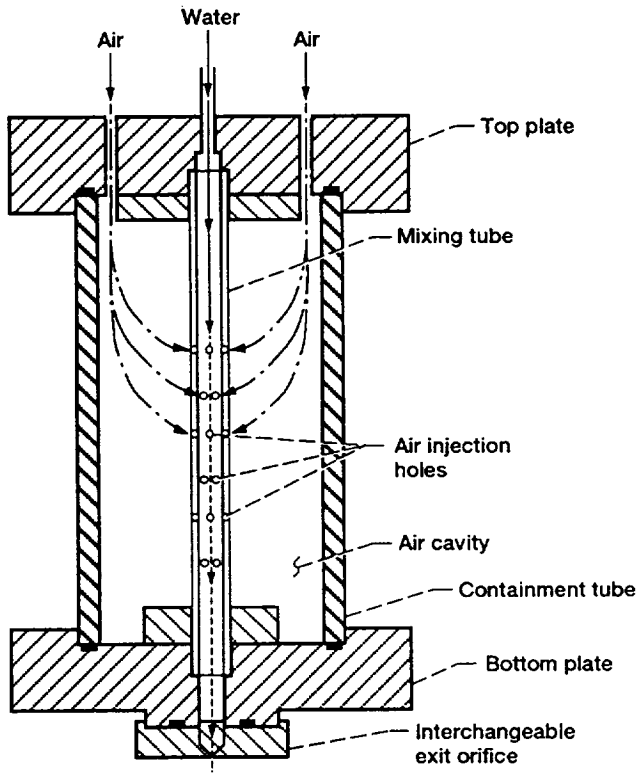

Figure 2.15.—Plain-orifice effervescent atomizer (Whitlow, 1990).

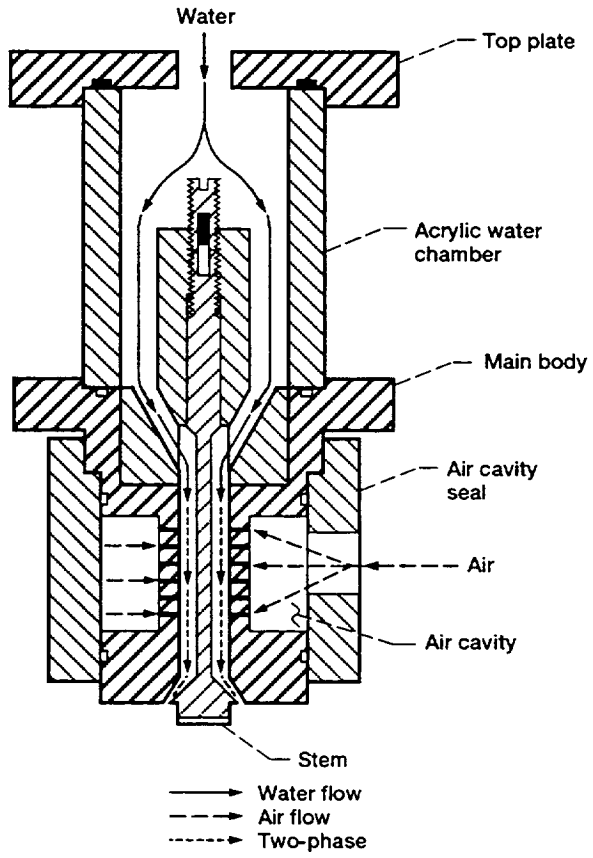

Figure 2.16.—Conical-sheet atomizer (Whitlow, 1990).

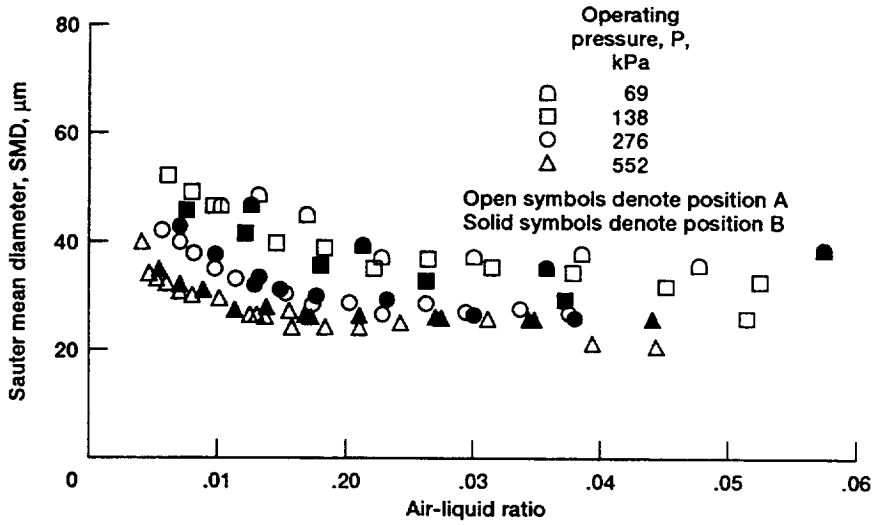

Figure 2.17.—Comparison of SMD versus air-liquid ratio for conical-sheet atomizer; discharge gap width, 0.20 mm (Whitlow, 1990).

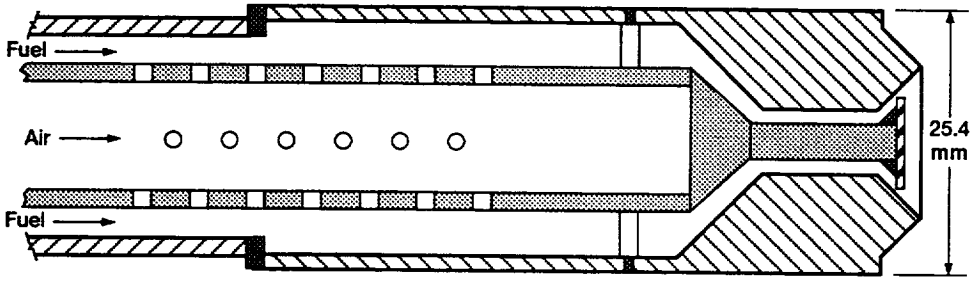

Figure 2.18.—Effervescent atomizer fitted to T-56 combustor (Lefebvre, Chin, and Rollbuhler, 1991, Purdue University, NASA Lewis Research Center, unpublished report).

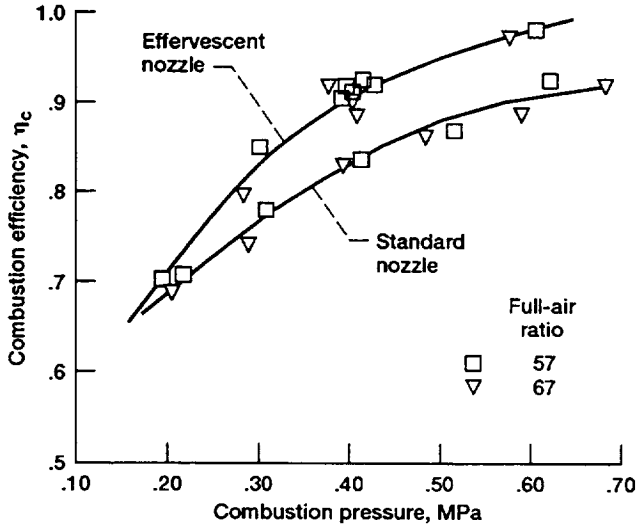

Figure 2.19.—Comparison of combustor performance with standard and effervescent fuel nozzles (Lefebvre, Chin, and Rollbuhler, 1991, Purdue University, NASA Lewis Research Center, unpublished report).

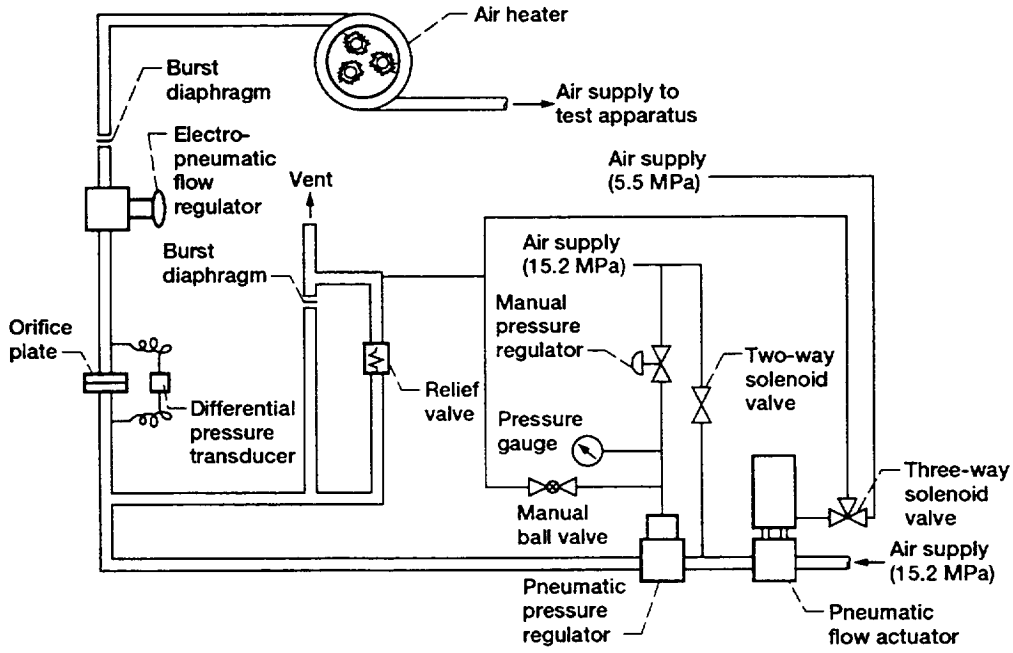

Figure 3.1.—Main air system.

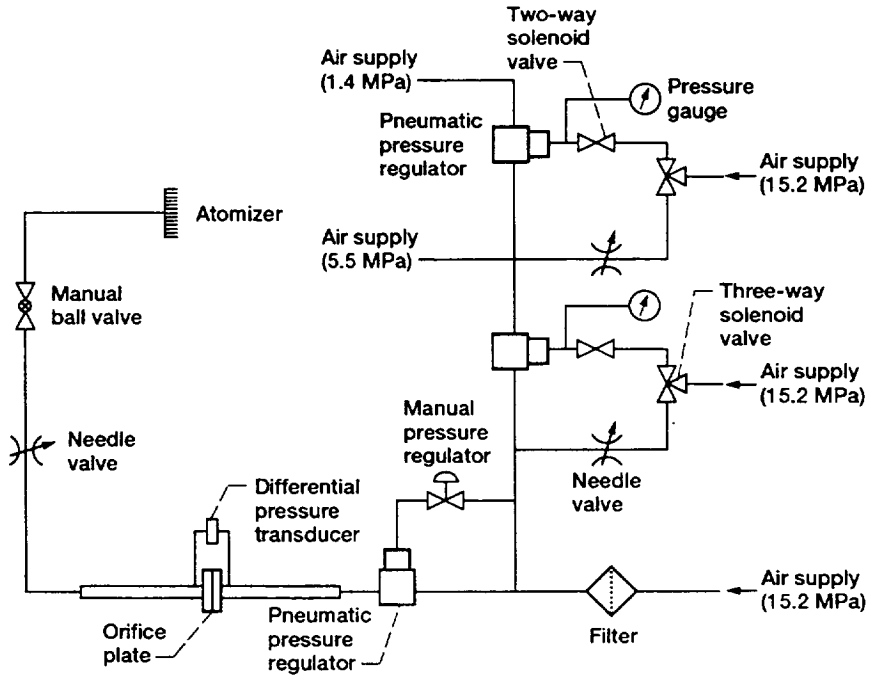

Figure 3.2.—Effervescent air system.

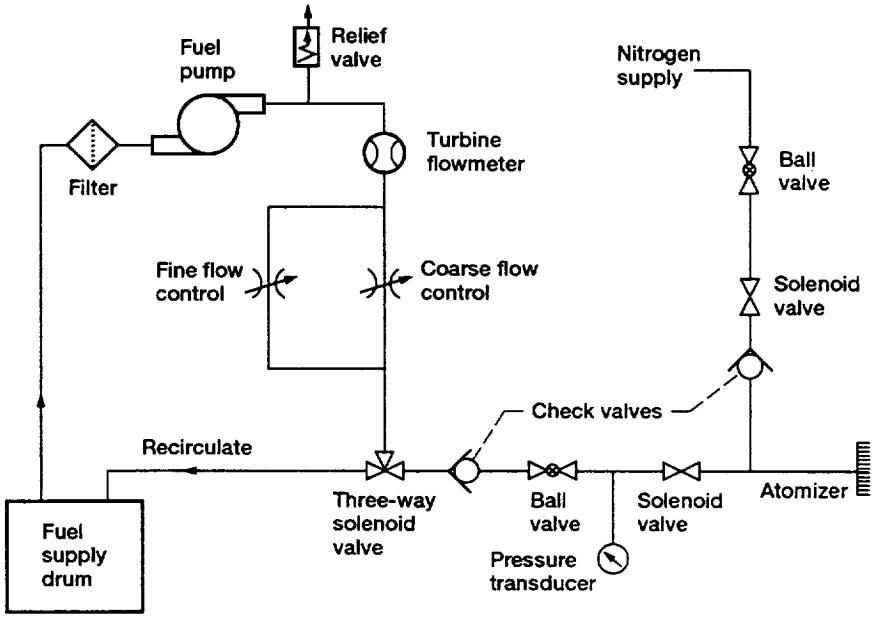

Figure 3.3–Fuel supply system.

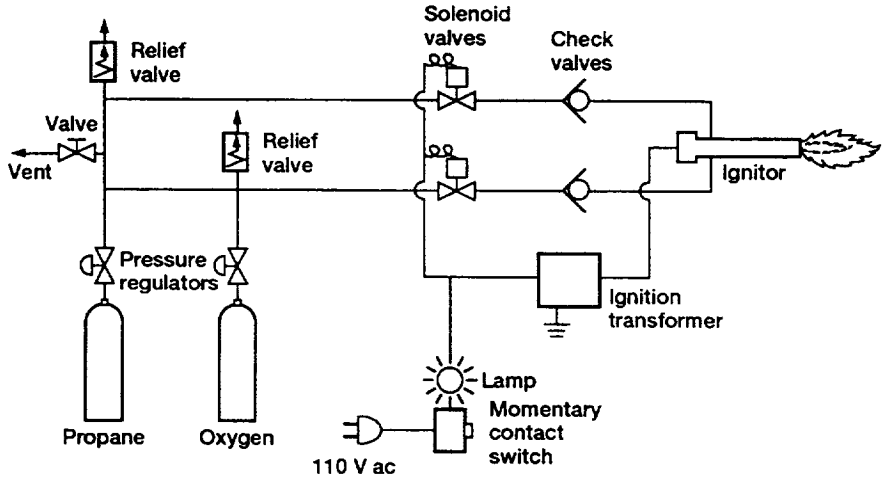

Figure 3.4.—Ignition system.

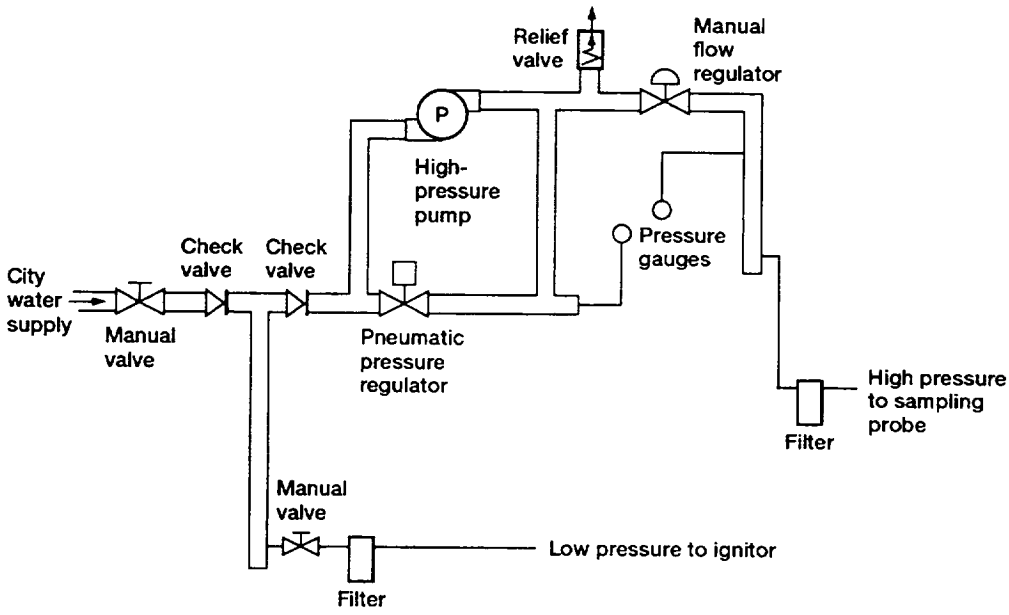

Figure 3.5.—Water supply system.

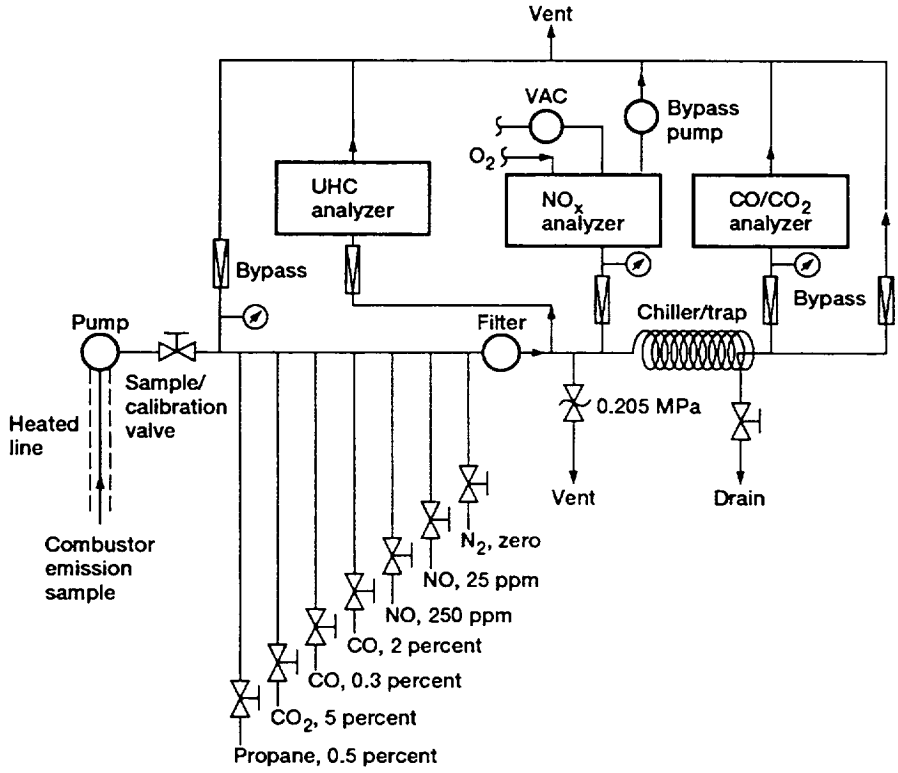

Figure 3.6.—Gas analysis system.

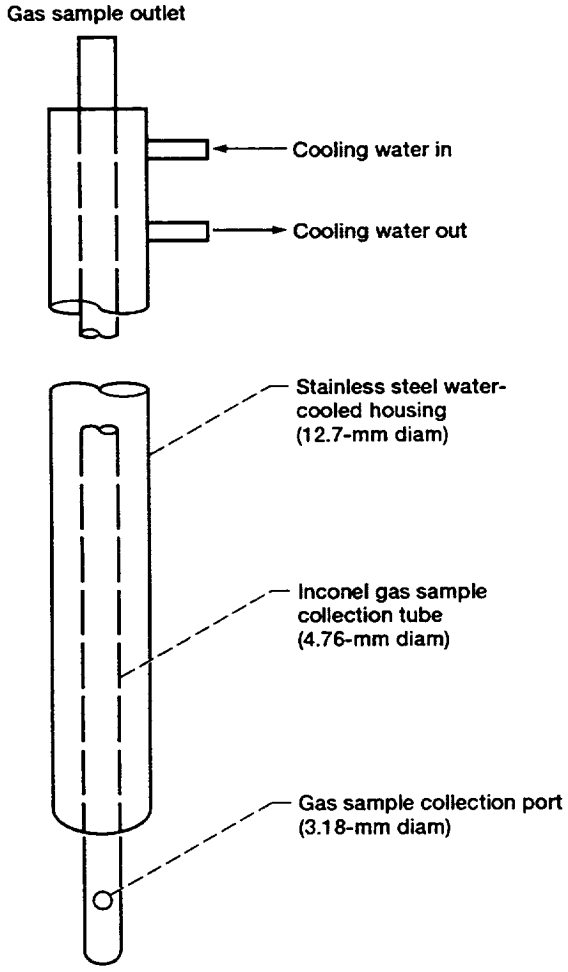

Figure 3.7.—Single-port, water-cooled gas sampling probe.

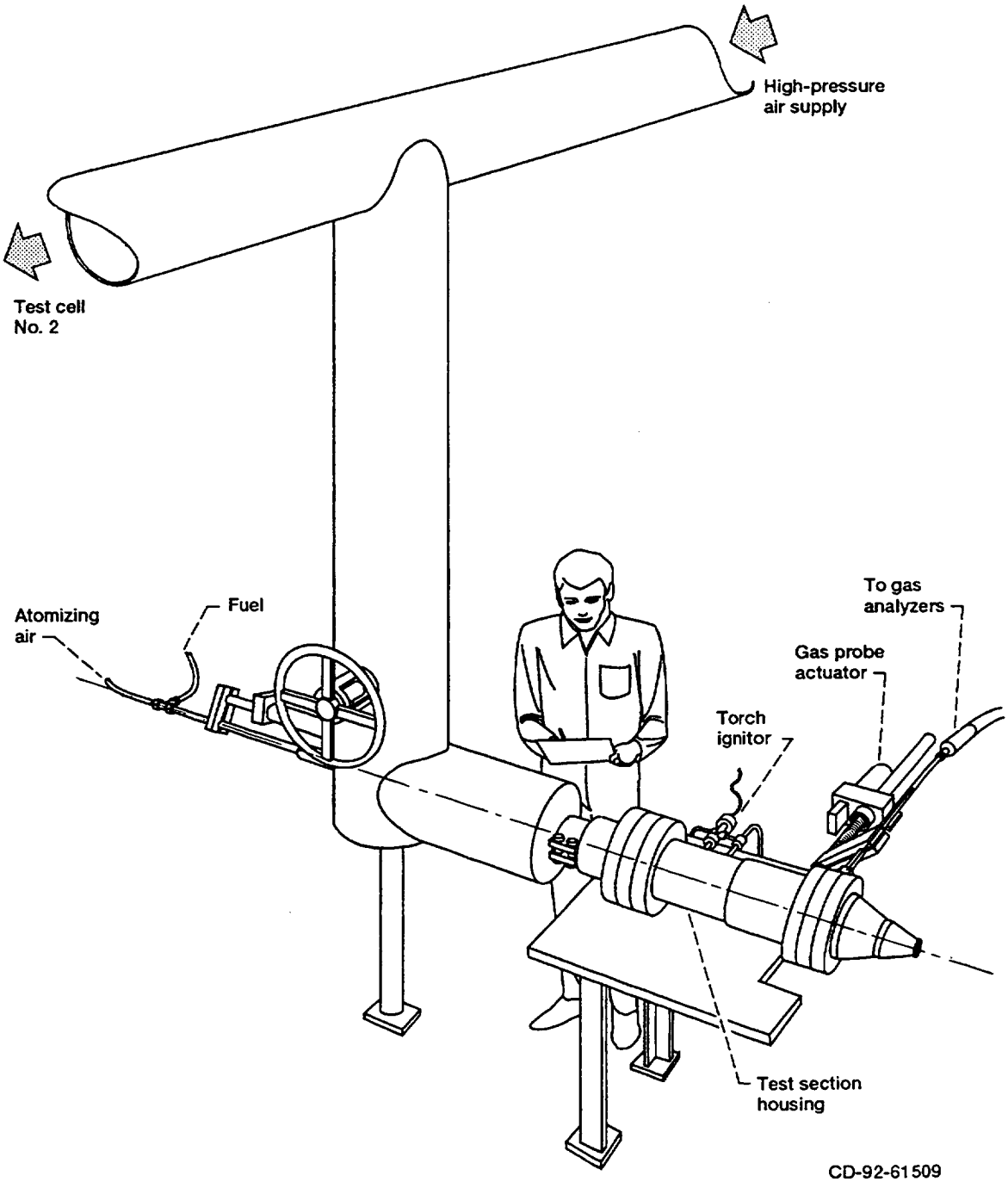

Figure 4.1—High-pressure combustor test facility at the Thermal Sciences and Propulsion Center, Purdue University.

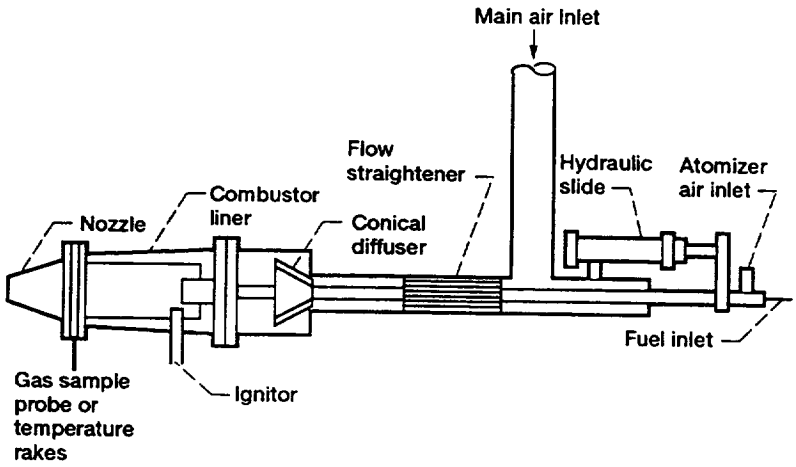

Figure 4.2.—Test section configuration.

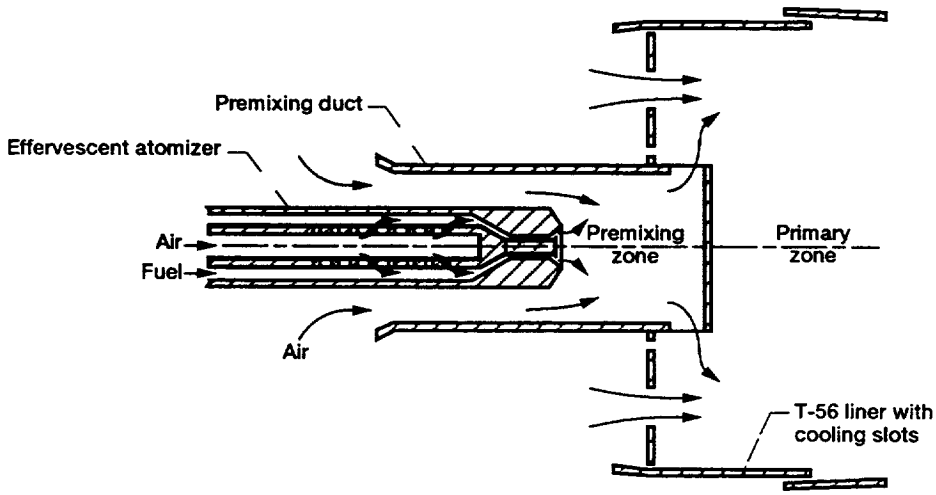

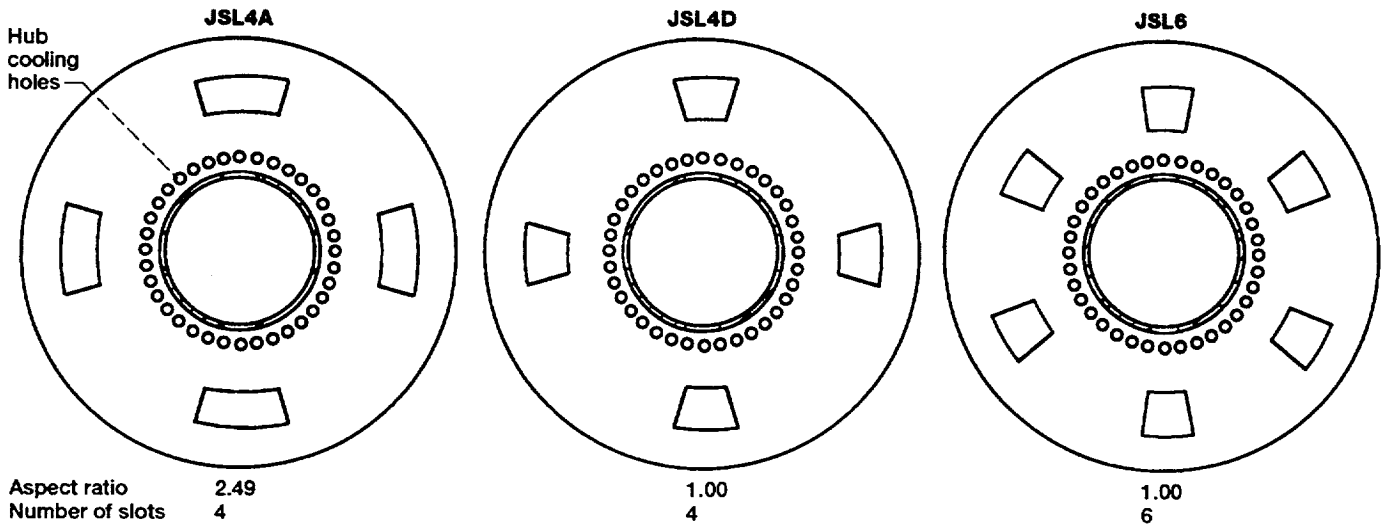

Figure 4.3.—Jet-Shear-Layer combustor configurations.

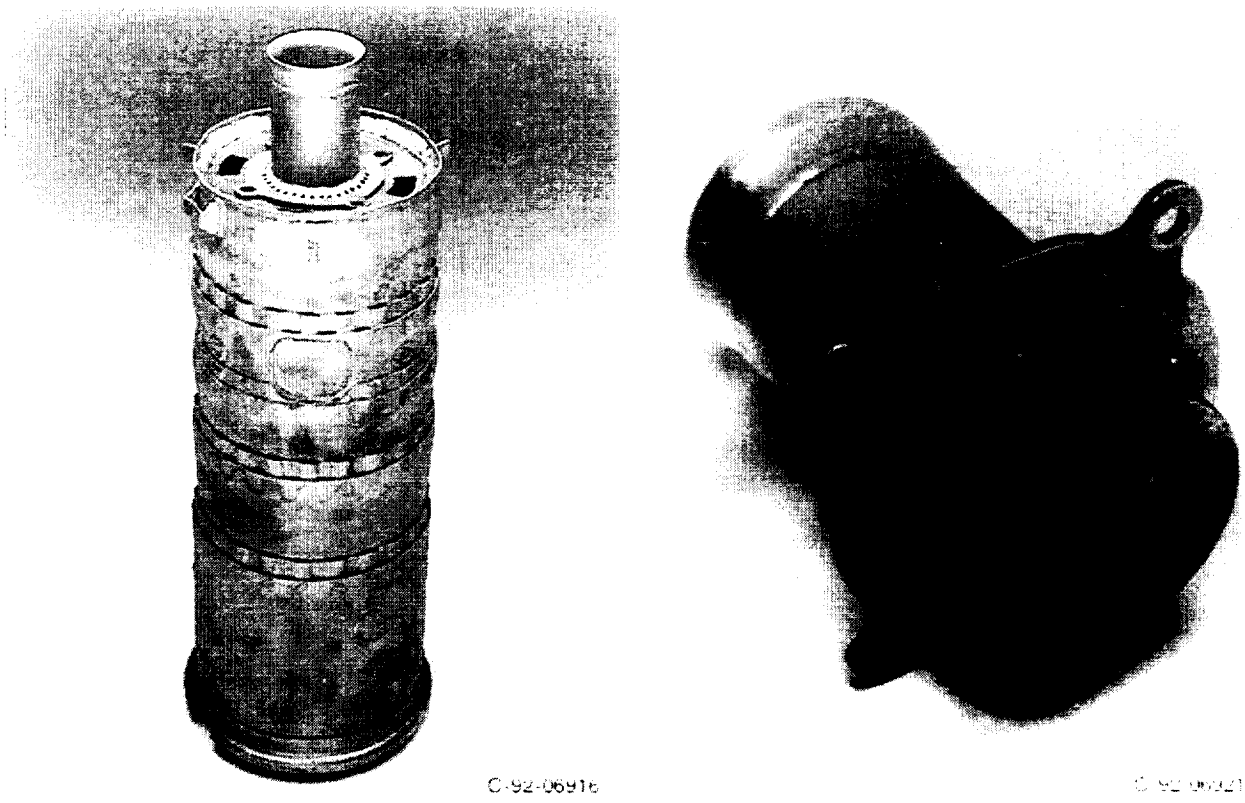

Figure 4.4.—JSL4A combustor (left) and premixing duct with hub cooling holes (right).

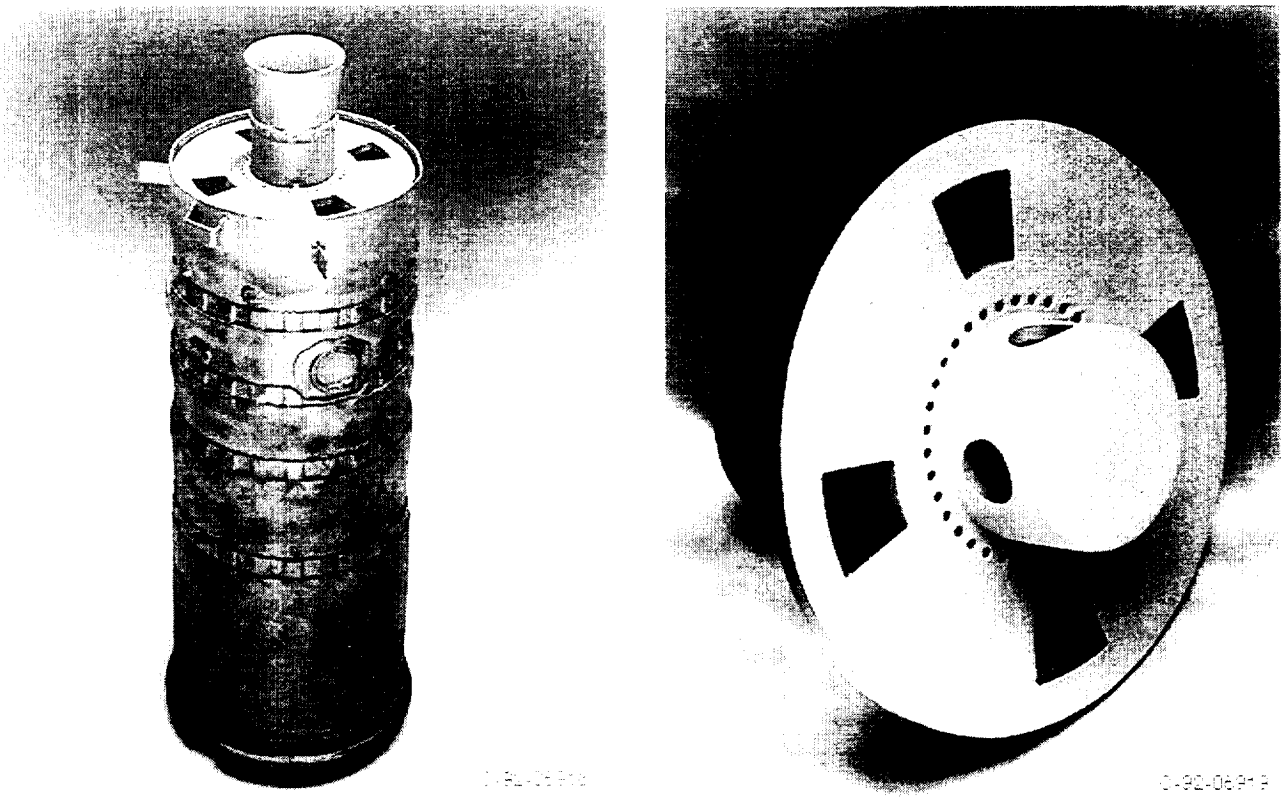

Figure 4.5.—JSL4D combustor (left) and dome section (right).

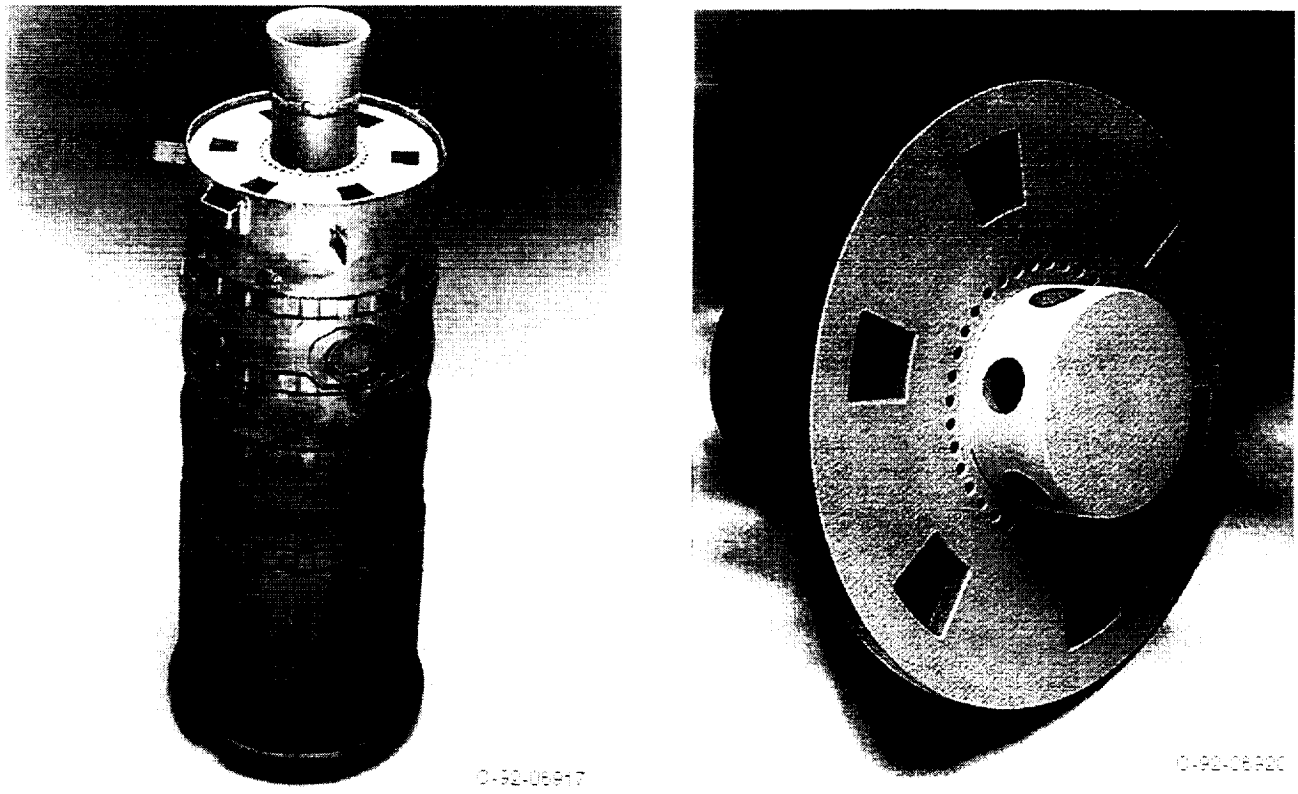

Figure 4.6.—JSL6 combustor (left) and dome section (right).

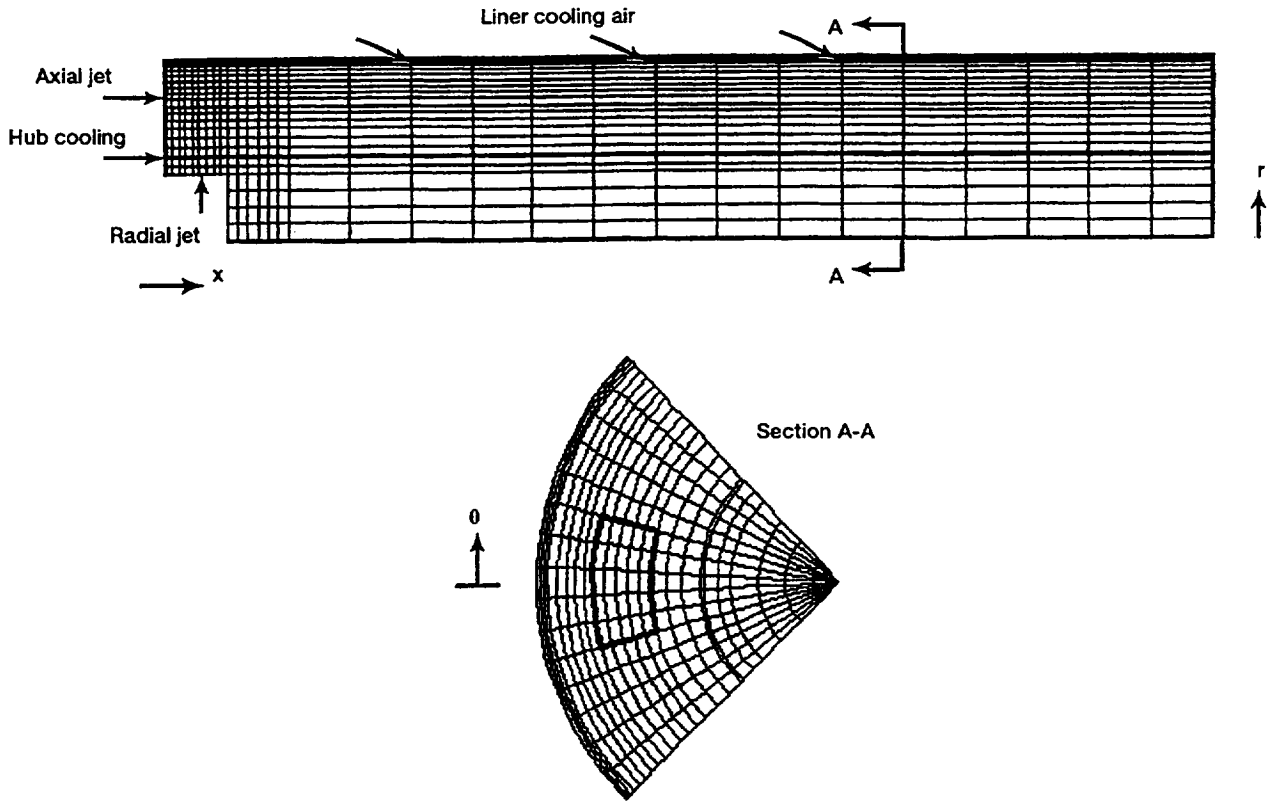

Figure 5.1.—Grid configuration for CFD model.

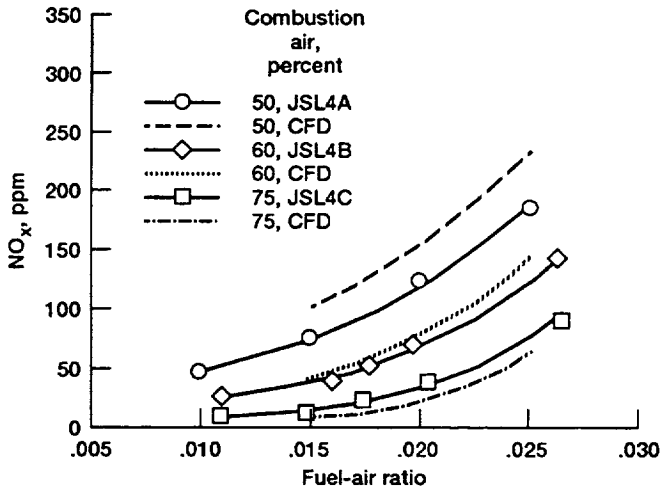

Figure 6.1.—Effects of fuel-air ratio and combustion air quantity on NO_x emissions; combustor inlet temperature, 551 K; combustor inlet pressure, 0.48 MPa.

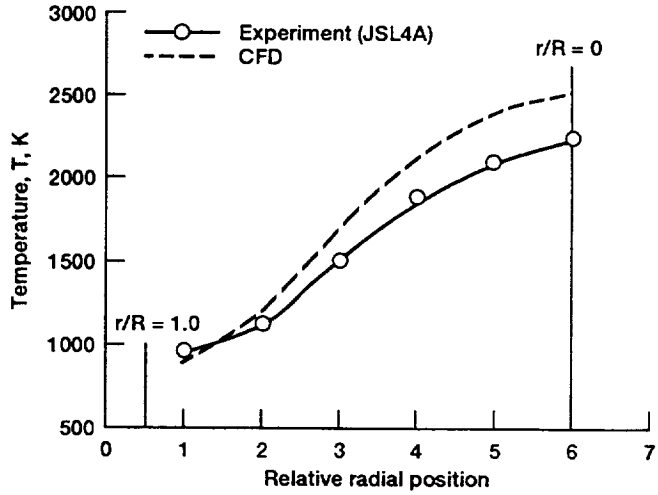

Figure 6.2.—Comparison of combustor exit temperature profiles obtained from experimental testing and CFD results; combustor inlet temperature, 551 K; combustor inlet pressure, 0.48 MPa; fuel-air ratio, 0.025.

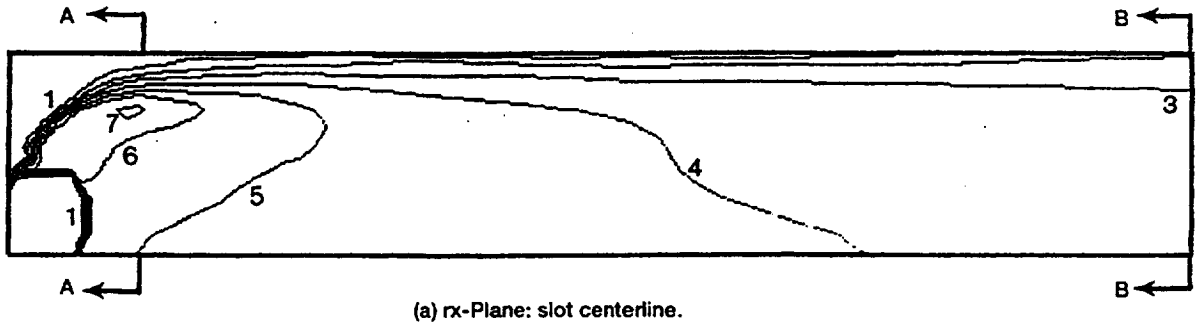

(a) rx-Plane: slot centerline.

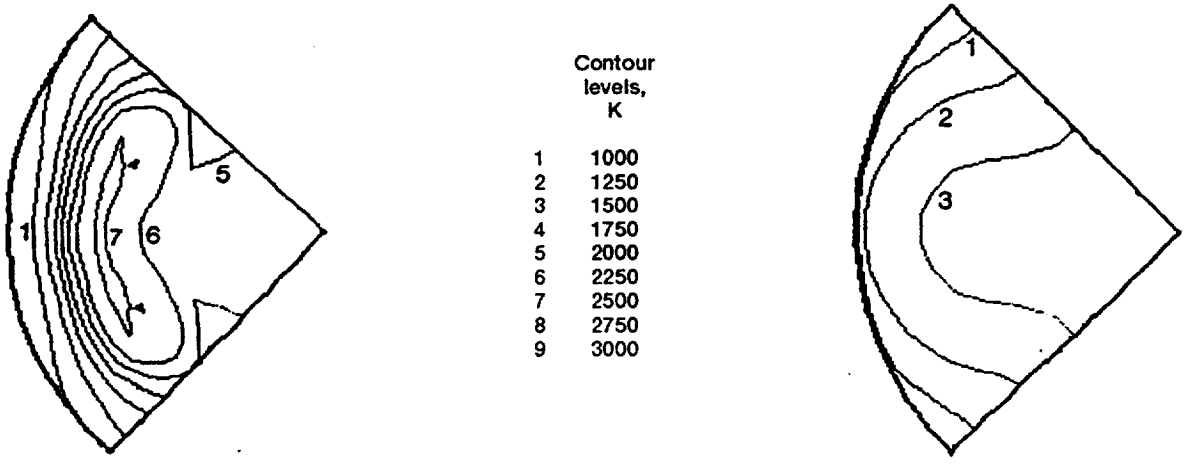

(b) rθ-Plane.

Figure 6.3.—Calculated temperature profiles within a JSL4C combustor; combustion air, 75 percent; fuel-air ratio, 0.020.

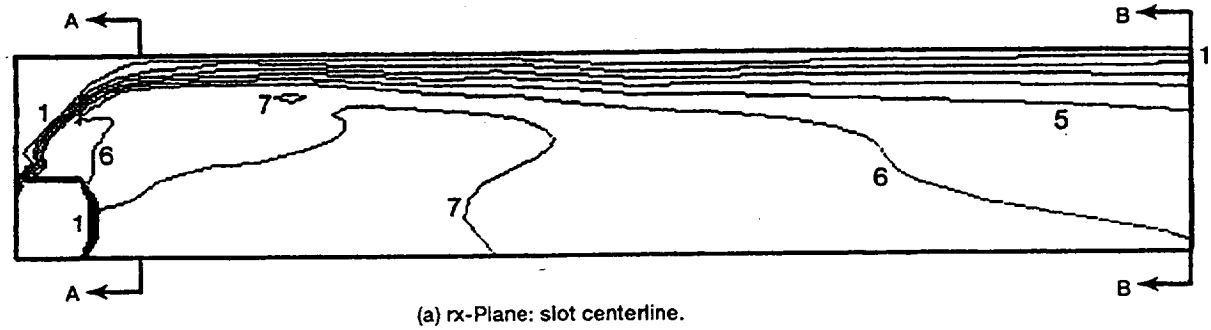

(a) rx-Plane: slot centerline.

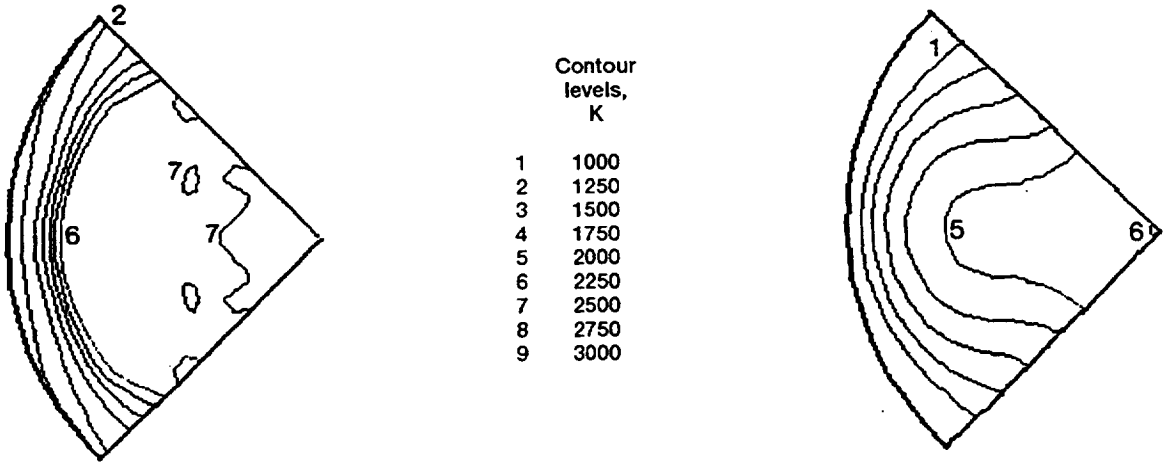

(b) rθ-Plane.

Figure 6.4.—Calculated temperature profiles within a JSL4A combustor; combustion air, 50 percent; fuel-air ratio, 0.020.

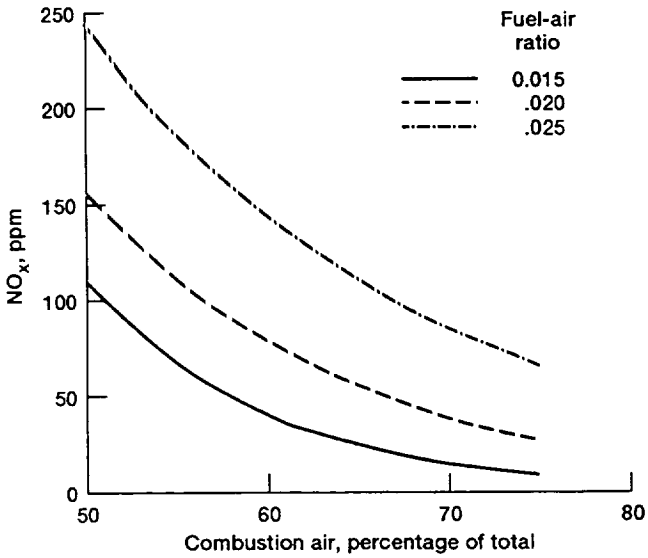

Figure 6.5.—CFD predictions of the effects of combustion air quantity and fuel-air ratio on NO_x emissions; combustor inlet temperature, 551 K; combustor inlet pressure, 0.48 MPa.

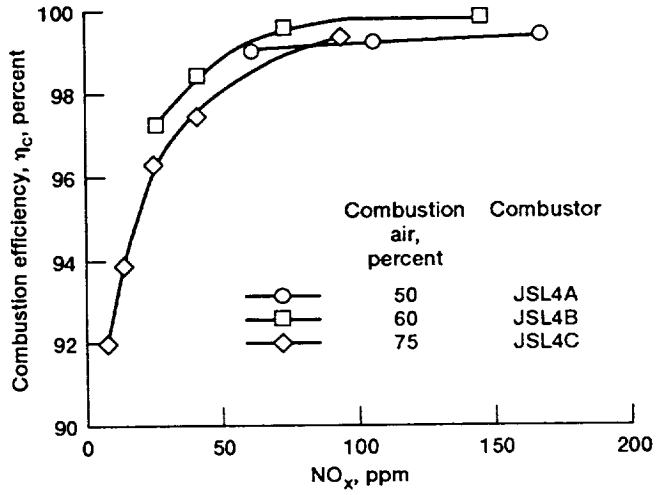

Figure 6.6.—Experimental results showing the effects of combustion air quantity on NO_x emissions; combustor inlet temperature, 551 K; combustor inlet pressure, 0.48 MPa.

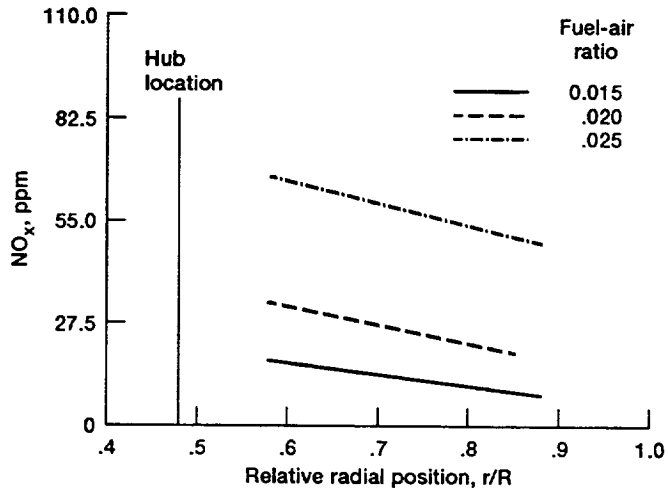

Figure 6.7.—CFD predictions of the effects of axial slot radial position and fuel-air ratio on NO_x emissions; combustor inlet temperature, 551 K; combustor inlet pressure, 0.48 MPa.

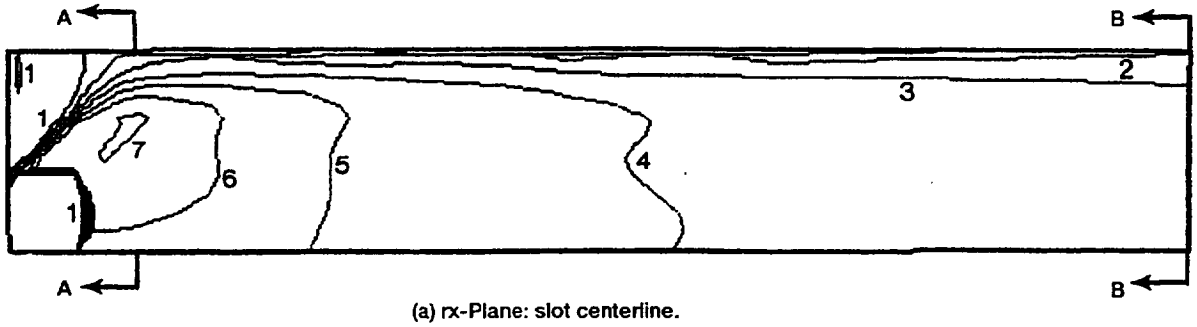

(a) rx-Plane: slot centerline.

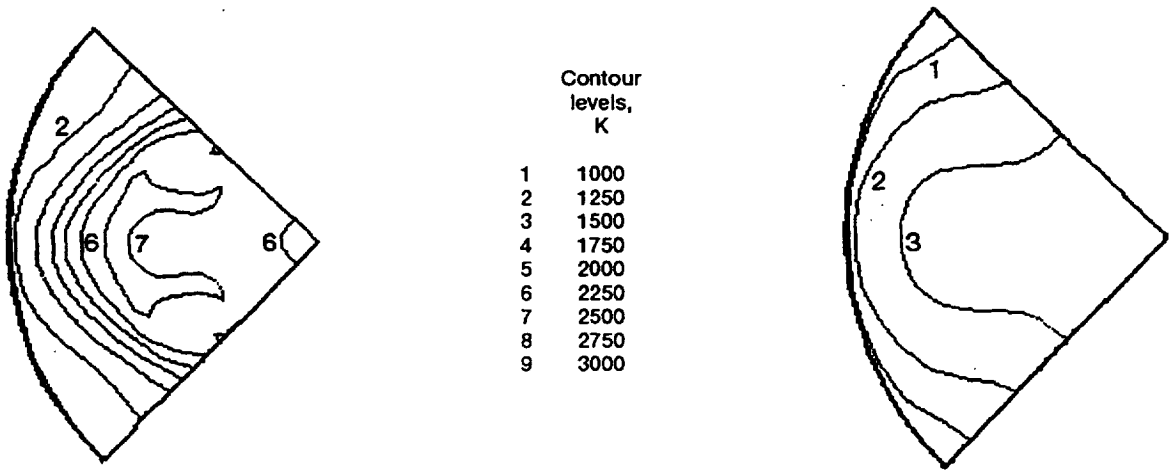

(b) rθ-Plane.

Figure 6.8.—Calculated temperature profiles within a JSL combustor with axial air slots located at radial position of 0.63; combustion air, 75 percent; fuel-air ratio, 0.020; axial slot aspect ratio, 2.49.

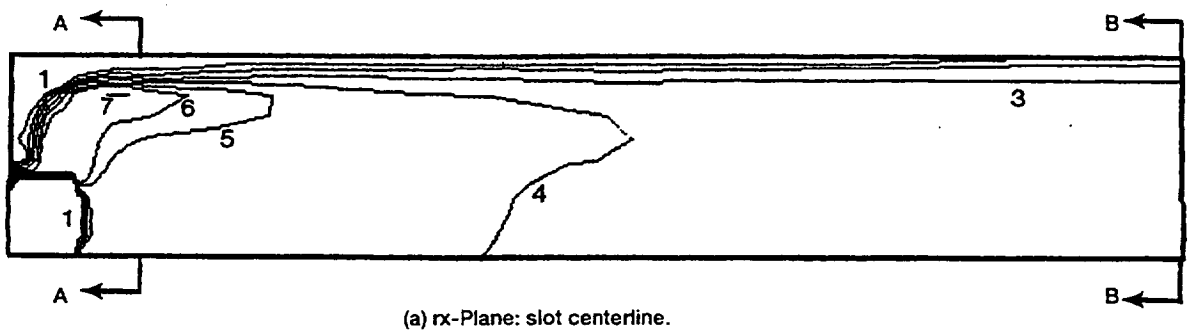

(a) rx-Plane: slot centerline.

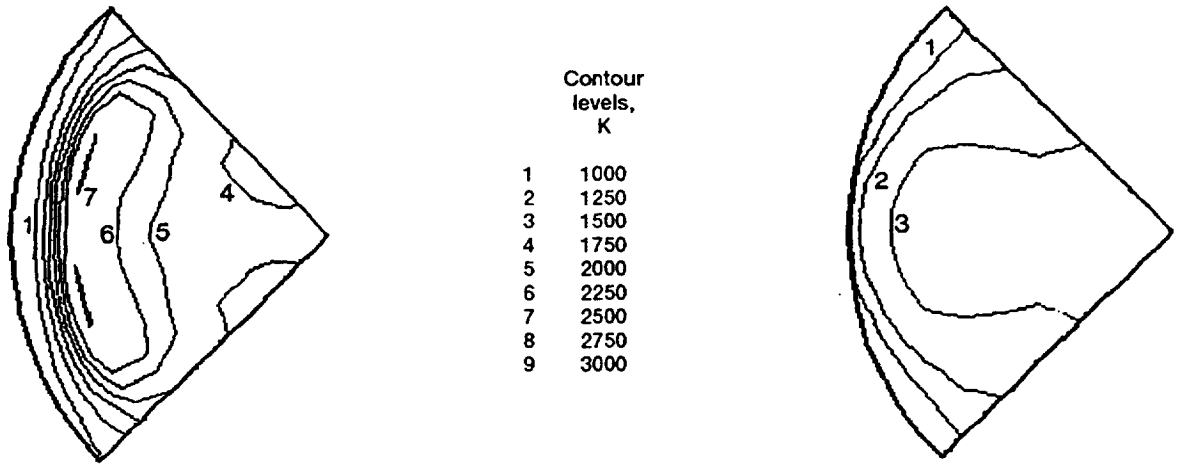

(b) rθ-Plane.

Figure 6.9.—Calculated temperature profiles within a JSL combustor with axial air slots located at radial position of 0.88; combustion air, 75 percent; fuel-air ratio, 0.020; axial slot aspect ratio, 2.49.

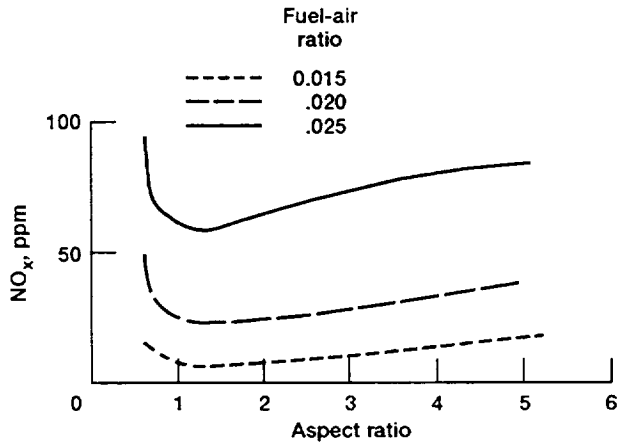

Figure 6.10.—CFD predictions of the effects of axial slot aspect ratio and fuel-air ratio on NO_x emissions; combustor inlet temperature, 551 K; combustor inlet pressure, 0.48 MPa.

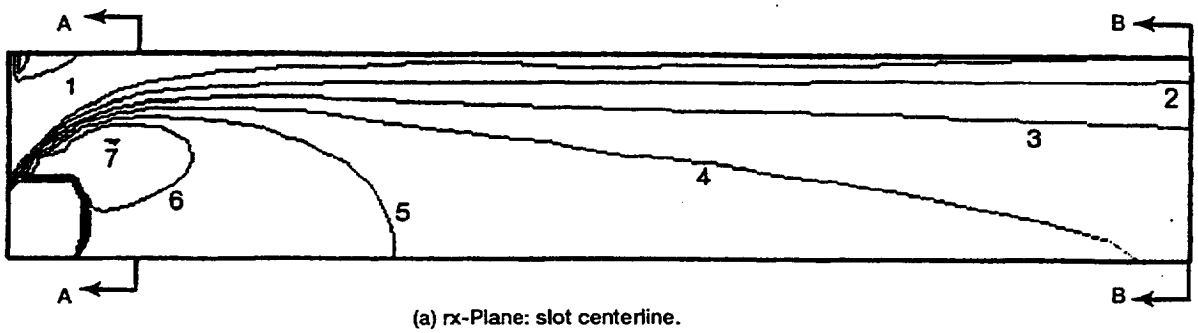

(a) rx-Plane: slot centerline.

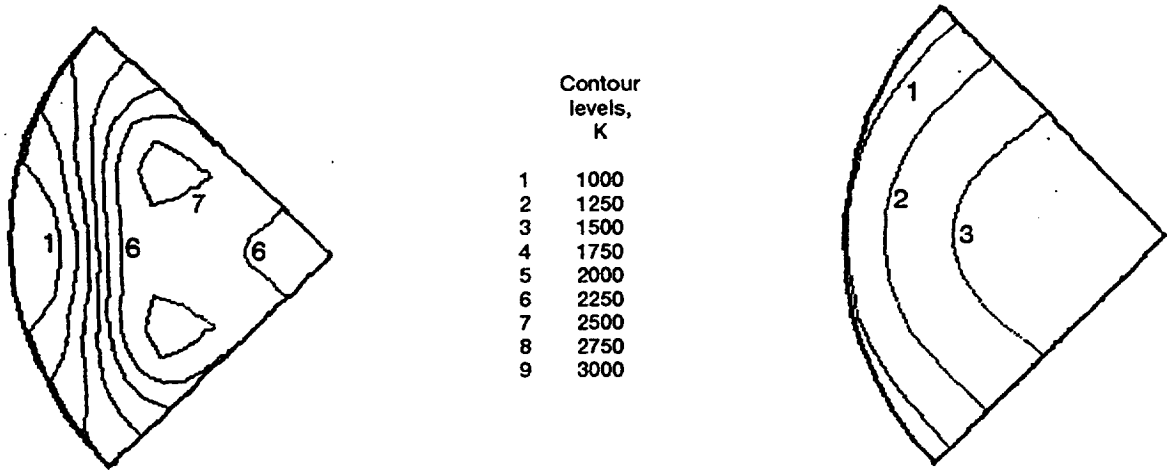

(b) rθ-Plane.

Figure 6.11.—Calculated temperature profiles within a JSL combustor with an axial slot aspect ratio of 0.62; combustion air, 75 percent; fuel-air ratio, 0.020; axial slot radial position, 0.72.

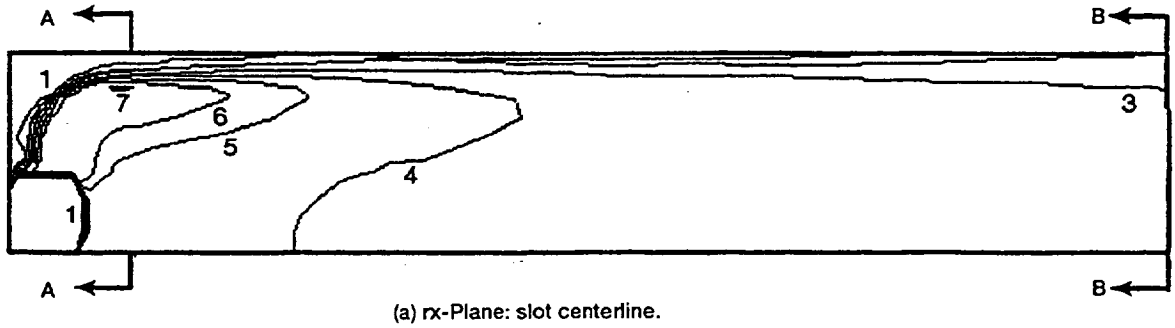

(a) rx-Plane: slot centerline.

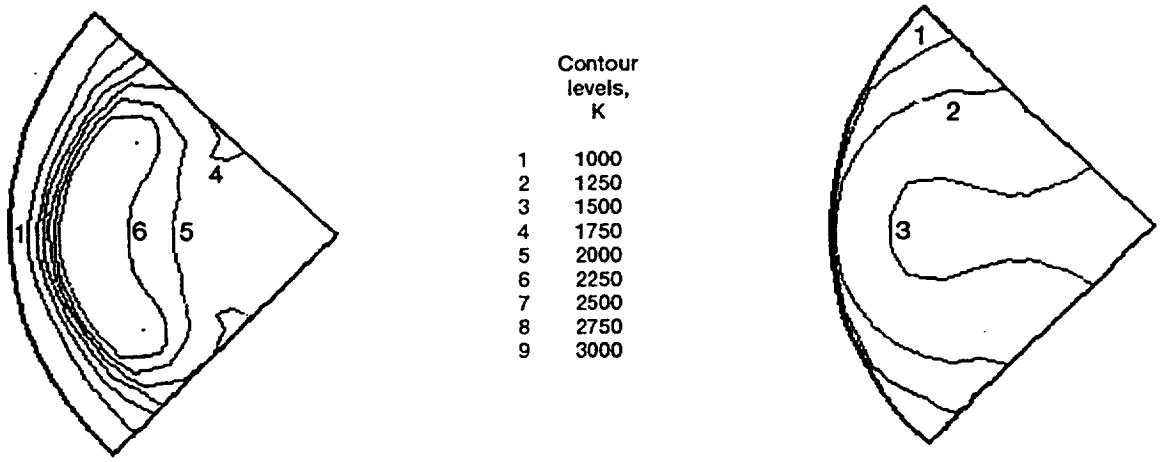

(b) r0-Plane.

Figure 6.12.—Calculated temperature profiles within a JSL combustor with an axial slot aspect ratio, 5.22; combustion air, 75 percent; fuel-air ratio, 0.020; axial slot radial position, 0.72.

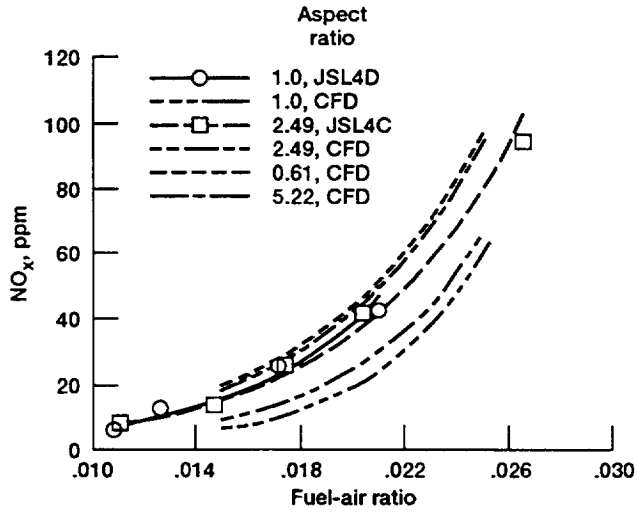

Figure 6.13.—Effects of fuel-air ratio and axial slot aspect ratio on NO_x emissions; combustor inlet temperature, 551 K; combustor inlet pressure, 0.48 MPa.

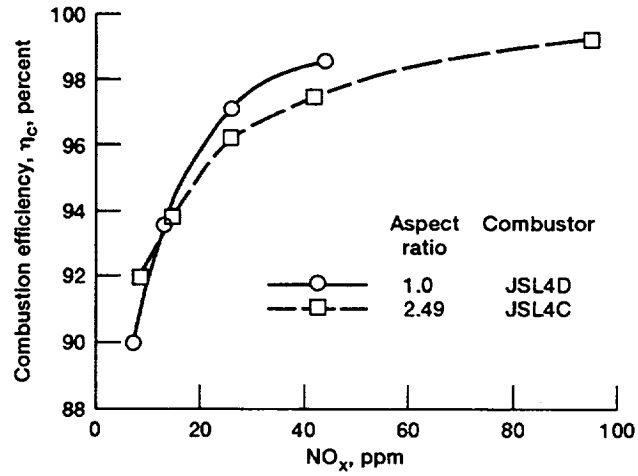

Figure 6.14.—Experimental results showing the effects of combustion efficiency and axial slot aspect ratio on NO_x emissions; combustor inlet temperature, 551 K; combustor inlet pressure, 0.48 MPa.

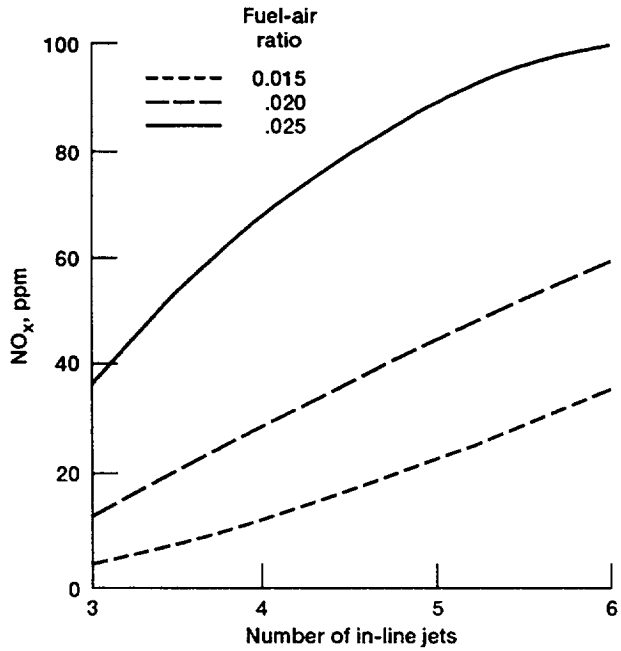

Figure 6.15.—CFD predictions of the effects of number of in-line jets and fuel-air ratio on NO_x emissions; combustor inlet temperature, 551 K; combustor inlet pressure, 0.48 MPa.

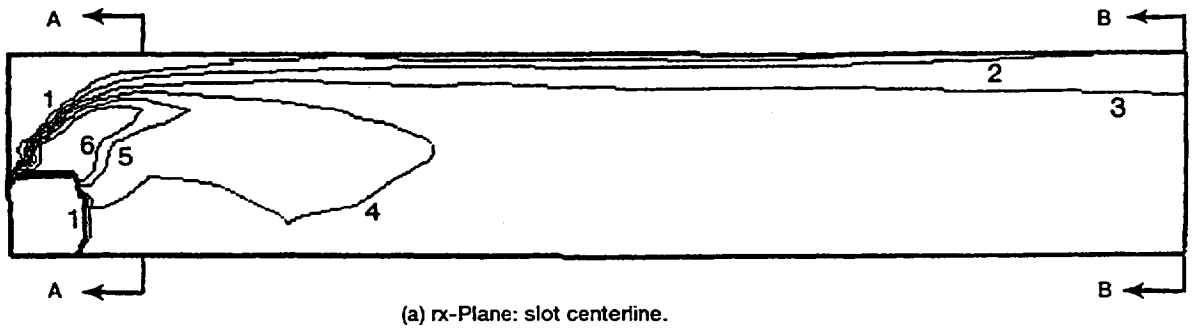

(a) rx-Plane: slot centerline.

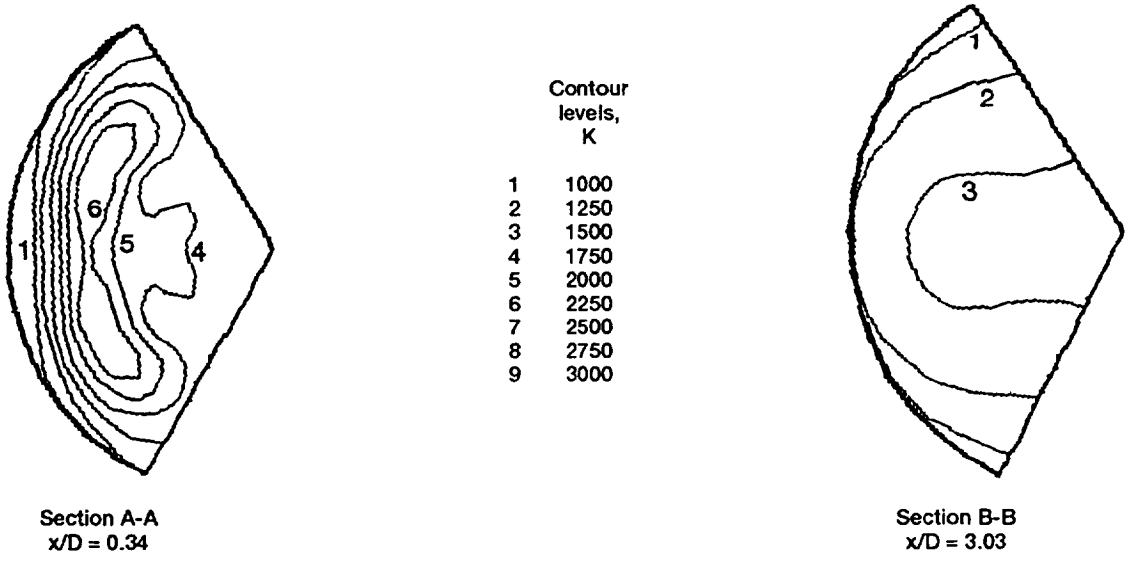

(b) rθ-Plane.

Figure 6.16.—Calculated temperature profiles within a three-slotted JSL combustor; combustion air, 75 percent; fuel-air ratio, 0.020; axial slot radial position, 0.72; axial slot aspect ratio, 1.00.

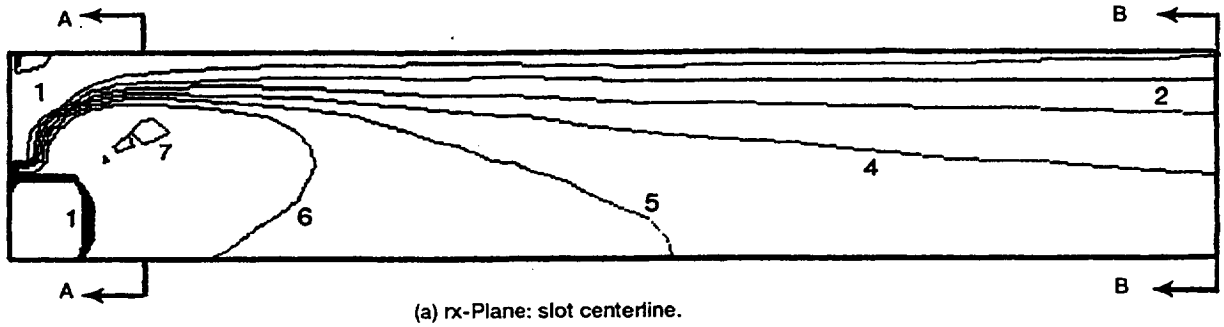

(a) rx-Plane: slot centerline.

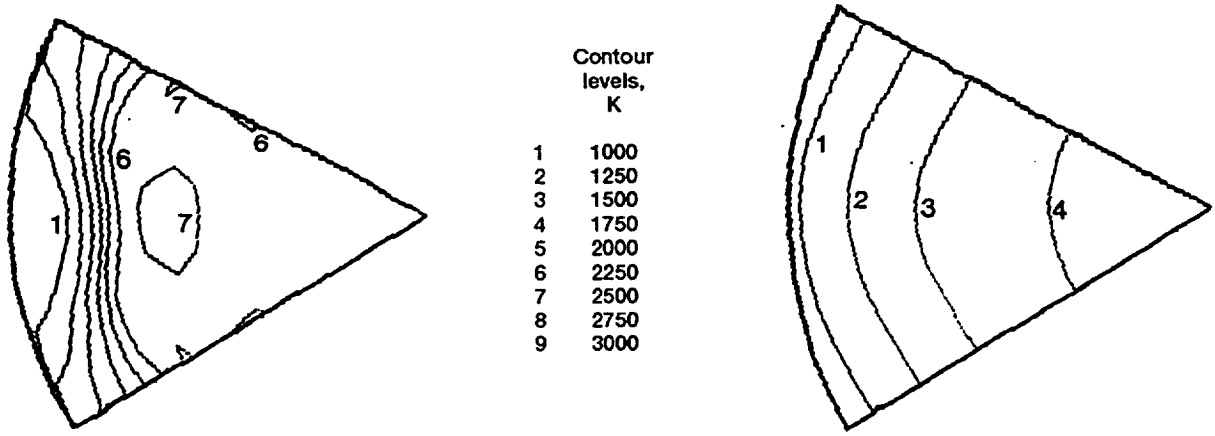

(b) rθ-Plane.

Figure 6.17.—Calculated temperature profiles within a six-slotted JSL combustor; combustion air, 75 percent; fuel-air ratio, 0.020; axial slot aspect ratio, 1.00; axial slot radial position, 0.72.

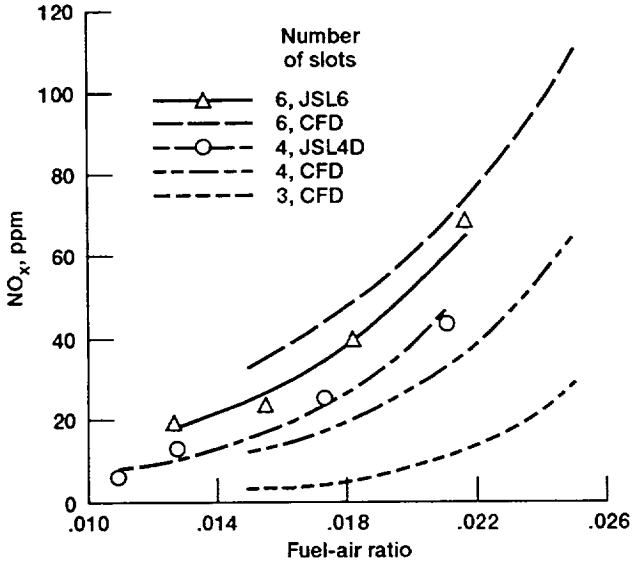

Figure 6.18.—Effects of fuel-air ratio and number of in-line jets on NO_x emissions; combustor inlet temperature, 551 K; combustor inlet pressure, 0.48 MPa.

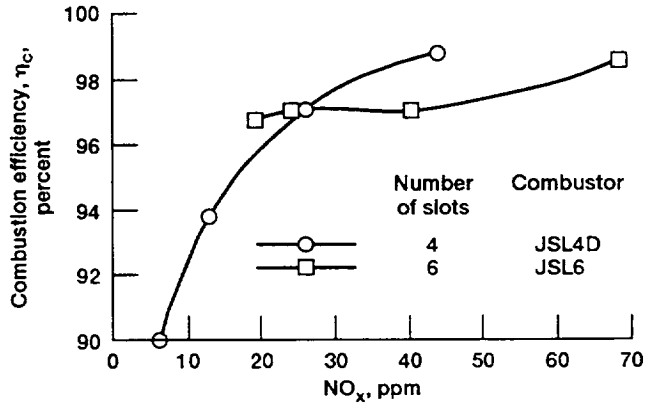

Figure 6.19.—Experimental results showing the effects of combustion efficiency and number of in-line jets on NO_x emissions; combustor inlet temperature, 551 K; combustor inlet pressure, 0.48 MPa.

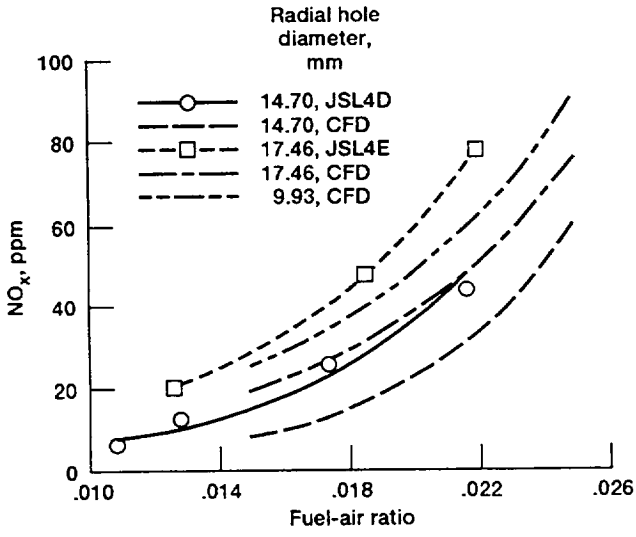

Figure 6.20.—Effects of fuel-air ratio and radial hole diameter on NO_x emissions; combustor inlet temperature, 551 K; combustor inlet pressure, 0.48 MPa.

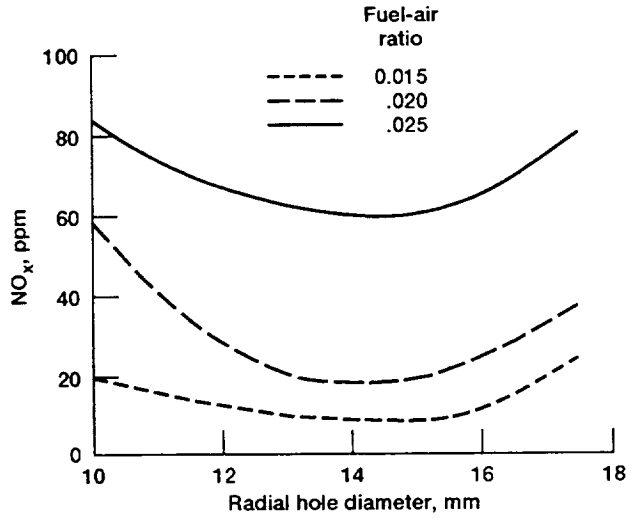

Figure 6.21.—CFD predictions of the effects of radial hole diameter and fuel-air ratio on NO_x emissions; combustor inlet temperature, 551 K; combustor inlet pressure, 0.48 MPa.

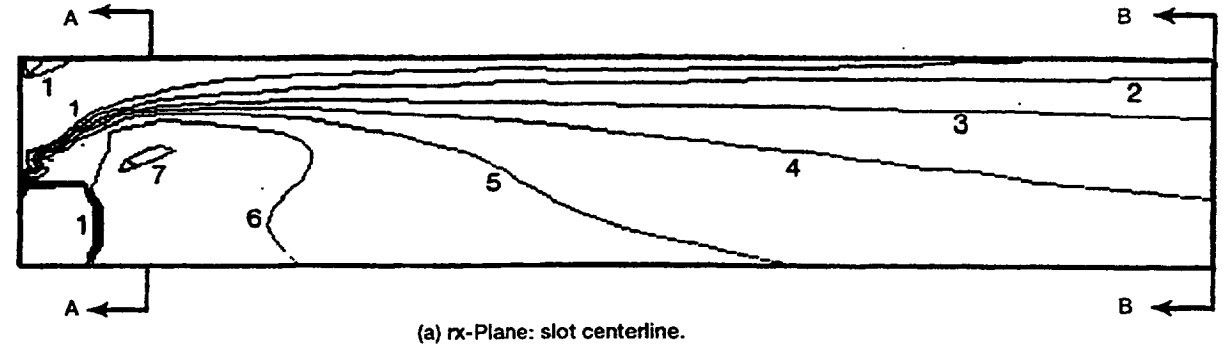

(a) rx-Plane: slot centerline.

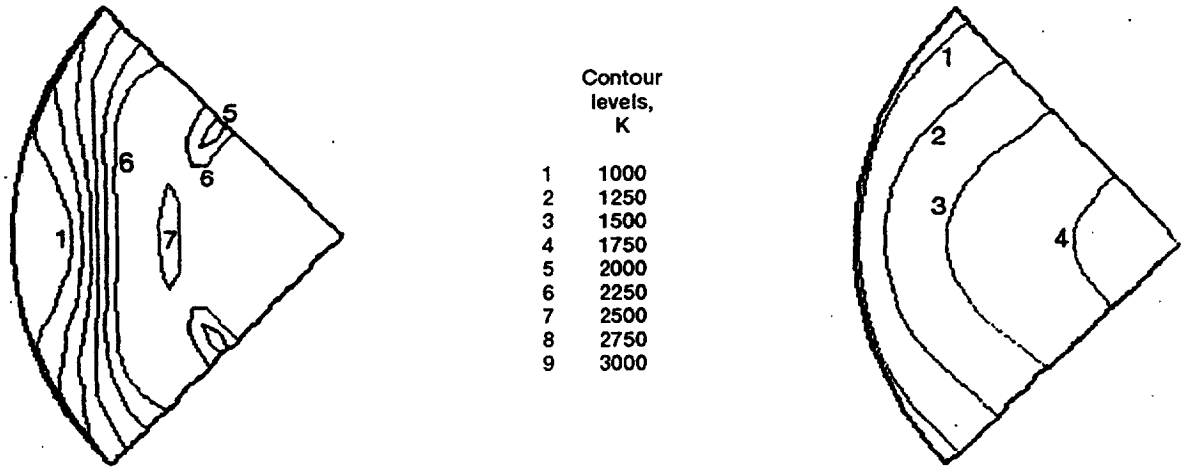

Contour levels,	K
1	1000
2	1250
3	1500
4	1750
5	2000
6	2250
7	2500
8	2750
9	3000

Section A-A
x/D = 0.34

Section B-B
x/D = 3.03

(b) rθ-Plane.

Figure 6.22.—Calculated temperature profiles within a JSL combustor with 9.93-mm-diameter radial holes; combustion air, 75 percent; fuel-air ratio, 0.020; axial slot aspect ratio, 1.00; axial slot radial position, 0.72.

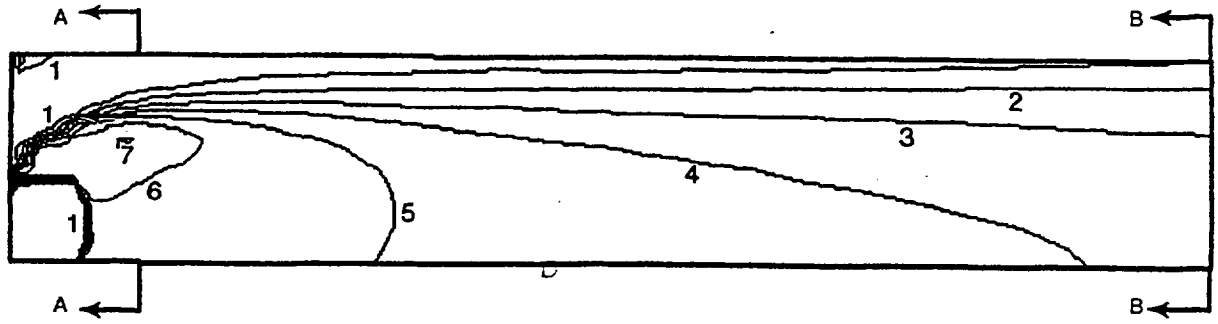

(a) rx-Plane: slot centerline.

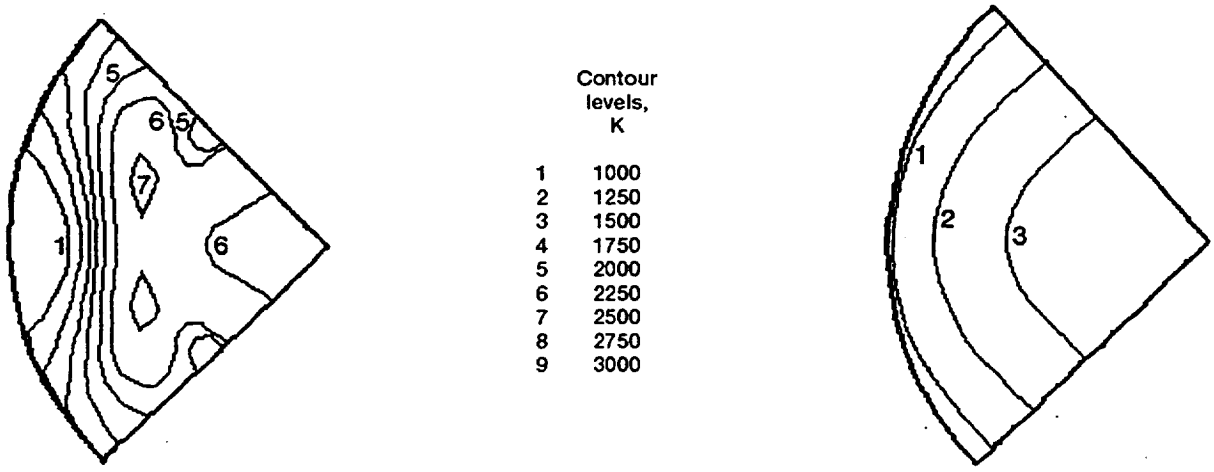

(b) rθ-Plane.

Figure 6.23.—Calculated temperature profiles within a JSL combustor with 17.46-mm-diameter radial holes; combustion air, 75 percent; fuel-air ratio, 0.020; axial slot aspect ratio, 1.00; axial slot radial position, 0.72.

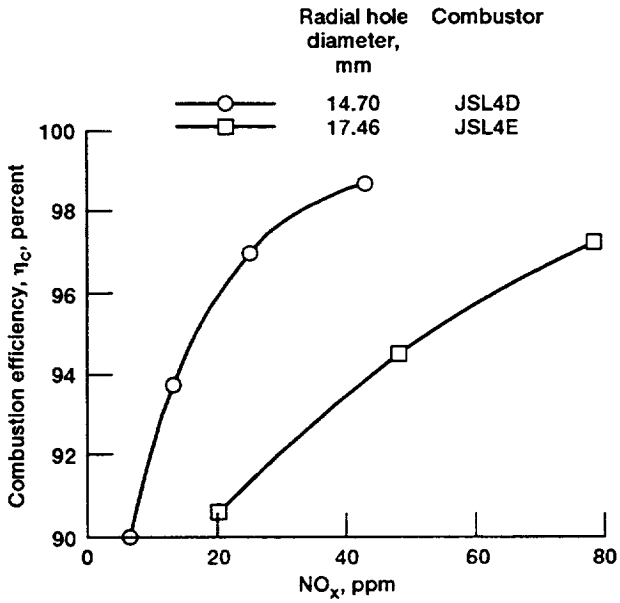

Figure 6.24.—Experimental results showing the effects of combustion efficiency and radial hole diameter on NO_x emissions; combustor inlet temperature, 551 K; combustor inlet pressure, 0.48 MPa.

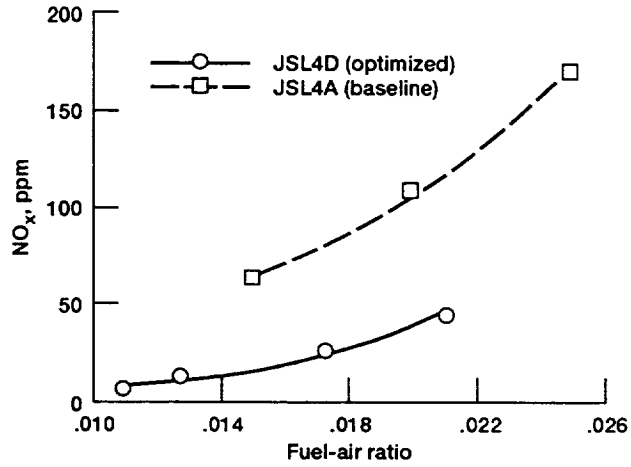

Figure 6.25.—Comparison of experimental data on NO_x emissions for the JSL baseline and optimized combustors; combustor inlet temperature, 551 K; combustor inlet pressure, 0.48 MPa.

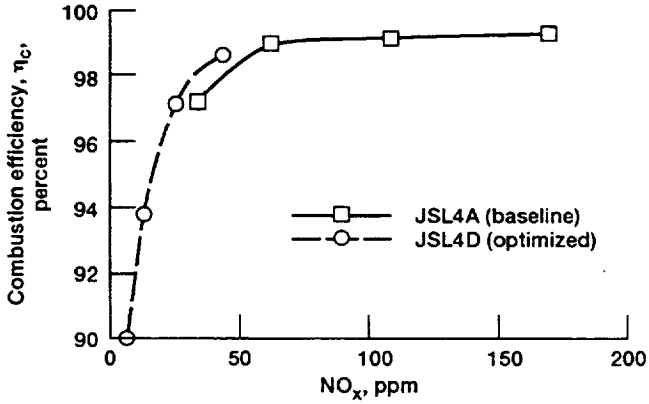

Figure 6.26.—Comparison of experimental data on combustion efficiency for the JSL baseline and optimized combustors; combustor inlet temperature, 551 K; combustor inlet pressure, 0.48 MPa.

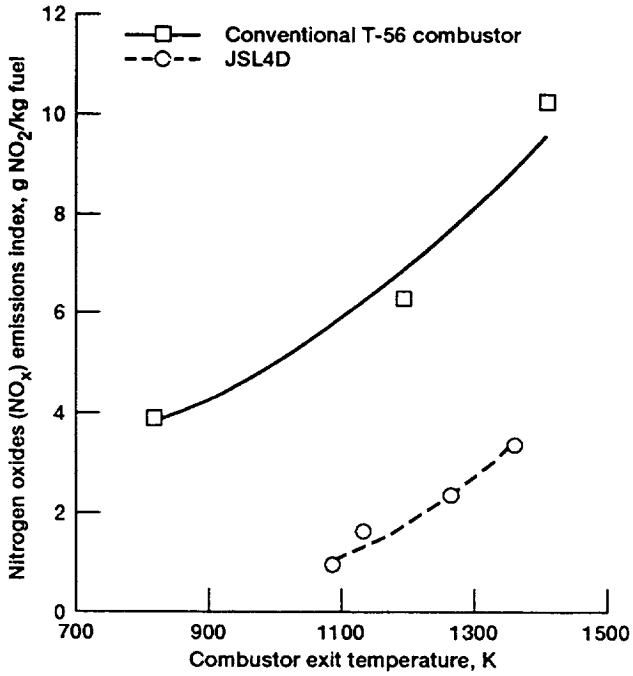

Figure 6.27—Comparison of experimental data on NO_x emissions for conventional and JSL combustors.

REPORT DOCUMENTATION PAGE

Form Approved
OMB No. 0704-0188

1. AGENCY USE ONLY (*Leave blank*)	2. REPORT DATE	3. REPORT TYPE AND DATES COVERED
	June 1993	Technical Memorandum

4. TITLE AND SUBTITLE

Application of Jet-Shear-Layer Mixing and Effervescent Atomization to the Development of a Low-NO_x Combustor

5. FUNDING NUMBERS

WU–535–05–10

6. AUTHOR(S)

Renato Olaf Colantonio

7. PERFORMING ORGANIZATION NAME(S) AND ADDRESS(ES)

National Aeronautics and Space Administration
Lewis Research Center
Cleveland, Ohio 44135–3191

8. PERFORMING ORGANIZATION REPORT NUMBER

E–7353

9. SPONSORING/MONITORING AGENCY NAME(S) AND ADDRESS(ES)

National Aeronautics and Space Administration
Washington, D.C. 20546–0001

10. SPONSORING/MONITORING AGENCY REPORT NUMBER

NASA TM–105888

11. SUPPLEMENTARY NOTES

Report was submitted as a dissertation in partial fulfillment of the requirements for the degree Doctor of Philosophy to Purdue University, West Lafayette, Indiana, 47907. Responsible person: Renato Olaf Colantonio (216) 433–6370.

12a. DISTRIBUTION/AVAILABILITY STATEMENT

Unclassified - Unlimited
Subject Category 07

12b. DISTRIBUTION CODE

13. ABSTRACT ***(Maximum 200 words)***

An investigation was conducted to develop appropriate technologies for a low-NO_x, liquid-fueled combustor. The combustor incorporates an effervescent atomizer used to inject fuel into a premixing duct. Only a fraction of the combustion air is used in the premixing process to avoid autoignition and flashback problems. This fuel-rich mixture is introduced into the remaining combustion air by a rapid jet-shear-layer-mixing process involving radial fuel-air jets impinging on axial air jets in the primary combustion zone. Computational analysis was used to provide a better understanding of the fluid dynamics that occur in jet-shear-layer mixing and to facilitate a parametric analysis appropriate to the design of an optimum low-NO_x combustor. A number of combustor configurations were studied to assess the key combustor technologies and to validate the modeling code. The results from the experimental testing and computational analysis indicate a low-NO_x potential for the jet-shear-layer combustor. Key parameters found to affect NO_x emissions are the primary combustion zone fuel-air ratio, the number of axial and radial jets, the aspect ratio and radial location of the axial air jets, and the radial jet inlet hole diameter. Each of these key parameters exhibits a low-NO_x point from which an optimized combustor was developed. Using the parametric analysis, NO_x emissions were reduced by a factor of 3 as compared with the emissions from conventional, liquid-fueled combustors operating at cruise conditions. Further development promises even lower NO_x with high combustion efficiency.

14. SUBJECT TERMS	15. NUMBER OF PAGES
Low-NO_x combustor; Jet-shear-layer combustor; Lean-direct injection; Effervescent atomization	70
	16. PRICE CODE A04

17. SECURITY CLASSIFICATION OF REPORT	18. SECURITY CLASSIFICATION OF THIS PAGE	19. SECURITY CLASSIFICATION OF ABSTRACT	20. LIMITATION OF ABSTRACT
Unclassified	Unclassified	Unclassified	